A thesis entitled

SOME COMBINATION REACTIONS OF FREE ATOMS

by

Abul Kasem Chowdhury

Submitted to the Faculty of Science for the

Degree of Doctor of Philosophy in the

University of London

Department of Chemistry

Bedford College,

London N.W.1

September 1978

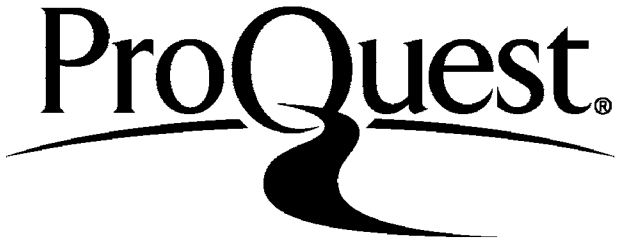

Abstract

A kinetic study has been made of the reactions:

$O + O_2 + M \longrightarrow O_3 + M$ ($M = O_2, CO_2, He, Ar$) 1.1

$O + SO_2 + M \longrightarrow SO_3 + M$ ($M = SO_2, N_2, He, Ar$) 2.1

and the rate constants determined at different temperatures.

An improved discharge flow apparatus was designed and used for the work; the first order decay of oxygen atoms was followed by chemiluminescence techniques. Rate constants for surface reactions were measured by an extension of the technique; this permitted the measurement of surface recombination efficiencies in the presence and absence of O_2. Recombination coefficients for each third body were determined and the corresponding recombination efficiencies were evaluated.

For reaction 1.1, the rate of reaction decreased with increasing temperature. The Arrhenius plots in the presence of all third bodies, except CO_2, were non-linear; this was indicative of the presence of different reactions each with its own energy of activation. A possible mechanism for the reaction is advanced. The high surface recombination efficiency depended on the ambient gas, decreasing in the order $Ar > He > CO_2$. This suggests that physical adsorption reduces the catalytic efficiency; this could explain the large range of values of the catalytic efficiency reported in the literature.

The rate of reactions 2.1 increased with increase of temperature; the energy of activation ($M = SO_2$), determined for the first time, is compared with literature values using other third bodies. The importance

of the complete exclusion of water from the apparatus and reagents was essential. Unless great precautions are taken, an oily film, possibly of H_2SO_4, is formed on the walls of the reactor; this has a pronounced catalytic effect on the reaction. The mechanism of this reaction is discussed in terms of the attainment of a steady state concentration of SO_3.

This thesis comprises a report of full-time research undertaken by the author in the Physical Chemistry Laboratories of Bedford College, University of London, from February 1975 to September 1978.

A. K. Chowdhury.

ACKNOWLEDGEMENTS

I am very grateful and indebted to my supervisor Dr. F. S. Larkin for giving me constant guidance, encouragement, constructive criticism, friendly advice throughout the course of this investigation.

I owe a great debt of gratitude to Prof. G. H. Williams and Prof. A. M. James for their keen interest, inspirations and providing all research facilities during the process of the work.

I am very grateful to my parents for their continuous monetary support, to my brothers and uncles for their encouragements.

I extend my sincere thanks to Mr. and Mrs. Sharif for their declaration concerning my maintenance and educational expenses in England.

Thanks are also due to Mr. Z. Hossain, Mr. Shahidul Alam, Mr. Ezaj Ahmed, Mr. Iqbal Bhanger and Mr. H. K. Siddiquee for their great help and cheerful company.

I also owe many thanks to Mr. N. A. Chowdhury for his nice gift, technical help and encouragement.

My sincere thanks also to Mr. Liquiroish, Mr. Mitchell and Mrs. D. Storey for their technical help.

Finally, I would like to thank British Council for an OSFAS award and Bedford College for Paterson Memorial Scholarship.

CONTENTS

CONTENTS (Continued)

CHAPTER 1

INTRODUCTION

Studies of many gas-phase chemical reactions show that they proceed by a complex process rather than by a simple one-step process. One of the criteria and symptoms of such complex reactions is the existence of reactive atoms and free radicals as transitory intermediates. These transitory intermediates are known to play important roles in many gaseous reactions such as oxidations, explosions and in flames etc. The study of the reactions initiated by these intermediates is important for two reasons. First, as the reactions are complex, it is essential to study the reactions of the intermediates involved in other simple systems under more easily controlled conditions. Secondly, experimental data on elementary reactions is needed for comparison with theoretical predictions. In the last decade, therefore, the emphasis on reaction kinetics has shifted to measurement of the rate of elementary reactions and study of the energy distributions and products.

Atomic reactions were of interest to chemists from the early part of the present century. In 1911, Strutt[1] produced oxygen and nitrogen atoms by using a high frequency electrical discharge. Wood,[2] in 1920, produced high concentrations of hydrogen atoms by a low frequency discharge. During this period Langmuir showed that hydrogen could be dissociated on a heated tungsten filament at very high temperatures. It was first shown by Wood[3] that hydrogen atoms could be pumped out of a glow discharge and carried for a considerable distance before they recombine. Steacie[4] has reviewed the work on atomic and free radical reactions carried out in the period up to 1953. More recent reviewers have dealt exclusively with O atoms[5] and

with H atoms,[6,7] although in the first two cases the emphasis is on reactions with a simple inorganic molecules.

This thesis describes an experimental study of the kinetics and decay rate of oxygen atoms by the three-body processes:

$$O + O_2 + M = O_3 + M \qquad 1.1$$

and

$$O + SO_2 + M = SO_3 + M \qquad 2.1$$

Chapters 5 and 6 describe experimental results obtained for various third bodies M for reactions 1 and 2 respectively. Rate constants for these reactions have been measured in a conventional type of discharge flow system and oxygen atom concentrations were measured by a chemiluminescence technique. The rate constants have been determined over a range of temperatures between 196 - 500 K. A full description and discussion of the discharge apparatus, flow system, photomultiplier and other essential parts of the apparatus is given in chapter 2.

Before discussion of some earlier work on these two atomic combination reactions, some salient features of the kinetics of atomic recombination reactions will be discussed.

1.1. Combinations of Atoms and Radicals

Atoms and radical recombinations are the reverse of unimolecular dissociation reactions and show similar pressure dependent kinetics. When two atoms A and B (where B may be the same atom as A or different) recombine to form a stable molecule, they do so along a Morse type potential energy curve (Fig. 1). For a head-on collision between two atoms A and B, the distance of closest approach depends on their relative velocity. The total energy is conserved in a collision, and it can be represented by the horizontal line XZ. The relative kinetic energy ΔE is the difference

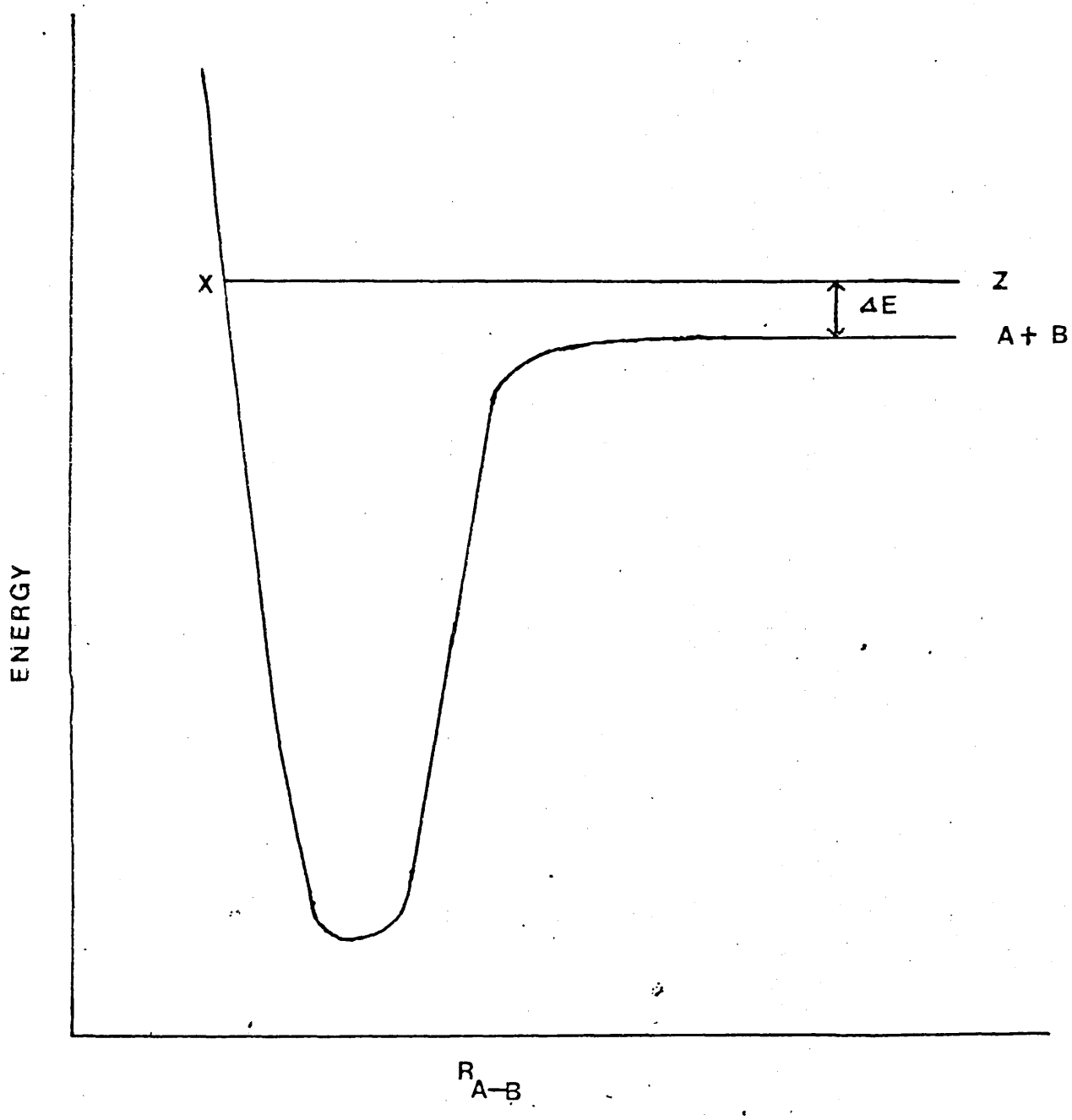

FIG:1 POTENTIAL ENERGY DIAGRAM FOR ATOM RECOMBINATION

between the potential energy curve and XZ. As the atoms approach they attract one another and the kinetic energy increases, until the repulsive limb is reached, when the kinetic energy decreases and reaches zero at X. At this point, the atoms reverse their relative motion and move away from one another unless energy in excess of ΔE is removed during the collision. Collision of AB* with a third body M, generally provides the most efficient means of removing this energy, the excess energy being channelled into relative motion of AB* and M, or into the internal degrees of freedom of M. The overall combination reaction:

$$A + B + M \longrightarrow AB + M \qquad 3$$

can usually be considered to involve three basic reactions, Viz.:

$$A + B \longrightarrow AB^* \qquad 4$$

$$AB^* \longrightarrow A + B \qquad -4$$

$$AB^* + M \longrightarrow AB + M \qquad 5$$

where AB* is a complex which possesses all the energy liberated by the two particles A and B. Applying the steady state approximation to AB* gives:

$$[AB^*] = \frac{k_4\ [A]\ [B]}{k_{-4} + k_5\ [M]}$$

The rate of formation, P of AB is $k_5\ [AB^*]\ [M]$, and so

$$P = \frac{k_5\ k_4\ [A]\ [B]\ [M]}{k_{-4} + k_5\ [M]}$$

It follows that at sufficiently low pressures of M, ie. $k_5\ [M] << k_{-4}$ the overall reaction is third order with a rate constant $k_5\ k_4/k_{-4}$ while at sufficiently high pressures, the overall reaction is of second order and independent of the concentration M; it has a rate constant equal to k_4. The mechanism of the reaction 3 discussed above is known as "Energy transfer" mechanism (ET).

The reverse reaction of 3 viz. the unimolecular decomposition of AB has long been considered to involve the basic reactions:

$$AB + M \longrightarrow AB^* + M \qquad 6$$

$$AB^* \longrightarrow A + B \qquad 7$$

$$AB^* + M \longrightarrow AB + M \qquad 8$$

and to have the complete rate expression:

$$\frac{-d\,[AB]}{dt} = \frac{k_6\, k_7\, [AB]\, [M]}{k_7 + k_8\, [M]}$$

It follows that provided AB* in the two sets of basic reactions means the same thing, a termolecular reaction of type 3 will be the second or third order when the reverse unimolecular reaction is first or second order respectively.

The change from the third to second order in the case of combination of atoms, generally occurs only at very high pressures. This pressure depends on the lifetime of AB* if the energy transfer mechanism is operative. For H_2, O_2, N_2 and I_2 a very high pressure is necessary. For O_3* the pressure has been calculated to be about 60 atmospheres.

Third order rate constants have been obtained for the combinations of hydrogen,[8] bromine[9] and iodine[10-16] atoms and of methyl[17,18] and other radicals. Many of the reactions have small negative activation energies. The third order rate constants for atom combination reactions fall into two classes: with the inert gases and certain simple molecules (such as hydrogen) the values at ordinary temperatures are about 3×10^{15} cm^6 mol^{-2} s^{-1} while with more complex molecules much higher values are observed. The recombination of atoms in the presence of benzene, mesitylene or I_2 molecules (but not of the inert gases, hydrogen, nitrogen, oxygen and ~~carbondioxide~~ carbon dioxide), the overall rate constant is considerably greater than 10^{15} cm^6 mol^{-2} s^{-1}. In such cases, the equations 4-5 must be

replaced by the following mechanism:

$$A + M \longrightarrow AM^* \qquad 9$$

$$AM^* \longrightarrow A + M \qquad -9$$

$$AM^* + B \longrightarrow AB + M \qquad 10$$

This mechanism is known as Radical-molecule-complex mechanism (RMC). The radical molecule complex theory was suggested by Rabinowitch,[19] and since then has been considerably refined.[20-22,14,15]

Applying a steady state treatments for [AM]*, gives:

$$\frac{d[AM]^*}{dt} = k_9 [A] [M] - k_{-9} [AM]^* - k_{10} [AM]^* [B] = 0$$

and the stationary concentration of $[AM]^* = \frac{k_9 [A] [M]}{k_{-9} + k_{10} [B]}$

Thus: $\frac{d [AB]}{dt} = k_{10} [AM]^* [B] = \frac{k_{10} k_9 [A] [B] [M]}{k_{-9} + k_{10} [B]}$

If $k_{-9} >> k_{10} [B]$ then $\frac{d [AB]}{dt} = K_9 k_{10} [A] [B] [M]$

where $K_9 = k_9/k_{-9}$ is the equilibrium constant for the formation AM* from A and M. The bond dissociation energy, D_o (A - M) is usually taken to be in the range D (A - M) = 3500 $\pm$ 1500 cal mol^{-1}. k_{10} is considered to be near the gas collision frequency. The measured third order recombination rate constant k (M) comes from:

$$\frac{d [AB]}{dt} = k [A] [B] [M]$$

$$k = K_9 k_{10},$$

$$K_9 = e^{-\Delta G/RT} = e^{\Delta S/R} e^{-\Delta H/RT}$$

$$k = k_{10} e^{\Delta S/R} e(+3500 \pm 1500)/RT$$

There is some temperature dependence in k_{10} because of the collision frequency α $T^{1/2}$. Qualitatively this expression accounts for the negative activation energy observed experimentally.

To compare theories with experiment several criteria may be considered. A good theory should predict three parameters (a) the absolute value of the rate constant; (b) its variation with temperature and (c) its variation with the nature of the third body. Most theoretical studies have aimed at these objectives.

Porter[23] believes that energy transfer is less successful in predicting temperature coefficients for iodine recombination in the presence of twelve chaperons and concluded that the radical-molecule-complex theory predicts both the absolute rate and the dependence on chaperon. The main objection which can be raised to the complex theory concerns the nature of the AM complex. Laidler[24] has questioned whether the binding energy can be great enough when the foreign gas is inert and has concluded that the energy transfer mechanism applies in such cases. The interaction between A and M is unspecific, since even iodine itself, the most efficient chaperon, fits the correlation with boiling point, ionization potential and similar properties found by Russell and Simons.[10] Attempts to interpret recombination rates in terms of van der Waals[14] forces were not, however, successful since these forces are too small, and show too little variation between chaperon molecules, to account for either temperature coefficients or relative rates. This difficulty is removed in the charge-transfer complex theory of Porter and Smith.[25] Evidence has been provided for this theory by the direct observation of the absorption spectra of the charge transfer complexes in flash photolysis experiments.[26,27] In case of free radical recombinations i.e. when A and B is free radical rather than atoms, the life-time of AB* (or A_2^*) is usually sufficiently long for the ET mechanism to be more important. Atom combinations in the presence of poly-atomic and particularly of chemically reactive foreign molecules, occurs largely by the RMC mechanism, the reason is that the AM*, because of

its complexity has a long life and is readily deactivated to give the more stable species AM which brings about the recombination species. The greater the energy released in the conversion of AM* into AM the greater the rate for the combination process. However, the situation is not so clear-cut for the combination of atoms in the presence of simple foreign molecules such as inert gas, hydrogen and oxygen. The question of the binding between A and M and of the possible energy levels of the complex AM, is important in deciding whether the RMC mechanism plays a role in these reactions. This question has been theoretically examined by Eusuf and Laidler.[24] They estimated the binding energies between iodine atoms and various chaperon molecules taking dispersion forces and charge transfer into account. The binding energies obtained for certain simple molecules including inert gas are less than the average thermal energy. These complexes AM*, therefore, cannot be deactivated to AM and play no role in atom recombinations. With n-butane, benzene and molecular iodine as chaperons, however, complex formation plays a role in the reaction.

1.2 Reactions of Excited Species.

From the discussion in the previous section it is apparent that an excited product can result whenever the elementary processes involve atoms and radicals. The excess energy of the excited species instead of being removed by a third body may be emitted as electromagnetic radiation. A chemical reaction which emits light is called a chemiluminescence reaction. Visible and ultraviolet chemiluminescence results from the production of electronically excited species whereas infrared chemiluminescence arises from vibrationally excited species. Electronically excited species have in a limited number of cases been established.[28] Most of these reactions involve atoms or free radicals, eg. the recombination of nitrogen atoms[29,30]

or the combination of oxygen atoms with nitric oxide.[31,32] The infrared chemiluminescence from reaction 1.1 has been reported by Rosenberg and Trainor.[33-35] Thomas and Thrush[36] also measured infrared emission by the vibrationally excited H_2O molecules produced in the quenching of O_2 ($^1\Sigma g^+$). The formation of electronically excited species in the reactions of stable molecules is unusual and the only examples appear to be the reactions of ozone with nitric oxide[37] and sulphur monoxide.[38]

A chemiluminescent reaction can be divided into two stages: the formation of an electronically excited molecule and its subsequent radiation or quenching. The absolute intensity of radiation is thus the product of the absolute rate of formation of the electronically excited molecules and their probability of radiation or fluorescence efficiency. Chemiluminescence emitted from a combination reaction may be a two body or three body process.[39]

1.3 Three Body Combination Reactions.

Three body chemiluminescence emanates from levels immediately below the dissociation threshold as these are the levels corresponding to newly stabilized molecules. It rarely comes from a state which correlates with ground state atoms so that several electronic states are usually involved.

The general mechanism requires the atoms to approach each other on a stable potential energy curve and make a collision induced crossing to the emitting state.

Population: $A + B + M = \overset{*}{AB} + M$ 3.1

radiation: $AB^* = AB' + h\nu$ 3.2

quenching: $AB^* + M = AB' + M$ 3.3

Where AB′ is either a ground or vibrationally excited state.

The intensity of radiation I may be represented by

$$I = k_{3.2}\,[AB^*] \qquad 3.5$$

Applying the steady state treatment for [AB*] gives

$$\frac{d[AB^*]}{dt} = k_{3.1}\,[A]\,[B]\,[M] - k_{3.2}\,[AB^*] - k_{3.3}\,[AB^*]\,[M] = 0$$

$$[AB^*] = \frac{k_{3.1}\,[A]\,[B]\,[M]}{k_{3.2} + k_{3.3}\,[M]}$$

Therefore equation 3.5 gives

$$I = \frac{k_{3.1}\,k_{3.2}\,[A]\,[B]\,[M]}{k_{3.2} + k_{3.3}\,[M]}$$

Many three body chemiluminescence reactions are represented by this scheme, in particular the yellow nitrogen afterflow from:

$$N + N + M = N_2^* + M \qquad 3.4$$

and the grey-green air afterglow from:

$$O + NO + M = NO_2^* + M$$

If the quenching parameters $k_{3.3}/k_{3.2}$ are known, the effective rate constant for the combination into the emitting state $k_{3.1}$ can be calculated from the absolute intensity of the chemiluminescence.

1.4 Two Body Combination Reactions.

The association of two atoms into a state with thich they do not correlate is the inverse of predissociation. For two body emission then, the atoms must approach on a non-repulsive potential curve and cross to the emitting state and this state is confined to levels immediately above the dissociation threshold.

The most important types of reactions of excited atoms and molecules other than chemiluminescence are:

(i) spontaneous dissociation:

$$AB^* \longrightarrow A + B$$

(ii) spontaneous isomerization:

$$AB^* \longrightarrow BA$$

(iii) physical quenching, if the electronic energy of the excited molecule is removed without chemical reaction:

$$A^* + B \longrightarrow A + B$$

(iv) transfer of electronic energy to the colliding molecule:

$$A^* + B \longrightarrow A + B^*$$

this can lead to sensitized fluorescence;

(v) quenching accompanied by dissociation of colliding molecule:

$$A^* + BC \longrightarrow A + B + C$$

this is the process of sensitized dissociation;

(vi) chemical quenching:

$$A^* + BC \longrightarrow AB + C$$

(vii) quenching accompanied by dissociation of excited molecule:

$$AB^* + C \longrightarrow A + B + C$$

(viii) quenching accompanied by isomerization of the excited molecule:

$$AB^* + C \longrightarrow BA + C$$

(ix) association between the excited molecule and a colliding molecule in the presence of a third body:

$$A^* + B\ (+M) \longrightarrow AB\ (+M)$$

1.5 The Early Work on the Recombination of Atoms.

Considerable interest has been shown recently in the reactions of oxygen atoms with molecular oxygen. The recombination of oxygen atoms in the presence of molecular oxygen in gas phase may be represented by the following processes:

$$O + O_2 + M \longrightarrow O_3 + M \qquad 1.1$$

$$O_3 + M \longrightarrow O + O_2 + M \qquad 1.2$$

$$O + O_3 \longrightarrow 2O_2 \qquad 1.3$$

$$O + O + M \longrightarrow O_2 + M \qquad 1.4$$

where 'M represents a third body.

Reaction 1.1 is one of the fundamental reactions in the upper atmosphere which predominantly governs the O and O_3 concentrations in the stratosphere[40] and polluted air.[41] Rate equations derived from studies of the kinetics of both the photochemical[42-44] and the thermal[45-47] decompositions of ozone indicate that reaction 1.1 is third order at pressures up to at least 1 atmosphere.

Until 1956 one could do little more than guess at the rate of this 1.1 reaction, and estimates by different investigators varied by more than three order of magnitudes. Benson and Axworthy[45] had, by this time, experimentally investigated the pyrolysis of ozone in an effort to discover its mechanism. The analysis of their results was based on the long recognised fact that, except at high temperatures or high ozone concentrations, the kinetics of the thermal decomposition of ozone are capable of explanation by a first step consisting of the reverse reaction 1.2.

This is then followed by competition between molecular oxygen and ozone for oxygen atoms ie. reactions 1.1 and 1.3.

They inferred that reaction 1.3 which produces two oxygen molecules with the liberation of 93.7 k cal of excess energy does not produce more than one excited electronic state of oxygen and these hot O_2 molecules are not very efficient in exciting ozone to decomposition. This indicates that high quantum yields found in the photolysis of ozone at short wave-lengths

probably are attributable to metastable O atoms (^1D) produced in the primary process which can generate a chain.

From the value of the rate constant of the reaction 1.2 and the knowledge of the equilibrium constant of the same reaction, Benson and Axworthy calculated the rate constant $k_{1.1}$ for reaction 1.1. From the positive exponent of temperature variation of $k_{1.1}$ they concluded that it has an apparent negative activation energy. Eucken[48] also found that the rate of photochemical ozone formation from oxygen at very low pressures has a negative temperature coefficient. In this case, reaction 1.1 may be supposed to occur in steps:

$$O + O_2 \xrightarrow{a} O_3^*$$

$$O_3^* \xrightarrow{b} O + O_2$$

$$O_3^* + M \xrightarrow{c} O_3 + M$$

It seems that when oxygen atoms combines with O_2, excited ozone forms by process (a) which again may dissociate to its original state by process (b). Finally, the excited ozone molecule can dissipate its excess energy to a third body M and then form a ground state ozone.

Herron and Klein[49] determined the rate constant k_a by the isotopic exchange of O^{18} atoms with $O_2^{16.16}$ and suggested the formation of an excited intermediate O_3^* in the course of the reaction O^{16} and $O_2^{16.16}$; similar results were also found by Brenner and Niki.[50]

The Benson-Axworthy mechanism does not correspond to a chain reaction as there are no chain propagating steps. To explain the higher decomposition rate of ozone at high pressures or temperature, Ritchie[51] proposed a thermal chain involving a reaction between ozone molecules and energy rich oxygen molecules from reaction 1.3. A chain reaction was suggested by

Glissman and Schumacher[46] and discussed again by Schumacher,[52] it involves excited oxygen molecules which are supposed to be involved in the following chain propagating steps:

$$O + O_3 \longrightarrow O_2 + O_2^*$$

$$O_2^* + O_3 \longrightarrow 2O_2 + O$$

On the basis of the critical examination of the problem, Benson and Axworthy[53] concluded that chain reaction is unimportant and the excess rate is due to thermal gradients within the reaction vessel. By considering the potential energy surfaces for the reaction, McKenney and Laidler[54] also reached a similar conclusion. A similar conclusion has also been drawn by Kaufman.[55]

The photochemical decomposition of ozone has also been studied in considerable detail. The decomposition isbrought about by red light and also by radiation of higher frequency, such as uv. radiation. It appears that the reaction brought about by red light does not involve energy chains, like the thermal decomposition, but the reaction in uv. does involve energy chains. Both in the thermal decomposition and decomposition in red light the atoms produced are in their ground (^3P) state, and do not have enough energy to give rise to excited O_2 molecules that are sufficiently energetic to propagate a chain. In uv., on the other hand, O^* (^1D) atoms are produced and these undergo the reaction:

$$O^*(^1D) + O_3 \longrightarrow O_2 + O_2^* \ (^3\Sigma g^-)$$

The O_2^* $(^3\Sigma\text{-}_g)$ molecules produced in this then propagate the chain as follows:

$$O_2\ (^3\Sigma\text{-}_g) + O_3 \longrightarrow 2O_2 + O\ (^1D)$$

As the Benson and Axworthy's value of $k_{1.1}$ is dependent on the thermal data for the equilibrium constant K_{eq}, any uncertainty in this

constant will be reflected in $k_{1.1}$. Two years later, direct investigations of the rate of the reaction 1.1 appeared in the literature. The experimentally determined values of $k_{1.1}$ reported by Kaufman[57] and Elias[58] are in agreement with the values obtained indirectly by Benson and Axworthy (calculated from the decomposition rate constant of ozone, $k_{1.2}$ and the equilibrium constant of reaction 1.2). Kaufman produced oxygen atoms by a microwave discharge in a flow system; a small amount of nitric oxide was introduced into the system and the disappearance of 0 atoms was monitored at varying distances down the flow tube by measuring the intensity due to chemiluminescence reaction:

$$0 + NO \longrightarrow NO_2 + h\nu$$

The NO_2 in the system was regenerated by the fast reaction:

$$0 + NO_2 \longrightarrow NO + 0_2$$

By use of this reaction, the concentration of 0 atoms was titrated, the end-point was indicated by the complete extinction of the glow along the tube. With a knowledge of the velocity of flow down the tube, rate constants are obtained for the first order disappearance of 0 atoms by this method, with

$k = (2.3/t_{xy}) \log_{10} (I_x/I_y)$, where I_x and I_y are the luminescent intensities at positions x and y, and t_{xy} is the flow time between the positions. From a consideration of some of the limitations of the system such as the effects of viscous pressure drop along the tube (which is particularly large at high pressure and high flow rate), wall effects and the effect of recombination on the flow, Kaufman obtained a value of $k_{1.1} = 4 \times 10^{14}$ cm^6 mol^{-2} s^{-1} for M = 0_2. Since 0 atoms compete to combine by two other processes 1.3 and 1.4 the actual value of $k_{1.1}$ would

be less than this. Since the observed decay rate in the presence of added nitrogen and argon was entirely explained by the pressure drop correction and wall effects, and the observation that, with varying reactant concentrations, the rate constants calculated on the basis of $0 + 0_2 + M$ remained nearly constant while those calculated on the basis $0 + 0 + M$ did not, it was concluded that their contribution of recombination reaction is unimportant. On the other hand, the reaction of oxygen atoms with ozone is important and Kaufman estimates that allowance for this reaction would reduce the value of $k_{1.1}$ to a value in the range $2 - 4 \times 10^{14}$ cm^6 mol^{-2} s^{-1}.

Elias, Ogryzlo and Schiff[58] produced oxygen atoms by passing molecular oxygen through an electrodeless discharge in the pressure range 0.1 - 3 mmHg. The concentration of oxygen atoms was measured as a function of time in a flow system by means of a movable atom detector which consisted of a platinum wire coated with a suitable catalyst for atom recombination. Values of 7.7×10^{-5} and 1.0×10^{14} cm^6 mol^{-2} s^{-1} were obtained for the recombination coefficient (γ) on pyrex and for the termolecular reaction $k_{1.1}$ respectively. Elias _et al_. compared the concentration of oxygen atoms measured by their wire detector with those measured by a wrede gauze, and by the NO_2 titration method of Kaufman. The wrede gauze gave concentrations about 10% lower and NO_2 titration gave values about 25% lower than those obtained by the wire detector. The authors concluded that the difference between the NO_2 titration and the wire detector was due to the presence of excited 0_2 molecules, possibly in the $^1\Delta g$ state in the gas stream. Foner and Hudson,[59] (1956) using mass spectrometry, also found the excited $^1\Delta g$ oxygen in fairly large concentrations. Kaufman[60] (1964) in his experiments with discharge-flow system showed the presence of some

metastable species capable of dissociating O_3 and of generating additional O atoms downstream of the discharge. He provided evidence for the presence of these metastable species by adding O_3 to discharged oxygen. He found no metastable species when O atoms were produced by thermal decomposition of ozone and suggested that heat of formation of ozone $\Delta H_f(O_3)$ must be changed so as to change equilibrium constant for agreement with $k_{1.1}$. A value of 34.5 k cal mol^{-1} for heat of formation of ozone at 0 K was recommended in this case. Clyne, Thrush and Wayne[61] reported the spectroscopic evidence for the existence of such species and identified them with O_2 ($^1\Sigma_g^+$). However, their concentration was too small to account for the large amount of O_3 decomposition and O atom generation. Again, by mass spectrometric studies Herron and Schiff[62] found large concentrations (10% - 20%) of $O_2(^1\Delta_g)$. Oxygen molecules in the $^1\Sigma_g^+$ state react with ozone regenerating oxygen atoms.

$$O_3 + O_2(^1\Sigma_g^+) \longrightarrow O\ (^3P) + 2O_2(^3\Sigma_g^-)$$

$$\Delta H = -12 \text{ k cal mol}^{-1}$$

and similar process can also occur with higher excited states of O_2. The reaction of more abundant ($^1\Delta_g$) state:

$$O_2\ (^1\Delta_g) + O_3 \longrightarrow 2O_2 + O \qquad 1.5$$

is endothermic (ΔH = 3 k cal mol^{-1}) and does not appear to occur readily. However, the earliest studies of electronically excited O_2 suggested the occurence of reaction 1.5 might explain the anomalous rates for the reaction

$$O + O_2 + O_2 \longrightarrow O_3 + O_2$$

measured in discharge flow systems.

Reaction 1.5 has been studied by different groups[63,64,65] using different techniques such as photoionization technique, optical emission, etc. to detect O_2 ($^1\Delta_g$).

Another important effect which can also lead to a large spread in the reported values of $k_{1.1}$ was reported by Larkin and Thrush.[66] They found that even small amounts of hydrogen through the discharge catalyses the removal of atomic oxygen by the reaction sequence:

$$H + O_2 + M \longrightarrow HO_2 + M$$

$$O + HO_2 \longrightarrow OH + O_2$$

$$O + OH \longrightarrow H + O_2$$

Mathias and Schiff[67] obtained reproducible results only when molecular oxygen was passed through traps cooled in liquid air which they suggested prevented catalylic decomposition by hydrogeneous impurities. The considerable discrepancies of the rate constant $k_{1.1}$ appearing in the literature before 1964 was, therefore, due to the presence of impurities such as hydrogen and electronically excited O_2 which are known to affect the reaction significantly.

Kaufman and Kelso[60] eliminated these species, hydrogen atoms and electronically excited oxygen molecules, by generating the atoms by pyrolysis of ozone in a quartz tube at 1000°C. They obtained a value of 2.7×10^{14} cm^6 mol^{-2} s^{-1} for $k_{1.1}^{O_2}$. Clyne, McKenney and Thrush,[68] on the other hand retained the discharge and relied upon rigorous purification of the gases and the great dilution of the oxygen with argon passing through the discharge to eliminate unwanted species. They obtained a value of

$$k_{1.1}^{Ar} = 1.9 \times 10^{14} \text{ cm}^6 \text{ mol}^{-2} \text{ s}^{-1} \text{ at } 290 \text{ K.}$$

Benson and Axworthy[69] in 1964 reconsidered the rate constant obtained from the thermal decomposition of ozone and reported that values obtained for the efficiencies of various third bodies calculated on the basis of pyrolysis data (of Glissman[46] and Schumacher) are in exact agreement with the values of Castellano[70] and Schumacher.

Kaufman and Kelso[71] determined the efficiciencies of 9 third bodies in the reaction $O + O_2 + M \longrightarrow O_3 + M$ by producing O atoms thermally in a flow system. The values of $k_{1.1}^{M}$ showed the dependence on the nature of M increasing with molecular complexity and increasing more strongly with the dipolar interaction in the case of $M = H_2O$. By considering the efficiencies for O_2, He, Ar, N_2 and CO_2, they found a good agreement with those of pyrolysis and photolysis.

Mulcahy and Williams[72] using a stirred-flow reactor studied the rate constant of reaction 1.1 at total pressures from 1 to 8 torr, generating oxygen atoms by pyrolysis of ozone at 1300 K. The rate constant obtained in the temperature range 213 - 386 K when M = Ar and $M = CO_2$ can be represented by $k_{1.1}^{Ar} = (1.7 \pm 0.2) \times 10^{13} \exp \frac{846 \pm 50}{T}$ $cm^6\ mol^{-2}\ s^{-1}$ $k_{1.1}^{CO_2} = (8.4 \pm 1.1) \times 10^{13} \exp \frac{730 \pm 70.5}{T}$ $cm^6\ mol^{-2}\ s^{-1}$.

The values obtained for $k_{1.1}$ are greater than those calculated from previous investigations of the kinetics of pyrolysis of ozone, even allowing for the accepted error in the equilibrium constant for reaction 1.1 . The relative efficiencies of O_2, Ar and CO_2 also differ from those derived from earlier work on the pyrolysis and photolysis of ozone.

A few measurements of the rate constant $k_{1.1}$ in the static system also appeared in the literature after 1965. Sauer[73] et al. used the

method of pulse radiolysis to study the kinetics of ozone formation in gaseous argon-oxygen systems. The value of $k_{1.1}$ was determined by a fast reaction method in which the reaction was initiated by a short-lived perturbation of the system. Ozone formation was monitored optically at 2600°A using a photomultiplier. In another experiment Sauer[74] used the same method to determine the rate constant of the reaction 1.1 in which different molecules were used as sources of oxygen atoms and in which the effects of different third bodies were determined. He concluded that the rate constant of the third body (Ar) controlled reaction of oxygen atoms with molecular oxygen is independent of whether the oxygen atom originates from O_2, CO_2 or NO_2. The third body efficiencies of He, CO_2 and N_2O relative to an Ar efficiency of 1.0 have been determined by them as 0.8, 5 and 5 respectively.

The techniques of pulsed-radiolysis, with spectroscopic detection of transients, have also been used by Meaburn[75] et al. to study some gas phase reactions of atomic oxygen produced in electron-irradiated CO_2, N_2O, and CO at pressures of about one atmosphere. In the presence of small amounts of added O_2, oxygen atoms were found to be removed from these systems mainly by reaction 1.1. The formation of ozone followed pseudo-first order kinetics with rate constant $k_{1.1}^{M}$ = 3.7, 3.2 and 1.6×10^{14} cm^6 mol^{-2} s^{-1} for M = CO_2, N_2O and CO respectively. Kinetic analysis of their results indicated the occurence of two parallel reactions in the system:

$$O\ (triplet) + O_2 + O_2 \longrightarrow O_3 + O_2 \qquad 1.1$$

$$O\ (singlet) + O_2 \longrightarrow O\ (triplet) + O_2$$

Hochanadel[76] et al. using the same technique found that the absorption

spectrum of ozone immediately after the pulse is considerably greater and the peak is a longer wave-length (~ 2860 Å) than that of ground state ozone (~ 2560 Å). The initial absorption was characterised by them as a vibrationally excited ozone produced by $O + O_2 \rightleftharpoons O_3^*$. Their results show that overall third order reaction 1.1 occurs by a sequence of steps.

Recently, the kinetics of ozone formation by 1.1 was studied by Bevan and Johnson.[77] Atoms were produced by irradiating molecular O_2 with a high dose-rate electron pulse and monitored by optical absorption. They interpreted their results in terms of three kinetically distinguishable, consecutive reactions.

The resonance fluorescence technique has been used by Slanger and Black[78] in which $O(^3P)$ atoms were produced by O_2 photodissociation at 1470 Å. They determined the rate constant $k_{1.1}^{Ar} = 1.69 \times 10^{14}$ cm^6 mol^{-2} s^{-1} for argon as third body.

Stuhl and Niki[79] determined the rate constants for a number of termolecular reactions of O - atoms at 300 K, producing O - atoms by pulsed vacuum - uv. photolysis of NO, O_2, CO_2 and N_2O and monitoring the $O(^3P)$ atoms by NO_2^* or CO_2^* chemiluminescent emission. Their values for $k_{1.1}$ are in good agreement with the recommended[83] values at room temperature.

The flash photolysis-resonance fluorescence technique was used by Huie, Herron and Davis[80] to measure the absolute rate constant for $k_{1.1}$. The temperature range covered was 200 - 346 K and the total pressure was varied from 50 - 500 Torr. Over the indicated temperature range, they represented their data by an Arrhenius expression $k_{1.1}^{Ar} = (2.38 \pm 0.21) \times 10^{13} \exp \frac{510.6 \pm 23.16}{T}$ cm^6 mol^{-2} s^{-1}

In some earlier work such as the thermal decomposition of ozone the reaction was studied by conventional manometric methods[81] in the temperature range 388 - 403 K, and in a shock tube[82] from 769 - 910 K.

Although different methods have been used to avoid contaminants the discrepancies in the values of $k_{1.1}$ are still considerably greater than the estimated experimental errors of 10 to 25% and these must be attributed to unknown sources of systematic error. Moreover, the temperature dependence of the reaction measured by flow system in some cases differ by a factor of 2 or 3 with that determined by static[80] methods and this discrepancy could lead to errors of nearly a factor of 2 in estimates of the rate of stratospheric ozone production. Since reaction 1.1 is of such importance in stratospheric chemistry and since its rate constant must be well established at temperatures and pressures corresponding to stratospheric condition, a re-examination of the temperature coefficient is important.

Following the development of a new discharge[93] flow technique in this laboratory, Ball[85] carried forward investigation of the reaction 1.1 in two flow systems - system A (movable detector) and system B (fixed detector). He measured the rate constants $k_{1.1}^{M}$, k_{w}^{*} (surface rate constant in the absence of O_2) and k_w (surface rate constant in the presence of O_2) in system A at 295 K for M = He, Ar, N_2, O_2, CO and CO_2. The room temperature correspondence between $k_{1.1}^{M}$ determined in systems A and B provided a check on each method. Although an attempt was made to elucidate the temperature coefficients for some of the third bodies, the development of the flow technique in system B was not completed. In the sense of extending the range of reaction conditions adopting the

correct technique, and the volume of experimental work, the present study may be considered a continuation of the earlier work by Ball. The main object of this work was to investigate the importance of reference measurements in system B and to show that the surface rate constant can be measured by the system B.

A very unsteady surface rate constant was observed by Ball for M = CO_2 which he suspected to be due to the back diffusion of CO_2 into the discharge producing various species which might attack on the surface. Difficulties of this sort were treated in this study using an improved technique. The overall object of this present work was to report reliable temperature coefficients for four third bodies over a wide range of temperature at the same time eliminating surface and other background reactions. Many interesting problems arose during this work, these are discussed in the appropriate chapter.

1.6 The Early Work on the Reaction: $O + SO_2 + M \longrightarrow SO_3 + M$.

The rate of the termolecular reaction:

$$O + SO_2 + M \longrightarrow SO_3 + M \qquad 2.1$$

is of great importance in the combustion of sulphur containing compounds and in the polluted atmosphere. This reaction was first examined by Geib and Harteck[84] who measured the extent of conversion of sulphur dioxide at liquid air temperatures.

Kaufman[32] studied the decay of oxygen atoms in the presence of SO_2 in a linear discharge flow system and obtained a value of 3×10^{16} cm^6 mol^{-2} s^{-1}. He also found that SO_3 changes the surface recombination efficiency of the glass tube. Although a very small addition of SO_3 had little effect, larger amounts made the flow die out

slowly all along the tube and reappear slowly when the SO_3 flow was shut off quickly. In order to understand reaction 2.1 clearly, it is important to know the part SO_3 plays in the reaction system. Investigation of the gas phase reaction between oxygen atoms and sulphur trioxide is made difficult by the heterogenous effect. Sulphur trioxide is strongly adsorbed on glass surfaces where it exerts a remarkable catalytic effect on the recombination of the atomic oxygen. Determination of the disappearance of oxygen atoms in the gas phase by reaction with SO_2 is further complicated by the strong affinity of the adsorbed sulphur trioxide for traces of water. However, from some preliminary flow tube experiments Kaufman concluded that oxygen atoms do not react rapidly with SO_3 in the gas phase at room temperature. On the other hand, studies[86] of the rate of production of oxygen in the radiolysis of liquid SO_2 have been interpreted to indicate that the reaction:

$$O + SO_3 \longrightarrow O_2 + SO_2 \qquad 2.2$$

is 10 times faster than the reaction:

$$O + SO_2 + M \longrightarrow SO_3 + M \text{ at } 256 \text{ K}$$

Jacob and Winkler[87] reported a gas phase bimolecular rate constant of 2.2 3.01×10^7 cm^3 mol^{-1} s^{-1} at 300 K from results of a discharge flow experiment with low temperature trapping of products; this value also indicates a very slow reaction. These authors noted SO_4 as being a probable intermediate.

Fenimore and Jones[88] concluded that a stationary concentration of SO_3 is reached when SO_2 is oxidized in flame gases. They suggested that SO_3 is formed by 2.1 but is destroyed as fast as formed by a faster reaction, than the reverse of 2.1.

Recently, Westenberg [89] and de Haas measured the rate of the reaction between 0, SO_3 and M under pseudo-first order conditions in a discharge flow reaction with ESR detection. They found this reaction is a fast third order process at pressures up to 7 torr. For M = He, they reported a value of $k_{2.2}^{He} = (7.3 \pm 0.2) \times 10^{17}$ cm^6 mol^{-2} s^{-1}.

Halstead [90] and Thrush using a flow-technique reported a value $k_{2.1}^{Ar} = (4.7 \pm 0.8) \times 10^{15}$ for the reaction:

$$0 + SO_2 + Ar \longrightarrow SO_3 + Ar$$

Mulcahy, Steven and Ward [91] using a stirred flow and ESR technique determined values for $k_{2.1}^{M}$ when M = 0_2, Ar and SO_2. Third order rate constants for $k_{2.1}^{M} = (2.7 \pm 0.5) \times 10^{15}$, $(2.4 \pm 0.15) \times 10^{15}$ and $(10 \pm 4) \times 10^{15}$ cm^6 mol^{-2} s^{-1} when M = 0_2, Ar and SO_2 respectively. Mulcahy et al. [92] later measured the kinetics of each SO_2 reaction at 300 K using both ESR spectrometry and chemiluminescence from the 0 + NO reaction to monitor the concentration of atomic oxygen. It was shown that 0 atoms disappear principally by the reactions:

$$0 + SO_2 + M \longrightarrow SO_3 + M \qquad 2.1$$

$$\text{and } 0 \xrightarrow{\text{wall}} \tfrac{1}{2}0_2 \qquad W$$

However, adsorption of SO_3 on the wall increases the rate of reaction 2.1 which therefore varies with the concentration of SO_3 in the gas phase. The increase in k_w as reaction proceeds causes the apparent value of $k_{2.1}$ to be too high and to depend on the concentrations of 0 atoms present. Nevertheless, by extrapolation to zero concentration of oxygen atoms it was shown that the true value $k_{2.1}^{Ar}$ is 1.4×10^{15} cm^6 mol^{-2} s^{-1} (by spectrometry) and 1×10^{15} cm^6 mol^{-2} s^{-1} (by the afterglow method). Furthermore, experiments[92] using ESR spectrometry have given

the value of $k_{2.1}^{SO_2}$ as 6.6×10^{15} cm^6 mol^{-2} s^{-1}.

The rate of the reaction 2.1 has also been determined by Jaffe and Klein[94] who produced oxygen atoms by the photolysis of nitrogen dioxide

$$NO_2 + h\nu \longrightarrow NO + O$$

In the presence of sulphur dioxide, there is competition between the reaction $O + NO_2$ and reaction 2.1. From the extent of the reduction of quantum yield for the disappearance of nitrogen dioxide (2 in the absence of sulphur dioxide) it was possible to obtain a value for $k_{2.1}^{M} = 1.4 \times 10^{16}$ cm^6 mol^{-2} s^{-1} when M is NO or SO_2.

Timmons *et al.*[95] studied the rate of reaction 2.1 using a linear discharge flow method in which the concentration of oxygen atoms was followed by ESR technique. The value of the rate constant for the reaction 2.1 was found to be 4.1×10^{16} cm^6 mol^{-2} s^{-1}.

The flash-photolysis resonance fluorescence technique has been used by Davis,[96] he reported a lower value for $k_{2.1}$ in comparison with other work. Atkinson and Pitts[97] determined rate constants for the reaction:

$$O + SO_2 + N_2O \longrightarrow SO_3 + N_2O$$

over the temperature range 299 - 392 K using a modulation technique. The Arrhenius expression:

$$k_{2.1}^{N_2O} / cm^6\ mol^{-2}\ s^{-1} = 3.32 \times 10^{16} \exp \frac{(1007.1 \pm 201.43)}{T}$$

This temperature dependence is in good agreement with that obtained from flash photolysis resonance fluorescence measurements using N_2 as the third body.

Very recently, Westenberg and de Haas[98] studied reaction 2.1 over the temperature range 248 - 415 K for M = He. They found that SO_2 is about 10 times as efficient as He as third body; during the course of the reaction SO_3 reaches a steady state concentration and reacts with O atoms forming SO_2 and O_2.

The values of the rate constant for reaction 2.1 obtained by the various workers are listed in Table 1 for comparison. The temperature dependence was measured in four of these studies, it was established that the reaction has a positive activation energy. There is a large measure of disagreement between the results of different workers. The rate constant measured at room temperature with an inert gas as a third body varies over a factor of 40. Extremely high third body efficiency has been attributed to SO_2 itself by some authors who reported a factor of 10 - 130 over rare gas efficiencies. It is clear from the above review that the O + SO_2 reaction should not be regarded as well-established.

In the present investigation it is intended to examine the rate of the reaction 2.1 by the newly developed discharge flow technique. It is proposed to measure rate constant, for M = SO_2 over the temperature range 240 - 500 K and for M = He, N_2 and Ar at 298 K.

T A B L E 1

Summary of results for the reaction: $O + SO_2 + M \longrightarrow SO_3 + M$

Workers	Method	Ref.	Third Body	$10^{-14} \times k^M_{2.1}$ / $cm^6\ mol^{-2}\ s^{-1}$ at 298 ± 2 K
Halstead and Thrush	Discharge flow chemiluminescence technique	90	Ar	47 ± 8
Timmons et al.	Linear discharge flow - ESR	95	He	8
			Ar	10
			SO_2	410
Mulcahy et al.	Homogeneous discharge flow ESR - NO glow	92	Ar	11 ± 3
			SO_2	66
Westenberg and de Haas	Linear discharge flow - ESR	98	He	3 ± 0.2
			N_2	7.2 ± 0.3
			SO_2	29 ± 8
Davis	Flash photolysis - resonance fluorescence	96	He	1.3
			Ar	2.5
			N_2	2.9
			SO_2	174
Atkinson and Pitts	Modulated Hg - photosensitized N_2O - NO glow	97	N_2O	11.5 ± 1.5
			SO_2	<60

CHAPTER 2

THE EXPERIMENTAL APPARATUS

2.1 Introduction.

The experimental apparatus and techniques which were used during the course of experimental work are described in this chapter. The techniques used for the preparation of reagents and the use of vacuum lines etc., are well documented in standard laboratory text books.[99-101]

2.2 The Reaction System.

The apparatus is of conventional design in which discharge flow technique was used to study the progress of reactions 1.1 and 2.1. Fig. 2 and 3 shows the essential parts of the flow system which consisted of a discharge tube, reaction tube and a photomultiplier. The reaction tube is made of pyrex glass of uniform bore (radius 1.25 cm) which has five multiple hole inlet jets at a distance of 15 cm from each other. These jets (J_1 to J_5) can be used for the introduction of reactatns at different positions of the reaction system with rapid mixing. There is another inlet jet at position D for addition of third bodies M. Nitric oxide may be added, if required, through the jet J_6 to facilitate oxygen atom detection. The whole system is connected to a vacuum pump, V,(E S 200 Edwards Vacuum Components Ltd.) of capacity 190 dm^3 min^{-1} which kept the reaction system within a low pressure range 5×10^{-3} to 3×10^{-1} torr. A large stainless steel valve located between the photomultiplier and vacuum pump, was used to control the flow; beyond the valve the gas passed through a large diameter trap

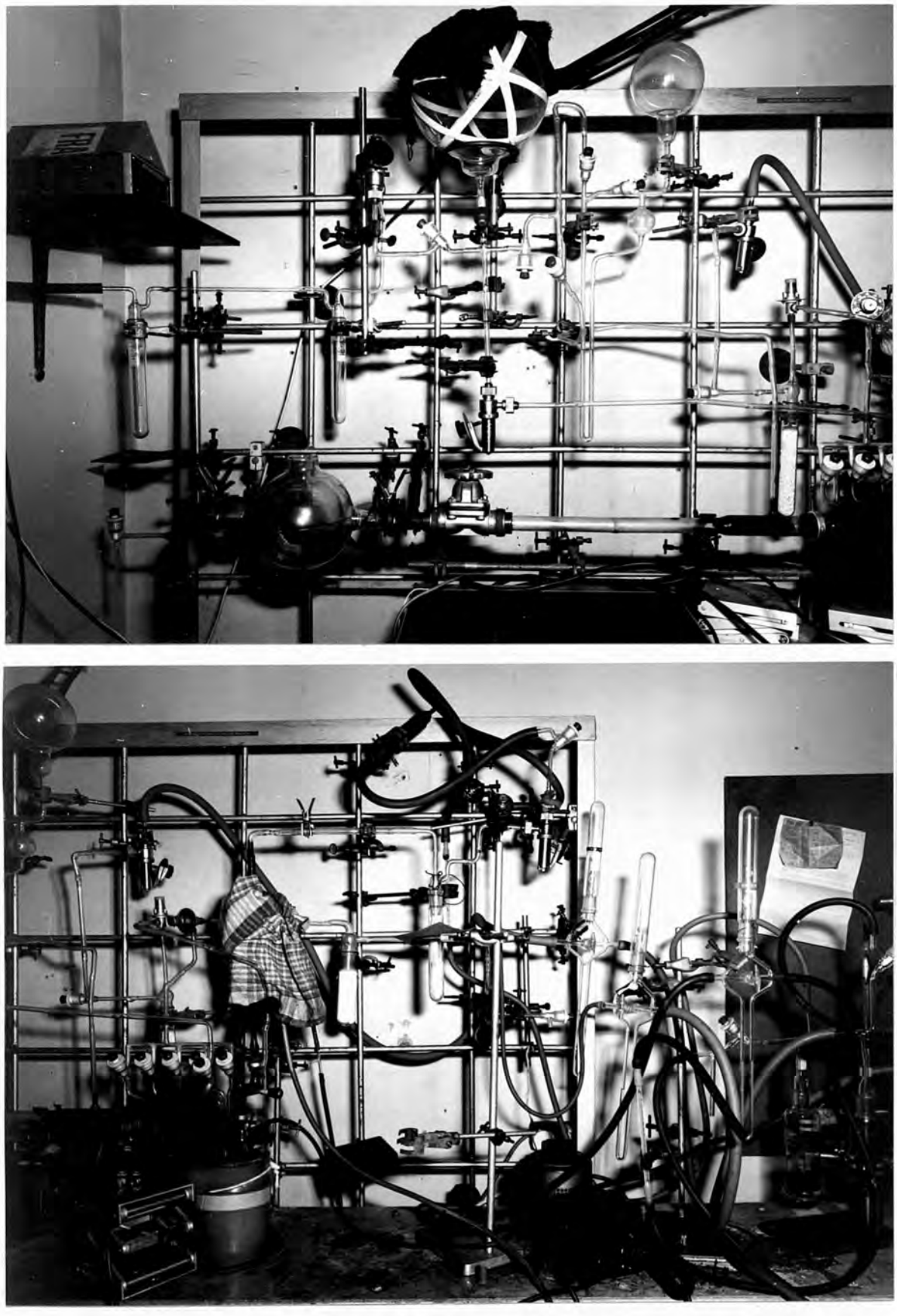

Fig. 2. Top: left hand side, bottom: right hand side of the apparatus.

FLOW SYSTEM B Fig. 3

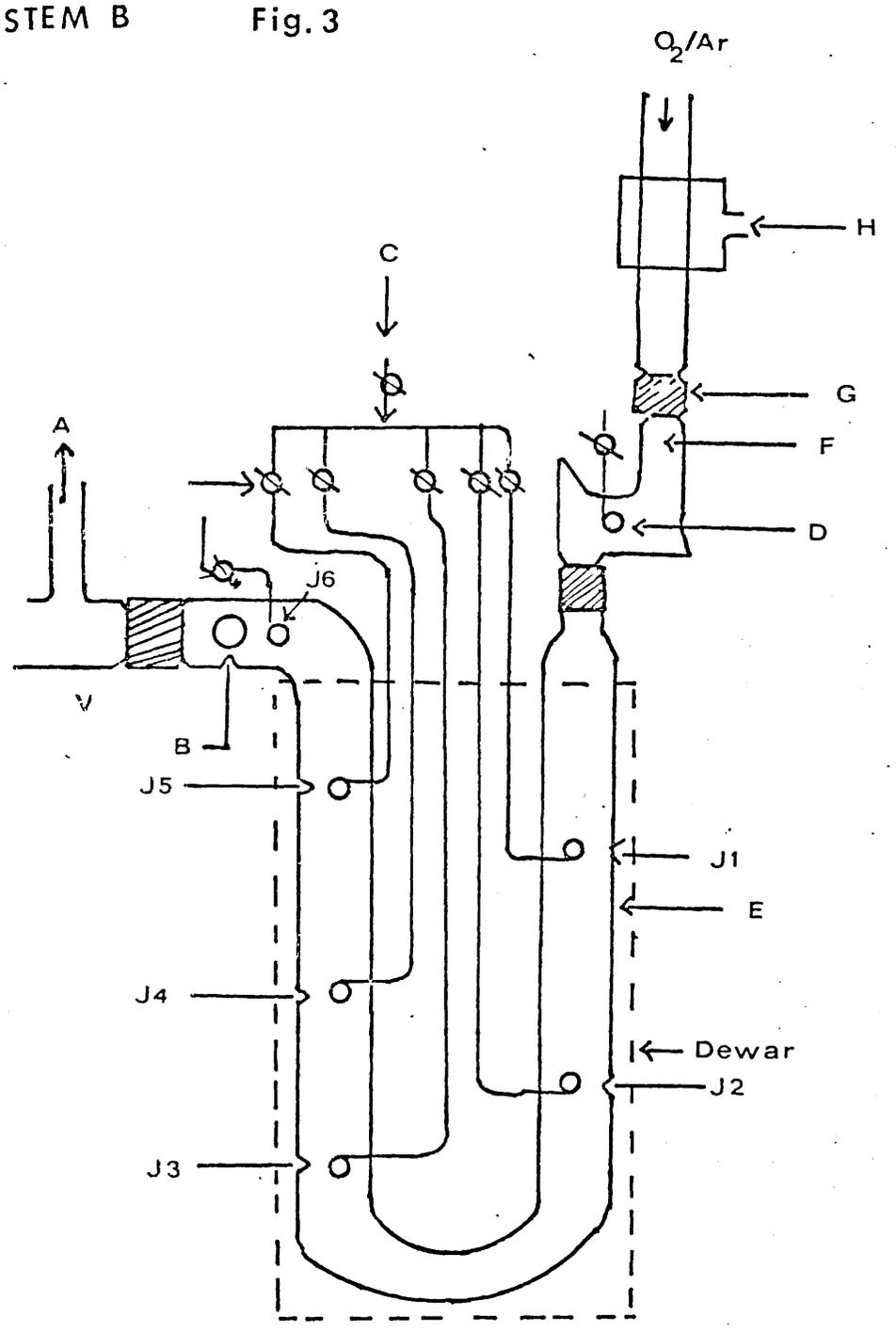

A = Oil manometer
B = Single observation point
C = To jets for O_2 addition
D = Jet for M addition
E = Pyrex flow tube
F = Wood's horn light trap
G = Greaseless screw joints
H = Microwave cavity
V = Vacuum pump

which was used to collect the reaction products at 77 K. A 10 dm^3 bulb was situated between the trap and pump to smooth the flow pattern and minimize pressure fluctuations. The reaction gases were pumped through the reaction system; the reaction time was varied by changing either the length of the reaction zone or the gas velocity. This reaction time was determined by dividing the length of the reaction zone by the linear flow velocity on the assumption that laminar (plug) flow prevailed and that there was rapid radial diffusion with negligible back diffusion. The conditions under which these assumptions are valid are discussed in greater detail in Chapter 3.

Oxygen atoms were generated by passing an inert carrier gas (Ar: 100 - 200 μ mol s^{-1}) containing < 500 ppm O_2 and < 5 ppm N_2 through an electrodeless discharge. The discharges were produced in a microwave cavity by a large C. W. magnetron 2450 - 3,000 Mc s^{-1} (up to 200 Watts microwave power). The molecular oxygen/argon mixture flowed through the cavity enroute to the reaction zone. The cavity had two screw controls which enabled it to be "tuned" to utilize the maximum amount of incident energy in the discharge and to produce the maximum amount of oxygen atoms for a determined total pressure. The position of the quartz discharge was of some importance as the highly ionized species produced by the discharge had to be allowed to decay to leave the mixture of uncharged atoms and molecules. If placed too close to the inlet jet of the flow tube the glass surrounding the inlet became hot, this created problems of definition of reaction temperature. The quartz discharge region was cooled by an internal air cooler since a cooled discharge gave a higher and more stable concentration of atoms

than when an uncooled discharge was used. A tesla coil was used to initiate the discharge.

The whole reaction tube was of U-tube design so that it could be immersed in a Dewar vessel. The Dewar vessel contained oil for experiments at or above room temperatures. Acetone-solid CO_2 mixtures were used to obtain temperatures in the range 196 - 240 K. A heating coil with a Variac and a thermometer was used in the oil to maintain the desired temperatures manually (298 - 500 K). For measurements at low temperatures an electronic platinum resistance thermometer was used to record the temperature, the temperatures were measured to $\pm$ 1 K. Reactor pressures during and between runs were measured by a silicone oil manometer. The reaction vessel and associated glass ware were washed with dilute phosphoric acid solution before assembly to reduce surface recombination.

2.3 The Discharge.

The dissociation of molecular gases in discharge is mainly due to the result of inelastic collisions between energetic electrons and molecules. The energy is supplied to the molecules by accelerating electrons under the influence of applied electric field. The high velocity electrons collide with molecules leading to dissociation either by excitation to an unstable electronic state or by a mechanism involving ions. Except in highly ionised plasmas, processes involving ions contribute little to the overall decomposition. The success of a discharge system in producing efficient and large amounts of dissociation thus depends on securing a large number of electron-molecule collisions in the discharge region. Oxygen[102-104] and hydrogen[2,3] have

traditionally been dissociated by the application of high voltages of either D.C. or A.C. between two large electrodes spaced about a metre or more apart in the low pressure gas. More recently, it has been found to be easier to dissociate these gases at low pressures using power of a higher frequency, such as radio frequency[105] and microwave power.[106] A review of the possible methods of producing free atoms in the gas phase has been given by Jennings[107] and by electrical discharge in particular by Shaw.[108]

Electrical discharges provide the most convenient method of producing a steady supply of atoms at relatively high concentration in a fast flow system. Low frequency electrode discharges have often been used but these suffer from the risk of contamination by electrode materials. Thus Linnett and Marsden,[109] have shown that, with O_2 at aluminum electrodes, aluminium oxide was entrained in the gas stream. This type of gross contamination undoubtedly has a pronounced effect on the rate of heterogeneous recombination of atoms in the system. Electrodeless radiofrequency discharges operation at few MHz do not, of course, give rise to contamination, but show a tendency to spread, and cannot be sustained at pressures above a few torr. It is also extremely difficult to screen sensitive electronic equipment satisfactorily from the effects of stray radiofrequency fields. A discharge operated at microwave frequencies suffers from none of these disadvantages, and was the method chosen for this work. Another advantage for this type of discharge is that microwave power can be coupled through a suitable glass without being significantly absorbed. To prevent stray light from the discharge reaching the reaction zone, a pair of woods horn light traps, coated with matt black paint were inserted between the discharge tube and the reaction vessel.

2.4 Flowmeters and Calibration.

The simple type of flowmeter consisted of a glass capillary tube which was attached by a cone and socket arrangement so that it could be readily removed or exchanged. The flow rates of gases passing through the capillaries were controlled by needle valves (Edwards) which were situated downstream from the flowmeters. The gas flows were measured with calibrated capillary flow-meters in which silicone oil was the manometric fluid. The calibration of flowmeters was accomplished in either of two distinct ways, which depend on the amount of gas passing through them.

For small flow rates, it is more accurate to calibrate the capillaries by measuring the rate of fall of pressure (-dp/dt) of a gas in a bulb of volume V and pressure p, for various valves of Δp, with the bulb situated upstream from the flowmeter. For small flow rates where the total change of p was small -dp/dt was obtained from a plot of p^{-1} against t and the flow rates calculated from the relation:

$$dm/dt = \frac{V}{RT} \frac{dp}{dt}$$

This equation is valid over a wide range of pressure, but for large flow rates deviations may be observed because of turbulence. Since large flow rates were used in the present experimental system, it was convenient to adopt the following procedure for calibration.

All flow gases were calibrated with a capillary flowmeter by passing directly to a gas meter (Alexander Wright and Co. Westminister Ltd.). The inlet of a gas meter was connected to a capillary flow meter and the outlet was connected to the flow line with a piece of rubber tubing. The meter was levelled by means of the levelling screws

in conjunction with spirit level. As soon as the gas passed through it, the gas meter indicator began to revolve. The time required for a given number of revolutions (one complete revolution = 250 cc) was measured. The flow rates in $cm^3\ min^{-1}$ were calculated corresponding to a pressure in the U-tube which recorded as cm of oil. Several such measurements were taken and the pressure was plotted against the flow rate ($cm^3\ min^{-1}$).

2.5 Purification System.

High purity gases (BOC) were used during all the experiments. All gases were passed through molecular sieve traps packed with finely divided silica gel or glass wool at 196 K or 77 K with pressures variable in the range 0 - 1 atmosphere. This prevented condensation while ensuring maximum residence times. Hydrogeneous impurities in the discharge gasses was reduced to < 1 ppm by a catalytic oxidation unit (Deoxo unit).

A rare gas purifier was also used in some cases which reduced impurities in commercial grades of rare gases to a level of less than 1 part in 10^7. It is most commonly used to purify argon or helium. The purification system consists of titanium granules at 973 K to remove nitrogen and oxygen, a copper oxide furnace to take out hydrocarbons, hydrogen and carbon monoxide and finally a molecular sieve to remove moisture and carbon dioxide.

The gases which were used in the experiments had the following purity levels according to the manufacturer:

High purity Ar $\geq$ 99.998%; He $\geq$ 99.9997%; $O_2 \geq$ 99.98%;

$CO_2 \geq$ 99.9996%; $N_2 \geq$ 99.9992%; $SO_2 \geq$ 98.98%.

2.6 Detection of O Atoms.

The chemiluminescence technique was used to monitor the decay of O atoms. This technique consisted of measuring intensities of the air afterglow emission spectrum which is produced by the indicator molecule, NO, which in turn is generated by dissociation of N_2 impurities in the discharge. Some pure NO was added to the reaction tube just before the detector during the study of reaction 2.1 to facilitate the detection of low concentrations of oxygen atoms. The reaction of atomic oxygen with nitric oxide is accompanied by a visible emission known as the air afterglow. The afterglow is a continuum extending from 388 nm into the infrared, with a maximum intensity at about 650 nm.[110] The emission results both from a bimolecular and a termolecular reaction.[111]

$$O + NO \longrightarrow NO_2 + h\nu$$

$$O + NO + M \longrightarrow NO_2 + M + h\nu$$

A concurrent non-radiative termolecular reaction also results in the loss of NO: $O + NO + M \longrightarrow NO_2 + M$. These reactions are relatively slow at the low pressures employed in discharge-flow systems and are followed by the very rapid reaction:

$$O + NO_2 \longrightarrow NO + O_2$$

If a very small amount of NO is added to a flowing gas containing atomic oxygen, the amount of atomic oxygen lost is negligible and there is no net loss of NO. Therefore, since the intensity of the chemiluminescence is proportional to the product of [NO] and [O], at constant [NO] the intensity is proportional to [O]. The decay of O-atoms caused by the introduction of O_2 or SO_2 was then determined by measuring

the relative intensity of emitted light with a photometer. A quantum photometer 9511 (Brookdeal Electronics Ltd.) with 5032 detector head was used for the purpose. The out-put of this instrument was monitored by a digital voltmeter. An RCA 931A photomultiplier with D.C. detection was also used in some earlier experiments to measure the light intensity.

The intensity of the afterglow may be calibrated by titration with NO_2, i.e. by measuring the amount of NO_2 required to consume all the atomic oxygen. This then permits absolute atom concentration to be calculated. The basic assumptions in the use of the NO chemiluminescence technique are that NO does not perturb the reacting system and that the concentration of NO remains constant. These assumptions could be invalid if were NO or NO_2 to react with other species, such as reaction products. This could result in a decrease in the NO concentration leading to a greater rate of decrease in the emission intensity, which in turn would lead to a rate constant that was too large. In the chemiluminescence technique, unlike resonance fluoresence, there is no need for the continuous illumination of the system to obtain a fluorescence signal and there is, therefore, no scattered light seen by the photodetector. This may lead to a greater ultimate sensitivity. A possible complication may arise if the reaction under study itself emits radiation and if these emissions are monitored by the photodetector, the apparent concentration of oxygen atoms would be in error. In the present investigation, no such visible light was observed when reactants were introduced into the reaction system, and a Wratten filter 61 was used in the detector to eliminate the unwanted light below 6000 Å.

2.7 The Quantum Photometer.

Photon counting by a quantum photometer is essentially a technique for measuring low levels of radiation. The systems of photon counting consist of five basic components, viz.: the photomultiplier, the photomultiplier anode load, a fast amplifier, a pulse height discriminator and a frequency meter. The basic advantages of this technique over the D.C. current measuring and analog lock-in techniques are:

(a) sensitivity to very low levels of radiation;

(b) improvement in the signal to noise ratio at low signal levels;

(c) direct digital processing of inherently discrete spectral information;

(d) drift-free long-term signal integration and reduced sensitivity to changes in voltage, temperature and photomultiplier gain;

(e) decrease of effective dark current from the photomultiplier.

A photomultiplier consists of a photoemissive cathode and a secondary emission multiplier which amplifies the signal before it leaves the tube. Photons falling on the photocathode cause the emission of photoelectrons with a probability, Q, the quantum efficiency. The photoelectrons are then accelerated through a potential gradient to the first dynode which causes the emission of secondary electrons. The multiplication factor for the first stage is normally in the range of 35-50 and for subsequent stages is of the order 3-6. A much higher multiplication factor for the first stage compared to later stages is desirable as the first stage has the greatest influence on the signal-to-noise ratio. The multiplication along the dynode chain results in an output signal which is a current pulse.

The photomultiplier tube is not an ideal detector because the tube itself emits pulses in the absence of light. This is known as the dark current, and arises from the following sources.

(i) Thermionic emission from the photocathode. With most photocathodes this type of emission represents the largest component of dark current. These pulses have a pulse height distribution almost identical to that of single photoelectrons. Thermionic emission is dependent on temperature, and one method of overcoming this is by cooling the photomultiplier tube.

(ii) Pulses from radioactive sources; these include photon pulses due to cosmic radioaction, known as Cerenkov photons. These pulses will have much larger amplitudes than single photoelectrons. In some photomultipliers pulses may result from radioactive emission from the ^{40}K isotope present in the glass.

(iii) Cold field emission; pulses arise from this source when the photomultiplier is operated at voltages higher than recommended.

(iv) Ohmic leakage gives rise to small unpulsed D.C. currents which are always present in photomultiplier tubes.

One great advantage of photon counting over the ~~analog~~ analogue techniques is the distinction which can be made between signal and noise pulses through pulse-height discrimination. The discriminator in the system is set such that only pulses with a larger amplitude than this fixed value are counted by the frequency meter. The discriminator level is low enough to include all the photon pulses. Thus each photon pulse, regardless of amplitude, is counted as one unit in the register.

Basically, there are two main sources of error in photon counting. Firstly, there is a condition known as pulse pile-up, which occurs at

very high levels of radiation. Pulse pile-up involves two or more pulses which are not resolved and hence are counted incorrectly. Secondly, at very low levels of radiation, e.g. 1 photon per minute, there will be a statistical error in the register when two low-amplitude background pulses arrive so closely together that they cannot be resolved. These will add together to form a resultant background pulse with an amplitude which exceeds the discrimination level, and hence is counted.

The 9511 Quantum photometer, used in this work, provides both photon counting and electrometer facilities in one instrument. In photon counting mode the 9511 gives both logarithmic and linear response in the range 10 - 10^6 cs^{-1}. In electrometer mode the 9511 gives a linear response from 10 nA-1 mA. The zero suppress is operative in both photon counting and electrometer modes. To bring the zero suppress into operation, the grey button marked ON was depressed. The variable ZERO SUPPRESS control was turned until the desired offset had been achieved; up to 10^3 cs^{-1} (photon counting) or 1 μA (electrometer) may be suppressed. Thus, the dark current signal can be eliminated in this instrument.

2.8 Surface Reactions.

Earlier workers[102, 112, 113] recognized the fact that wall reaction is an important factor in the study of recombination reaction in flow systems. Smallwood[112] observed that the surface reaction dominated the homogeneous reaction. To eliminate or minimize this problem, it is necessary to find experimental conditions under which the rate of the wall reaction is small compared with that of the homogeneous

reaction. Various kinds of surface poison have been recommended, usually they are substances containing sulphate or phosphate groups; metaphosphoric acid, orthophosphoric acid, a mixture of phosphorous pentoxide and orthophosphoric acid, sulphuric acid, potassium chloride and water vapour have all been used as surface poisons for preventing the recombination of atoms on glass. Phosphoric acid coatings are most commonly used and are put on in the form of a hot syrupy liquid which is cooled and degassed in a vacuum. These poisons reduce the amount of surface recombination of atoms. Even so, surface recombination remained an important factor in flow experiments and workers were obliged to take due consideration when estimating homogenous rate constants.

The work of Linnett *et al.* [109, 114-117] on the recombination of O atoms on glass surfaces, and several subsequent studies on various surfaces, showed that these reactions are first order. Several mechanisms for the first order recombination have been proposed, Johnson's[118] suggestion ~~observation~~ that atoms can be tightly packed on a glass surface without recombining, and Langmuir's [119] demonstration that surfaces are in general completely covered with a layer of ~~atoms~~ molecules, is strong evidence for a first order reaction in which a gas phase atom reacts with a surface atom. Linnett proposed a mechanism for recombination on glass or silica in which gas phase O-atoms recombine with loosely bound O-atoms from the SiO_2 surface and these are then rapidly replenished from the gas phase.

$$\text{Surface} - \underline{O} + O \longrightarrow \text{surface} + O_2$$

$$\text{Surface} - + O \xrightarrow{\text{fast}} \text{surface} - \underline{O}$$

where $\underline{O}$ represents loosely bound O atoms.

Surface recombination is usually measured in terms of surface recombination coefficient which may be expressed as follows:

$$\gamma = \frac{2r}{\bar{c}} \frac{k_w}{}$$

where γ is the fraction of total number of collisions with surface leading to recombination, r the radius of the tube, k_w the surface rate constant and $\bar{c}$ the mean kinetic velocity of atoms.

Kaufman's unpublished work shows that γ for vycor glass (96% SiO_2) increases less rapidly than those of Linnett et al. between temperature range 294 - 1073 K. The recombination coefficient often varies by a factor of five within the work of one laboratory, and by factors of 10 - 100 between different groups. Thus, for pyrex-glass, Kaufman[120] found $\gamma = 2 \times 10^{-5}$, Herron and Schiff[121] 7.7×10^{-5}, Harteck, Reeves and Mannella[122] estimated γ between 10^{-6} to 10^{-7} for Pyrex glass coated with orthophosphoric acid. In our system, the surfaces of the quartz discharge region and cylindrical flow tube were poisoned with syrupy phosphoric acid and pumped until the residual flow of volatile species was negligible in comparison with the total flow under typical experimental conditions. Experiments performed over a period of several years showed the wall loss to be small and easily controllable. Only infrequent recoating was required; the catalytic efficiency of the newly coated wall could be reduced through continued exposure to O/O_2 flows.

CHAPTER 3

GAS FLOW AND LIMITATIONS OF FLOW SYSTEM

Gas flow in vacuum systems can be divided into three distinct types: turbulent, viscous, and molecular. At high pressures and flow rates the flow is usually turbulent; as the pressure is reduced it merges into viscous flow; and finally at rather low pressures, it become molecular.

Turbulent flow is characterized by its complexity and lack of order; the gas swirls and eddies, and individual particles of the gas may have velocities and directions which are quite different from the average velocity and direction of the aggregate.

Viscous flow is much simpler than turbulent flow. It is smooth and orderly; every particle passing a point follows the same path as the preceeding particles that passed that point. The mean free path of the molecules is small compared to the dimensions of the tube during this type of flow, so that collisions between molecules will occur more frequently than collisions of molecules with tube walls. As a consequence, intermolecular collisions are predominant in determining the characteristics of flow, and flow rates will be affected by the viscosity of the gas.

Molecular flow is characterized by molecular collisions with the tube walls rather than with other gas molecules. As the pressure in the system is reduced, the mean free path of the gas molecules increases. The dependence of flow rate on viscosity begins to decrease because collisions between molecules are becoming less frequent. At pressures sufficiently low for the mean free path to be several times greater than the diameter of the containing vessel or tube, molecules migrate through a system freely and independently of each other.

It is clear from the above distinctions that turbulent flow and molecular flow are undesirable phenomena when kinetics is studied in a flow system. In gas phase reactions, the experimental conditions are most frequently those under which viscous flow occurs. The exact mathematical description of such flows becomes extremely complicated, however, if the effects of surface reactions, radial and axial diffusion, and the viscous flow are taken into account. In certain cases numerical analysis of the flow pattern have been made[123, 124] as in the case of second order volume recombination and first order surface recombination (neglecting the viscous pressure and axial diffusion). For simple interpretation, conditions are normally employed which give minimum viscous pressure drop, axial diffusion and wall reaction, and maximum radial diffusion. Such conditions are discussed in some detail by Kaufman[5] and a treatment essentially the same is given here. If these limitations are not taken into account the measured rate constants can be subject to serious systematic errors.

For laminar flow in the reaction tube, the viscous pressure drop can be calculated from the Poiseuille flow:

$$P_2^2 - P_1^2 = \frac{16FL\eta RT}{\pi r^4}$$

where F is the flow rate of gas, L the length of the reaction tube, r the tube radius and η the coefficient of viscosity. For small pressure differences, ΔP, the fractional change in pressure due to viscous flow is given by:

$$\Delta P/P = \frac{8\,\bar{v}\,L\eta}{r^2 P}$$

where $\bar{v}$ is the mean linear flow velocity. When P is expressed in mmHg, $\eta = 2 \times 10^{-4}$ g cm^{-1} s^{-1} for oxygen, the above expression may be written as:

$$\Delta P = \frac{1.2 \times 10^{-6}\ \bar{v} L}{r^2}$$

The most serious cases of pressure drop during experiments occurred in argon/oxygen mixtures, where for L = 48.8 cm, r = 1.25 cm and P = 3 mmHg, the pressure drop exceeds 1% if $\bar{v} > 800$ cm s^{-1}.

It thus seems that low flow rates are desirable because of the negligible pressure drop and rapid radial diffusion, but this may cause large axial concentration gradients and increased back diffusion. If radial convection and diffusion effects are neglected, the equation describing the flow assuming the first order decay of O atoms is,

$$\bar{v} \frac{dc}{dx} + kc - D \frac{d^2c}{dx^2} = 0$$

where D is the diffusion coefficient of O atoms into the gas, c is the concentration and x is the reaction distance. If the diffusion term is fairly small, the first order rate constant is given by

$$k = k'\left\{1 + \frac{k'D}{\bar{v}^2}\right\}$$

where k' is the observed, uncorrected rate constant, i.e.

$$k' = -\bar{v} \frac{d \ln c}{dx} = -\frac{d \ln c}{dt}$$

The condition for negligible back diffusion is therefore $Dk'/\bar{v}^2 \ll 1$.

The assumption of no radial concentration gradients is only valid if diffusion is sufficiently rapid to wipe out the gradients caused by viscous flow and surface recombination. For low flow rates, radial concentration gradients should be small if $r_o^2/4D \ll 2\, r_o/\gamma\bar{c}$ since then the diffusional process has the shortest relaxation time. Kaufman[5] has made an approximate estimate of concentration gradients assuming a parabolic radial velocity distribution. For first order volume

recombination, the stationary state equation for this case is:

$$v_o\left(1 - \left(\frac{r}{r_o}\right)^2\right) \frac{\delta[0]}{\delta x} + k\,[0] - D\left\{\frac{\delta^2[0]}{\delta x^2} + \frac{\delta^2[0]}{\delta r^2} + \frac{1}{r}\,\frac{\delta[0]}{\delta r}\right\} = 0 \qquad 21$$

where r is the radius of the reaction tube and v_o is the flow velocity at r = o. For the boundary conditions:

$$\frac{d(0]}{dr} = 0 \quad \text{at } r = 0, \text{ and } \frac{d[0]}{dr} = \frac{-k_s\, r[0]_s}{2D}$$

at $r = r_o$ (where 0_s is the concentration of 0 atoms at the surface) the solution takes the form

$$[0] = [0](r)\; e^{-\mu x} \text{ with } \mu = \left(\frac{k + k_s}{\bar{v}}\right)\left[1 - \frac{(k + k_s)\, D}{\bar{v}^2}\right]$$

for small D and radial variation [0](r). Integration of equation 21 then leads to an approximate radial concentration gradient given by

$$\frac{[0] - [0]_s}{[\bar{0}]} = \frac{r_o^2}{4D}\left[\mu\,\frac{\bar{v}}{2} + k_s\right] \approx \frac{r_o^2}{8D}\,(k + 3k_s)$$

where $[\bar{0}]$ is the mean radial concentration. For second order volume recombination k is replaced by $k_2[0]$. In the worst cases of radial gradients i.e. for high atomic concentrations and in argon carriers ($D \approx 1.0\ cm^2\ s^{-1}$ at 1 atmos.) at high pressures (5 mmHg), the concentration variation is between 1 and 2%, generally they were < 0.5%.

CHAPTER 4

KINETICS AND RATE MEASUREMENTS IN THE FLOW SYSTEM

4.1 Introduction.

This chapter is concerned with the mathematical form by which the kinetics of a reaction can be best discussed from a mechanistic and theoretical standpoint. The experimental data are records of concentrations of reactants or products at various times at constant temperature. On the other hand, theoretical expressions for reaction rates as functions of concentrations of reactants, and sometimes of products, are differential equations of the general form:

$$\frac{dc_1}{dt} = f(c_1, c_2, \ldots\ldots, c_n)$$

where, c is concentration of the particular product or reactant which is being followed to measure the rate of reaction. Before comparison of theory with experimental data, it is necessary either to integrate the rate equation or to differentiate the experimental concentration-time curve.

Many reactions can be explained in the form:

$$-\text{Rate} = k_R c_A^{\alpha} c_B^{\beta}$$

where k_R is the rate constant for the reactants A, B, ... For this type of expression α, β ..... are the orders of the reaction with respect to A, B, ...

In the present experimental system, when O_2 is added to a stream of O atoms in a carrier gas M, the possible reactions are:

$$O + \text{wall} \longrightarrow \tfrac{1}{2} O_2 + \text{wall} \qquad w$$

$$O + O_2 + M \longrightarrow O_3 + M \qquad 1.1$$

$$\left.\begin{aligned} O + NO + M &\longrightarrow NO_2 + M \\ O + NO_2 &\longrightarrow NO + O_2 \end{aligned}\right\} \qquad 12$$

$$O + O + M \longrightarrow O_2 + M \qquad 1.4$$

When the mixtures of inert gas-oxygen mixture contained less than 0.5% atoms, the rates of recombination were in accordance with the equation:

$$-d\,[O]/dt = k_w\,[O] + \sum_M k^M_{1.1}\,[O]\,[O_2]\,[M] + 2\,k_{12}\,[O]\,[NO]\,[M]$$

4.2 Adjustment of Experimental Conditions.

If the experimental conditions are suitably adjusted the kinetics of recombination can be dominated by any one of the terms in the rate equation, for example, the condition for kinetic domination by the second term is,

$$\frac{k_w + 2\,k_{12}\,[O]\,[NO]\,[M]}{\sum_M k^M_{1.1}\,[O]\,[O_2]\,[M]} \ll 1$$

This condition is approximately satisfied during the present recombination experiments by reducing γ by coating the walls of the reaction tube with phosphoric acid. The contribution by $2\,k_{12}\,[O]\,[NO]\,[M]$ is also negligible (see Chapter 2). In some experiments, however, γ was still too high to neglect surface recombination.

In most experiments the exact values of the rate constant were unknown and the required kinetic conditions had to be obtained by trial and error methods.

4.3 The Determination of Rate Constants.

Rate constants are most easily obtained from the integrated form of the rate equations. All of the possible reactions that might take place in the reaction system should be considered to develop an integrated rate equation.

Under the present experimental conditions, reaction 1.4 can be neglected since $k_{1.4}\ [O] \ll k_{1.1}\ [O_2]$. All the other reactions steps are first order in O atom concentrations. Therefore, the rate equation is,

$$\frac{-d\ [O]}{dt} = k_w\ [O] + k^M_{1.1}\ [O]\ [O_2]\ [M] + 2\ k_{12}\ [O]\ [NO]\ [M]$$

or,

$$\frac{-d\ \ln\ [O]}{dt} = k_w + k^M_{1.1}\ [O_2]\ [M] + 2\ k_{12}\ [NO]\ [M]$$

If at $t = 0$, $[O] = [O]^\circ$ and at $t = t$, $[O] = [O]^t$, then on integration the above equation becomes:

$$\frac{1}{t}\ \ln \frac{[O]^\circ}{[O]^t} = k_w + k^M_{1.1}\ [O_2]\ [M] + 2\ k_{12}\ [NO]\ [M] \qquad 14$$

The linear velocity of flow in the reaction tube is given by:

$$\bar{v} = \frac{\Sigma\ F_i\ RT}{\pi r^2\ P}$$

where $\Sigma\ F_i$ is the total flow rate (mol s^{-1}) of all gases i, r the radius of the tube and P the total pressure in the system.

If some point x, in the reaction tube is taken at t = o and some other point (x_2) corresponds to a reaction time t, then $t = \frac{\Delta x}{\bar{v}}$ where $\Delta x = (x_2 - x_1)$ is the reaction distance. Also the concentration of a species i in the reaction tube is given by:

$[i] = \frac{Fi}{\bar{v}\ \pi r^2}$ where $V = \bar{v}\ \pi r^2$ is the reaction volume swept out in 1 second.

Substituting $t = \frac{\Delta x}{\bar{v}}$, and $[i] = \frac{Fi}{V}$ for each gas in the mixtures, in equation 14 gives:

$$\frac{V^3}{V_R} \ln \frac{[0]^\circ}{[0]^t} = V^2 k_w + k^M_{1.1} F(O_2) F(M) + 2 k_{12} F(NO) F(M) \qquad 15$$

where $V_R = \Delta x \pi r^2$ is the reaction volume swept out in time t and F_i is the flow rate of species i. Equation 15 may be written in a more generalized way as,

$$\frac{V^3}{V_R} \ln \frac{[0]^\circ}{[0]^t} = V^2 k_w + \sum_M k^M_{1.1} F(O_2) F(M) + 2 \sum_M k^M_{12} F(NO) F(M)$$

Since [0] is proportional to intensity I (see Chapter 2) the equation therefore becomes:

$$\frac{V^3}{V_R} \ln I_1/I_2 = V^2 k_w + \sum_M k^M_{1.1} F(O_2) F(M) + k^{O_2}_{1.1} F(O_2)^2 +$$

$$2 \sum_M k^M_{12} F(NO) F(M) + 2 k^{O_2}_{12} F(NO) F(O_2) \qquad 16$$

A differential kinetic method is used to cope with the unwanted reaction taking place in the present investigation. The net rates of recombination are measured under two different sets of flow conditions and these are subtracted from each other. In this way the resultant net recombination can be made independent of reactions w and 12. This picture will be more clear from the decay diagram described in Fig. 4. The decay of 0 atoms is measured by a fixed detector (observation point). I_1 and I_2 are the measured intensities when 0_2 is introduced at position x_1 (inlet jet J5 and x_2 (inlet jet J1) respectively (Fig. 3). Similarly I^*_1 and I^*_2

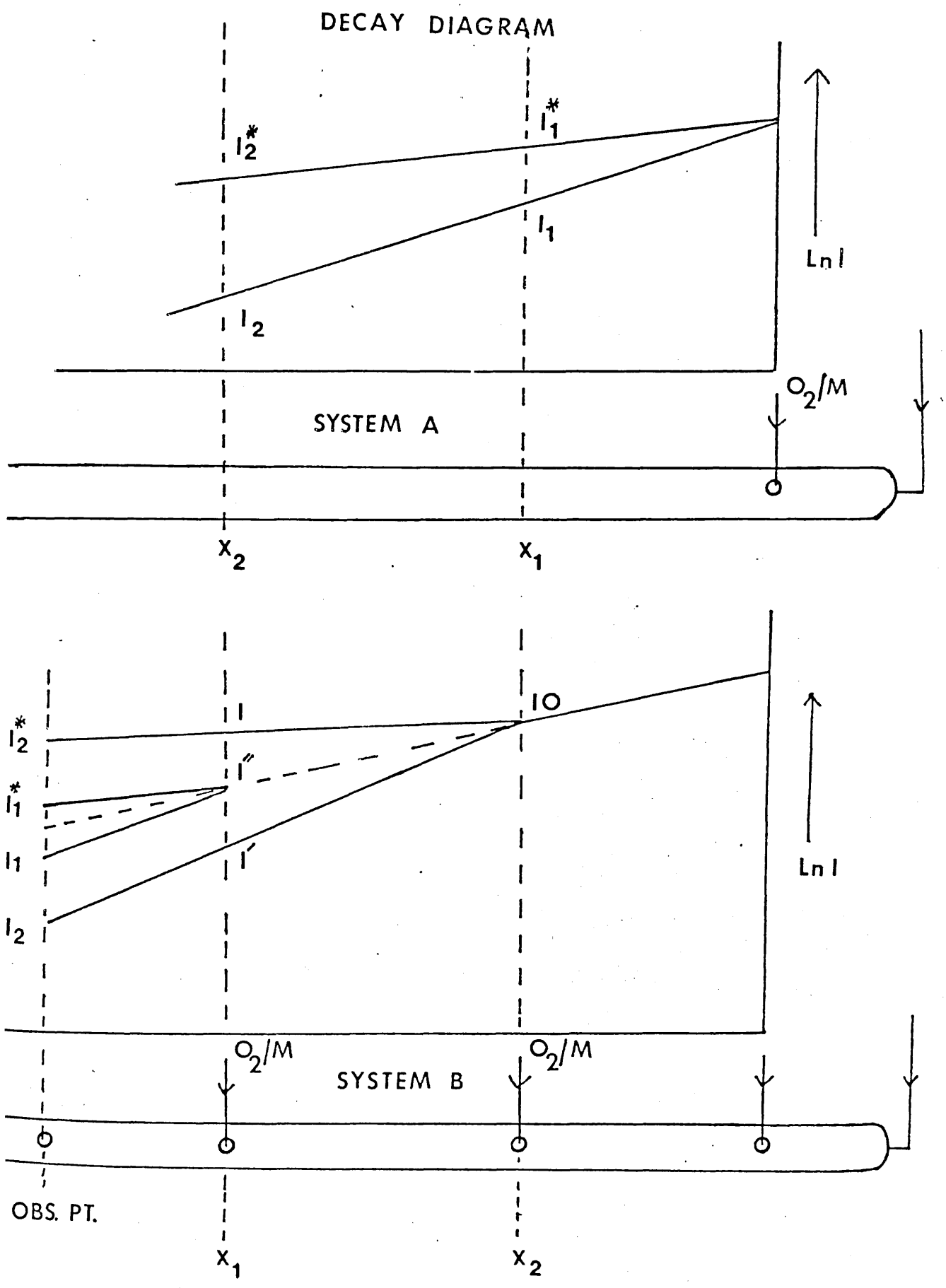
DECAY DIAGRAM
I_2^*
I_1^*
I_1
I_2
Ln I
O_2/M
SYSTEM A
X_2
X_1
I
IO
I''
I'
I_2^*
I_1^*
I_1
I_2
Ln I
O_2/M
O_2/M
SYSTEM B
OBS. PT.
X_1
X_2

FIGURE 4

are measured under the same conditions when an equivalent flow of inert gas, replacing oxygen, is introduced at positions x_1 and x_2 respectively. Since the pressure along the reaction tube is constant so that $V = V^*$, then it is necessary that:

$$F^*(M) + F^*(O_2) = F(M) + F(O_2)$$

In all experiments the flow of NO, F(NO), is maintained constant and hence this effects the kinetics to a negligible extent. Intensities I_1 and I_2 are measured for series of sets of flow conditions. If one set is made the reference set and indicated by an asterisk, then equation 16 can be written:

$$\frac{(V^*)^3}{V_R} \ln I_1^*/I_2^* = (V^*)^2 k_w^* + k_{1.1}^{O_2} F^*(O_2)^2 + k_{1.1}^{M'} F^*(O_2) F^*(M') + 2 k_{12}^{O_2} F^*(NO) F^*(O_2) + 2 k_{12}^{M'} F^*(NO) F^*(M') \quad 17a$$

For any other of the N sets, equation 16 becomes:

$$\frac{V^3}{V_R} \ln I_1/I_2 = V^2 k_w + k_{1.1}^{O_2} F(O_2)^2 + k_{1.1}^{M'} F(O_2) F(M') + 2 k_{12}^{O_2} F^*(NO) F(O_2) + 2 k_{12}^{M'} F^*(NO) F(M') \quad 17b$$

If equation 17a is subtracted from equation 17b the differential equation becomes:

$$\frac{V^3}{V_R} \ln I_1/I_2 - \frac{(V^*)^3}{V_R} \ln I_1^*/I_2^* = V^2 k_w - (V^*)^2 k_w^* + k_{1.1}^{O_2}\left\{[F(O_2)]^2 - [F^*(O_2)]^2\right\} + k_{1.1}^{M'}\left\{F(O_2) F(M') - F^*(O_2) F^*(M')\right\} + 2 k_{12}^{O_2} F^*(NO)\left\{F(O_2) - F^*(O_2)\right\} + 2 k_{12}^{M'} F^*(NO)\left\{F(M') - F^*(M')\right\}$$

Since $V^* = V$, $F^*(O_2) = 0$, and $F^*(NO) = F(NO)$, this equation becomes

$$\frac{V^3}{F(O_2)V_R} \ln\left(\frac{I_1 I_2^*}{I_2 I_1^*}\right) = \frac{V^2}{F(O_2)} (k_w - k_w^*) + k_{1.1}^{O_2} F(O_2) + \sum_{M'} k_{1.1}^{M'} F(M') + 2 F(NO)\left\{k_{12}^{O_2} - k_{12}^{M''}\right\} \quad 18$$

where M'' is the reference gas.

The rate constant is determined from a plot of $\frac{V^3}{F(O_2) V_R} \ln \frac{I_1 I_2^*}{I_2 I_1^*}$ against $F(O_2)$.

The rate constant $k_{1.1}^{M'}$ as third body is determined from a plot of $\frac{V^3}{V_R F(O_2)} \ln \frac{I_1 I_2^*}{I_2 I_1^*}$ against $F(M')$

4.4 Derivation of Surface Rate Equation for k_w^* in Flow System.

Assuming constant pressure along the reaction tube, the oxygen atom decay diagram in flow system B is shown in Fig. 4.

The equation for gas flowing downstream J_1 - J5 is

$$\frac{V^3}{V_R} \ln \frac{IO}{I} = V^2 k_w^* + 2 F(NO) \sum_M k_{12}^M F(M) \quad 19a$$

and the equation for upstream flow from J_1 - J5:

$$\frac{V_u^3}{V_R} \ln \frac{IO}{I''} = V_u^2 k_w^* + 2 F(NO) \sum_M^u k_{12}^M F(M) \quad 19b$$

where $V_u = \bar{v}_u \pi r^2$ for flow upstream from inlet jets J_1 - J5

$V = \bar{v} \pi r^2$ for flow downstream from inlet jets J_1 - J5

$\Delta V = (V - V_u)$

subtracting 19b - 19a gives:

$$\frac{1}{V_R} \ln \frac{I}{I''} = \frac{1}{V_R} \ln \frac{I_2^*}{I_1^*} = k_w^* \left(\frac{1}{V_u} - \frac{1}{V} \right)$$

$$+ 2 F (NO) \left[\sum_M^u \frac{k^M_{12} F (M)}{V_u^3} - \sum_M \frac{k^M_{12} F (M)}{V^3} \right]$$

This may be rewritten:

$$\frac{V}{V_R} \ln I_2^*/I_1^* = k_w^* \left(\frac{V}{V_u} - 1 \right)$$

$$+ 2 F (NO) k^{Ar}_{12} \left[\frac{V}{V_u^3} \sum_M^u x^M_{12} F (M) - \sum_M \frac{x^M_{12} F (M)}{V^2} \right]$$

where $x^M_{12} = k^M_{12}/k^{Ar}_{12}$

Hence:

$$\frac{V}{V_R} \ln I_2^*/I_1^* = k_w^* \frac{\Delta V}{V_u} +$$

$$2F (NO) k^{Ar}_{12} \frac{1}{V^2} \left[\left(\frac{V}{V_u} \right)^3 \sum_M^u x^M_{12} F (M) - \sum_M x^M_{12} F (M) \right]$$

which on rearranging becomes

$$\frac{V_u V}{\Delta V V_R} \ln I_2^*/I_1^* = k_w^* +$$

$$2 F (NO) k^{Ar}_{12} \frac{V_u}{\Delta V} \frac{1}{V^2} \left[\left(\frac{V}{V_u} \right)^3 \sum_M^u x^M_{12} F (M) - \sum_M x^M_{12} F (M) \right] \quad 20$$

since $\frac{V}{V_u} = \frac{\sum_M^u F (M)}{\sum_M F (M)}$, $\Delta V = (V - V_u)$

it follows that $\frac{\Delta V}{V_u} = \frac{\sum_{M}^{d} F(M)}{\sum_{M}^{u} F(M)}$

where $\sum_{M}^{d} F(M)$ is sum over all gasses not added of upstream from J_1 - J5. Equation 20 was used to calculate k_w^* since the of graph of

$$\frac{V_u}{\Delta V}\frac{V}{V_R} \ln I_2^*/I_1^* \text{ against } \frac{1}{V2}\frac{V_u}{\Delta V}\left[\left(\frac{V}{V_u}\right)^3 \sum_{M}^{u} x^M_{12} F(M) - \sum_{M} x^M_{12} F(M)\right]$$

gave k_w^* as intercept and 2 F (NO) k^{Ar}_{12} as slope.

4.5 The reliability of rate constant measurements.

Despite the most stringent precautions to eliminate and reduce errors, however good the design of the experiment, experimental errors will always remain in determination of experimental values of the rate constant. The reliability of such values can be assessed in a quantitative manner by estimating the total errors associated with them. Two types of errors are usually associated with an observation mainly systematic and random errors. Systematic errors which cause all results to be incorrect by approximately the same amount in the same direction. Random errors are those whose magnitude can vary in a random fashion.

The precision or reproducibility of a measurement depends upon the random errors involved, whereas the accuracy depends on the systematic errors or the deviation of a weighed mean of results from a defined "true" value.

In general if the quantity y is a function of n variables, x_1, x_2, ... i.e. $y = f(x_1, x_2, \ldots x_n)$ then $dy = \left(\frac{\delta y}{\delta x_1}\right)_{x_2, x_3 \ldots} dx_1 + \left(\frac{\delta y}{\delta x_2}\right)_{x_1, x_3 \ldots} dx_2 \ldots\ldots$

and small errors in y are given by

$$\Delta y = \left(\frac{\delta y}{\delta x_1}\right)_{x_2,\, x_3 \ldots} \Delta x_1 + \left(\frac{\delta y}{\delta x_2}\right)_{x_1,\, x_3 \ldots} \Delta x_2 \qquad 21$$

If it is assumed that the errors made in measuring each of the quantities x_1, x_2, ... etc are independent of each other then the expected resultant error in y is given by[125] the sum of the independent component vectors, i.e.

$$(\Delta y)^2 = \left(\frac{\delta y}{\delta x_1}\right)^2_{x_2,\, x_3 \ldots} \Delta x_1^2 + \left(\frac{\delta y}{\delta x_2}\right)^2_{x_1,\, x_2 \ldots} \Delta x_2^2$$

For systematic errors it is more convenient to consider the relative errors $\Delta y/y$, $\Delta x/x$ etc rather than the absolute error in each variable. If each term is divided by y^2 and then by multiplying and dividing each term by the square of the independent variable this equation becomes:

$$\left(\frac{\Delta y}{y}\right)^2 = \left(\frac{x_1\, \delta y}{y\, \delta x_1}\right)^2_{x_2,\, x_3 \ldots} \left(\frac{\Delta x_1}{x_1}\right)^2 + \left(\frac{x_2}{y}\, \frac{\delta y}{\delta x_2}\right)^2_{x_1,\, x_3 \ldots} \left(\frac{\Delta x_2}{x_2}\right)^2 \ldots$$

$$= \left(\frac{\delta \ln y}{\delta \ln x_1}\right)^2_{x_2,\, x_3 \ldots} \left(\frac{\Delta x_1}{x_1}\right)^2 + \left(\frac{\delta \ln y}{\delta \ln x_2}\right)_{x_1,\, x_3 \ldots} \left(\frac{\Delta x_2}{x_2}\right)^2 \qquad 22$$

The total error in the rate measurements obtained in the present work was estimated by estimating all the random and systematic errors associated with each of the measurements and applying equations 21 and 22.

The estimated systematic and random errors in each of the individual measurements are:

(a) Reaction distance. The position of the inlet jet in the reaction tube was measured with a standard metre rule to $\pm$ 0.5 mm. The total error associated with the measurement of reaction distances was estimated to be: $dx/_x = 0.05\ (x/_{cm})$

(b) Pressure: The total expected error in the pressure readings was estimated to be: $dp/_{p} = 0.05/_{12.7}$ (P/cm Hg)

(c) Temperature: The temperature of the reaction tube was kept to within $\pm$ 1 K by a Dewar flask containing either heated oil or acetone-solid mixtures. Estimated total errors $dT/_{T}$ were $< 5 \times 10^{-3}$.

(d) Radius of the reaction tubes. The volume of a measured length of the tubes was determined, and the radius estimated to within 1%.

There is also possibility of systematic errors arising from secondary recombination reactions or from the effects of diffusion and viscous flow. The former type of errors were avoided as far as possible by suitably adjusting the experimental conditions (page 56). The effects of diffusion and viscous contributed a total error of not more than 10% to the measured rate constant. The total error estimated in the rate constant was found to be about 15%. This can be compared with the 15% - 25% error reported by Kaufman and Kelso[71] for reaction 1.1.

CHAPTER 5

A STUDY OF THE REACTION $O + O_2 + M \longrightarrow O_3 + M$

5.1 Introduction.

The work described in this chapter consists of measurements of the rate of the reaction:

$$O + O_2 + M \longrightarrow O_3 + M \qquad 1.1$$

at temperatures between 196-500K. Rates of recombination were measured for three different third bodies, viz: M = O_2, Ar, CO_2 and He. The results of these experiments showed that there was no significant recombination by the reaction

$$O + O + M \longrightarrow O_2 + M \qquad 1.4$$

at the highest atomic concentrations used (0.5%). The rates of recombination were always found from equation 18.

The work described is a continuation of the earlier flow experiments made in this department (Ball[85]) but now using the improved flow technique and the controlled flow conditions. This enabled a more direct determination of recombination rate to be made.

Before presentation and discussion of experimental results, it is appropriate to describe and discuss the common procedures adopted in all of the measurements.

5.2 Experimental Procedure.

Measurements of the rate of recombination can be in error if there is a leak in the system. Atmospheric gases usually find their way into the system through such a leak and these interfere with the reaction under investigation. This interference is more prominent if there are some reactive atoms in the system. During this work many such problems

arose from leaks in the apparatus. A leak-free system is, therefore, essential in order to achieve reproducibility and reliability of the results. The whole flow system was evacuated to about 10^{-2} - 10^{-3} torr before testing for leaks. The whole flow line was checked very carefully with a tesla coil to ascertain whether there was any leak. When the discharge from the tesla coil was applied to a fracture or site of a leak, there was a bright white light from that point. Another way of checking the leak was to close the whole system by turning off the stainless steel stopcock and observing the pressure in the system; a steady pressure indicated a leak-free system. A leak detected in the apparatus was remedied either by glass-blowing or by a leak sealant spray, MS silicone vacuum leak sealant was used to seal leaks at metal joints. The leak sealant dries at room temperature to give a tough, flexible, non-melting film which retains its properties from sub-zero temperatures to 523K. Before applying the sealant, any dust or dirt from the area of the leak was removed and the area cleaned with solvent to remove oil and grease.

The surface of the pyrex reaction tube was poisoned with syrupy phosphoric acid (2.8). The photomultiplier was fittend perpendicularly to the reaction tube and the glass surface nearby was blackened with matte black paint. Black cloth was also used to cover the detector since this prevented stray light from the room falling on the detector. The quantum photometer 9511 was set for operation at the required line voltage (240V) and connected to the HV Discriminator input (9511)/Discriminator output (5032). The instrument was connected to the line supply and the power button switched on. The HV and linear

photon counting buttons were depressed and the voltage on the tube was checked. This voltage was displayed (in kV) on the bottom scale of the panel meter. The above procedure was also repeated by depressing electrometer button. Adjustments to the HV were made using the rear mounted 10-turn adjustable potentiometers. Mode selection was made by depressing the appropriate front panel button. The appropriate sensitivity scale was selected by means of the range switch, calibrated in 1, 3, and 10 steps. The zero suppress control was switched on by depressing the front panel ON push button. For measurements of small changes in signal level, the zero suppress control may be used to suppress the output upto 10^3 Hz for photon counting mode. In the electrometer mode, the zero suppress provides offset up to 1μA.

Argon, at a flowrate of 173.61 μ mol s^{-1}, in presence of traces of O_2 (less than 5 p.p.m.) was passed through the discharge. The purification of the gases is one of the most important factors in obtaining reliable data. Earlier workers[66] observed that a small trace of hydrogen or water vapour in the discharge can initiate a series of chain reactions. The decay of O atoms in the presence of these impurities would invalidate the present investigations. For these reasons, the gases were purified very carefully. Hydrogeneous impurities in the mixtures of argon and oxygen were reduced to < 1 p.p.m. by a catalytic oxidation unit (deoxo unit). In addition the gases were passed through molecular sieve traps at 77K. Similar molecular sieve traps were also placed in the flow line of inlet and third body inlet jets. Oxygen was purified by passing through a molecular sieve trap at 196K. The pressure in these traps was usually varied from 0 - 1 atmosphere. This prevented condensation while ensuring maximum residence time.

The Microton-200 generator was connected to the mains and to the discharge cavity. The generator took about five minutes to warm up; the green light button, POWER ON, in the generator was then pressed on and the discharge in the cavity was initiated by a testa coil. A luminous glow was observed in the discharge region, this was undoubtedly due to recombination of oppositely charged ions. Two screw controls in the cavity were adjusted to utilize the maximum amount of incident energy. This was confirmed by a minimum deflection of the reflected power indicator (by pressing on the reflected power button). The discharge cavity was kept cold by passing compressed air across it, stable and higher atom concentrations can only be achieved if the discharge is cold. The production of 0 atoms increased slowly and this was followed from the digital voltmeter. A visible grey-green afterglow also showed the existence of 0 atoms in the flow tube. 0 atom production was controlled either by: (a) varying the flow of molecular oxygen in the discharge gas, or (b) varying the microwave power in the discharge. It took about one hour to achieve a stable concentration of atoms at the required level. It was important to ensure that the intensity signal was stable before proceeding further with the experiment.

Let us consider the table associated with Fig. 5 to describe a typical run. F_1 and F_3 are the flow rates of oxygen in $cm^3\ min^{-1}$ admitted through the inlet jets. F_2 is the flow rate of argon through the discharge which was kept constant at 200 $cm^3\ min^{-1}$ in all successive measurements. When all the requirements for flow experiments had been established, 50 $cm^3\ min^{-1}$ of molecular oxygen was admitted through the inlet jet J_5 (Fig. 3) and the pressure in the reaction tube was adjusted

to 3.215 cm of silicone oil so that the flow velocity can be maintained at about 206.6 cm s^{-1}. The intensity signal I_1 i.e. 16.8 due to the decay of 0 atoms from inlet jet J5 to the observation point B was recorded. The intensity was measured at point B by a Quantum photometer (see 2.6 and 2.7). The flow of oxygen was then diverted through the inlet jet J2 and the inlet J5 was closed, the intensity I_2 i.e. 12.6 detected at point B was recorded at the identical pressure. The intensity I_2 here is due to the decay of 0 atoms from inlet jet J2 to observation point B. The distance between J5-J2 is 48.8 cm which is denoted by D on the top of the table associated with Fig. 5. For a distance of 48.8 cm, the intensity due to 0 atoms decreased from 16.8 to 12.6. The flow rate of oxygen was changed to 70 cm^3 min^{-1} and the flow velocity in the reaction tube was increased to 247.4 cm s^{-1} by adjusting the pressure in the silicone oil marometer. Intensities I_1 and I_2, both detected at point B, were noted. Similarly, successive variations of 0_2 up to 150 cm^3 min^{-1} at inlet jets J_5 and J_2 were made and the respective I_1 and I_2 signals were noted.

The reference measurements were accomplished in the same way as above, the only difference was that argon was passed through J5 and J_2 in place of oxygen. The oxygen flow in the flow line was shut off and replaced by flow of argon. Accordingly, Fl and F_3 are now the flow rates of argon through the inlet jets and F_2 (200 cm min^{-1}) is the flow rate of argon through the discharge. 50 cm^3 min^{-1} of argon was passed through inlet jet J_5. The pressure was adjusted to 3.215 cm of silicone oil to achieve a flow velocity of 206.6 cm s^{-1}. Intensity signal I01 (i.e. I_1^*) was measured at point B. Similarly IO_2 (i.e. I_2^*) was noted

when the same flow of argon was diverted through jet J2. Successive measurements of I01 and IO_2 were recorded by varying the flow rate of argon up to 150 cm^3 min^{-1} while the flow rate of argon through the discharge was kept constant. The pressure was also adjusted in each case to that shown in Table 5 associated with Fig. 5.

In table associated with Fig. 11, F_1 is the flow rate of oxygen, (F_2-F_3) is the flow rate of argon through the discharge and F_3 is the flow rate of third body M. I_1 and I_2, I01 and I02 were measured adopting the same procedure as above.

The data obtained in this way for I_1, I_2, I01 and I02 was inserted in equation 18 to calculate the various values of the term $\frac{V^3}{F(O_2)V_R} \ln\left[\frac{I_1\ 10_2}{I_2\ I01}\right]$ which was plotted against the flow rate (F_3) of the third body M. The rate constant $k^M_{1.1}$ was calculated from the slope of the straight line. The values of $(k_w - k^*_w)$ were found from intercepts. Similarly, the plot of the terms on the L.H.S of equation 20 against $\frac{V_u}{\Delta V}\ \frac{1}{V2}\left[\left(\frac{V}{Vu}\right)^3 \sum_M^u x^M_{12}\ F\ (M) - \sum_M x^M_{12}\ F(M)\right]$ gave the value of the k^*_w from the intercept and 2F (NO) k^{Ar}_{12} from the slope.

5.3 Experimental Results for the Reaction:

$$0 + O_2 + M \longrightarrow O_3 + M$$

The system used to measure the rates of this reaction was similar to that described in chapter 2. The first experiments were conducted with a cylinder of ordinary grade argon. This was purified from hydrogen by passing through a "deoxo" unit and then dried by passing through molecular sieve traps at 77K. Experimental flow rates for argon ranged from 150-200 μ mol s^{-1}, but in most cases, a constant flow

of 173.6 μ mol s^{-1} was passed through the discharge. Molecular oxygen (at a flow rate in the range 20.8-104.2 μ mol s^{-1}) was introduced into the reaction system through the inlet jet. Approximately 30 watts of microwave power was coupled into the argon-oxygen mixture passing through the discharge tube.

On the first occasion when the discharge was switched on, atoms could scarcely be detected by observation at point B (Fig. 3) situated at about 120 cm from the discharge. When the microwave power was increased slowly, the atomic concentration began to rise. The observations indicated that there was either a very small amount of dissociation or a serious loss of atoms on the walls of the reaction tube. In this case the former possibility was suspected and the power in the discharge was increased. This procedure raised the atomic concentrations some 5 to 10 times and enabled atomic concentration profiles to be measured.

A series of experiments were made in which relative atomic concentrations at two positions along the reaction tube were measured. Similarly, reference measurements were made by replacing molecular oxygen by an equivalent flow of argon. These initial experimental "runs" were in general far from reproducible. Some adjustment of the flow conditions was then made whereby $\frac{V^2}{F(O_2)}$ was kept constant. The ordinary argon was also replaced by high purity argon. Experiments made after this adjustment were now more reproducible. During the course of this work some 18 experimental runs were made at temperatures between 196 and 500K. The lower temperatures were obtained with acetone-solid CO_2 mixtures and were achieved and controlled by the following way.

The required temperatures in the Dewar flask was regulated by a lauda ultra thermostat which is maintained by an electronic temperature controller. The thermostat has both inlet and outlet tubes by which

fluid can be circulated quickly to the Dewar and back to the thermostat. This enabled temperature equilibrium in both the Dewar and thermostat to be established rapidly. The temperature in the thermostat is monitored by a thermocouple which is connected to the electronic controller. The required temperature was set on the controller. If the temperature in the Dewar flask was higher than that set on the scale, then cooling occurred automatically to achieve the required temperature. Some pieces of solid CO_2 were put in the Dewar flask containing solid CO_2-acetone mixture until the temperature dropped below the temperature set on the scale when this happened the cooling ceased (i.e. light switched off) and heating started automatically. Again, when the Dewar flask warmed up slowly and cooling light came on, a few pieces of solid CO_2 were added. It was more convenient to control the temperature by putting the thermocouple in the Dewar without using the thermostat. Higher temperatures were obtained with an oil bath. A heating coil connected to a variac was used for heating purpose. The desired temperature was controlled manually and maintained by changing the resistance in the variac until the temperature is within $\pm$ 1K. A mercury thermometer was used to note the temperature in the Dewar.

Typical graphs of $\frac{V^3}{v_R F(0_2)} - \ln\left[\frac{I_1\ I02}{I_2\ I01}\right]$ against $F(0_2)$ are shown in Figs. 5-9 at temperatures in the range 196-500K. The plots are reasonably straight line and this suggests that recombination by reaction 1.1 is dominant in the system. The rate constants $k_{1.1}^{0_2}$ for 0_2 as third body were obtained from the slopes and the rate constants $k_{1.1}^{Ar}$ and $(k_w - k_w^*)$ were calculated from the intercepts. The data I01 and I02 in tables associated with Figs. 5-9 were put in equation 20 to obtain the values of k_w^*. One of the typical plots is shown in

Figs. 5-9

Graphs of $\frac{V^3}{V_R\ F(0_2)}\ \ln\frac{I_1\ I_2^*}{I_2\ I_1^*}$ represented by Y

against $F(0_2)$ represented by X (equation 18) for the reaction

$$0 + 0_2 + 0_2 = 0_3 + 0_2 \qquad 1.1$$

In the tabulated data at the head of each graph:

T is the temperature (K);

D the distance (cm);

F_1 the flow rate of oxygen ($cm^3\ min^{-1}$);

F_2 the flow rate of argon ($cm^3\ min^{-1}$);

F_3 the flow rate of oxygen ($cm^3\ min^{-1}$);

I01 (computer notation for I_1^*) the intensity when argon was passed through jet J5;

I_1 the intensity when molecular oxygen was passed through jet J5;

I02 (computer notation for I_2^*) the intensity when argon was passed through jet J2;

I_2 the intensity when molecular oxygen was passed through jet J2;

VBAR is the flow velocity ($cm\ s^{-1}$);

P the pressure (cm-oil).

Fig. 5. $M = 0_2$, T = 196K

Fig. 6. $M = 0_2$, T = 246K

Fig. 7. $M = 0_2$, T = 295K

Fig. 8. $M = 0_2$, T = 400K

Fig. 9 $M = 0_2$, T = 500K

Fig.5

T	D
185.0	48.8

F1	F2	F3	I01	I1	I02	I2	P
50.0	250.0	50.0	13.6	16.8	19.4	12.6	3.215
70.0	250.0	70.0	18.7	22.1	26.1	17.2	2.663
90.0	250.0	90.0	19.9	20.9	29.0	16.0	2.731
110.0	250.0	110.0	20.7	18.5	28.8	14.3	2.595
130.0	250.0	130.0	20.1	17.8	28.4	13.5	2.510
150.0	250.0	150.0	18.8	16.4	26.8	12.4	2.468

VALUES OF Y= .8008E+11 .8931E+11 .1000E+12 .1094E+12 .1273E+12 .1380E+12

VALUES OF X== .3440E-04 .4816E-04 .6182E-04 .7568E-04 .8944E-04 .1032E-03

VALUES OF VBAR= .2066E+03 .2474E+03 .2756E+03 .3071E+03 .3352E+03 .3588E+03

SLOPE= .8570E+15

STANDARD DEVIATION= .4645E+14

INTERCEPT= .4838E+11

STANDARD DEVIATION= .3377E+10

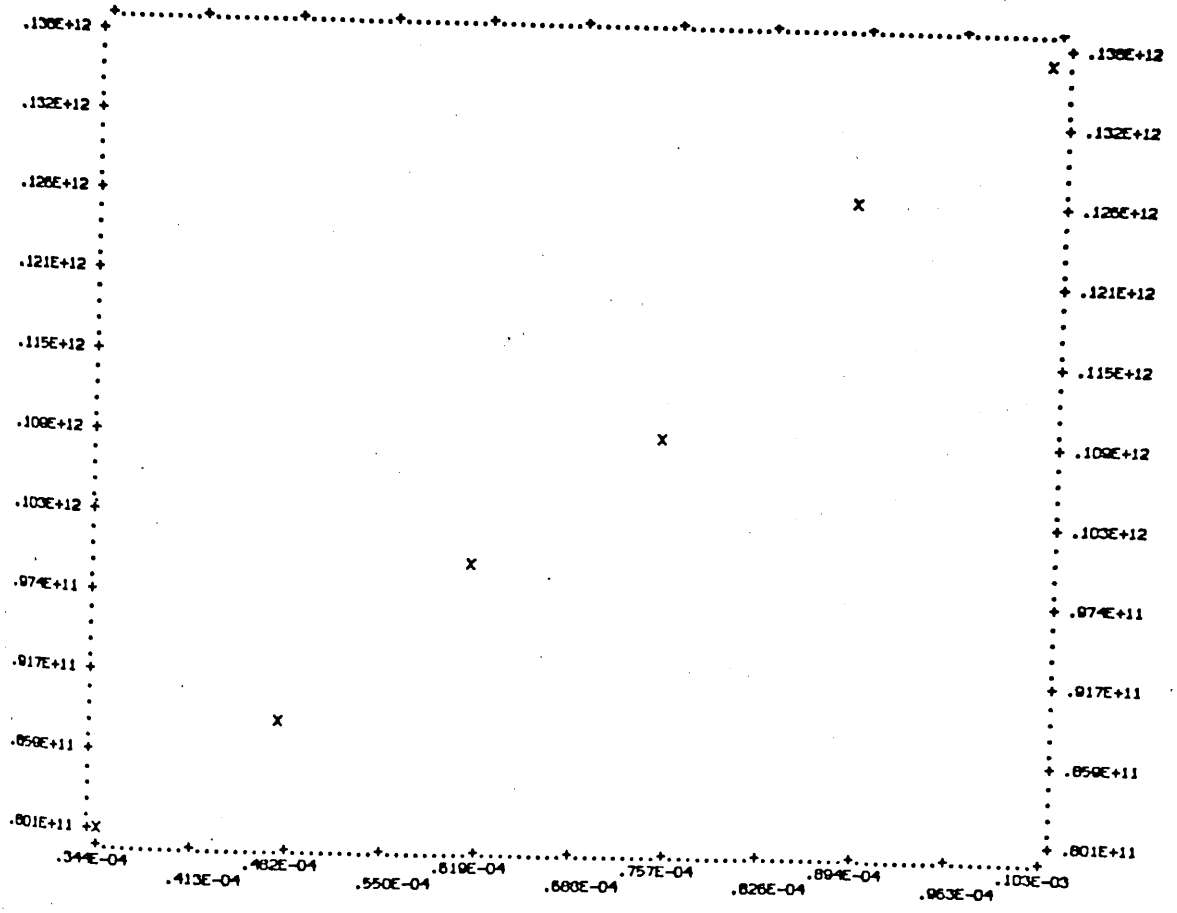

Fig. 6

T	D
246.0	48.8

F1	F2	F3	I01	I1	I02	I2	P
50.0	250.0	50.0	12.8	15.6	18.4	12.2	4.050
70.0	250.0	70.0	14.6	17.6	19.0	14.6	3.700
90.0	250.0	90.0	15.4	16.3	19.9	13.7	3.500
110.0	250.0	110.0	15.4	14.9	18.7	12.8	3.300
130.0	250.0	130.0	14.8	14.0	18.0	11.8	3.200
150.0	250.0	150.0	14.3	13.3	18.2	11.3	3.100

VALUES OF Y= .6055E+11 .6307E+11 .6562E+11 .7404E+11 .8214E+11 .8772E+11

VALUES OF X= .3440E-04 .4816E-04 .6192E-04 .7568E-04 .8944E-04 .1032E-03

VALUES OF VBAR= .2055E+03 .2402E+03 .2660E+03 .3031E+03 .3300E+03 .3585E+03

SLOPE= .4184E+15

STANDARD DEVIATION= .4388E+14

INTERCEPT= .4341E+11

STANDARD DEVIATION= .3190E+10

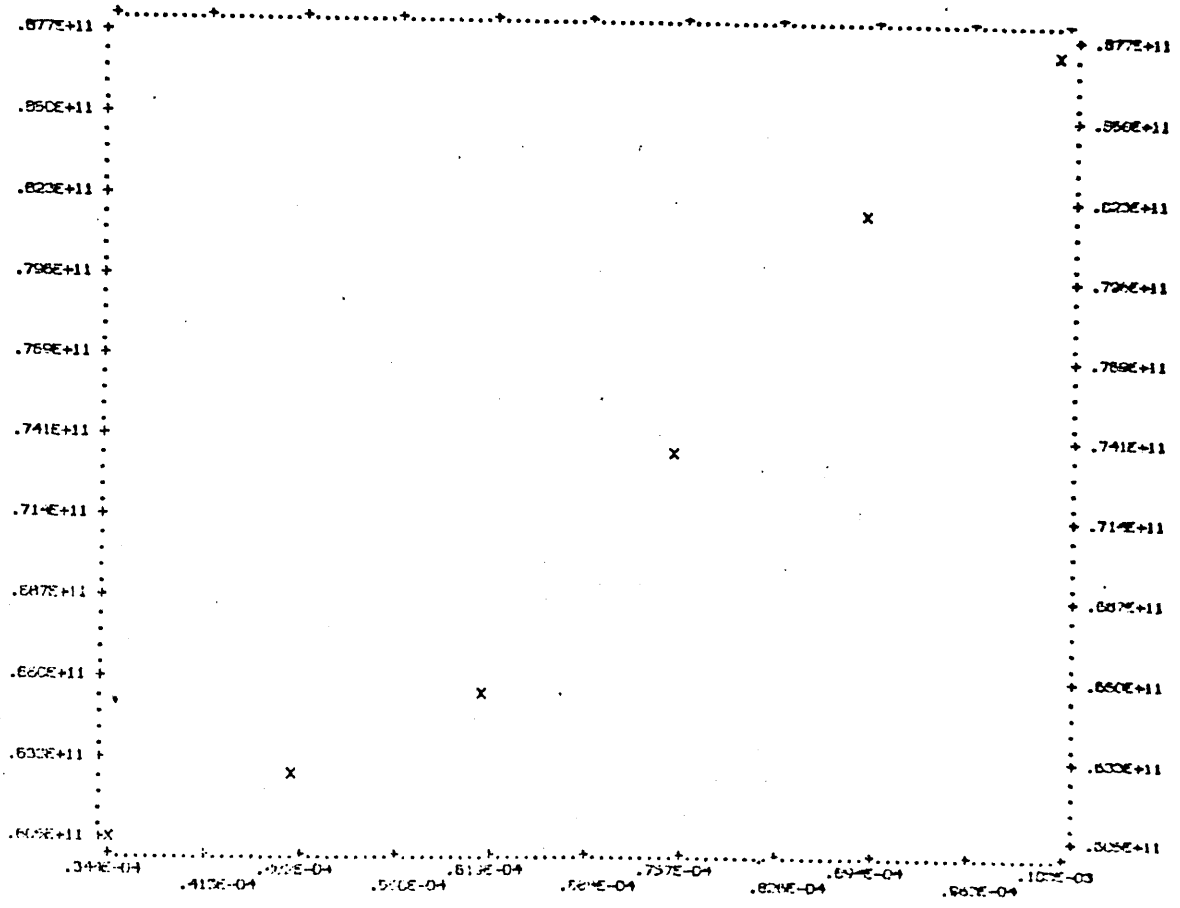

Fig.7

T	D
297.0	64.4

F1	F2	F3	I01	I1	I02	I2	P
30.0	200.0	30.0	9.9	16.5	12.1	10.1	5.713
50.0	200.0	50.0	12.1	28.7	14.5	20.0	4.687
70.0	200.0	70.0	13.5	34.3	15.7	24.3	4.418
90.0	200.0	90.0	11.9	37.1	14.2	27.2	4.186
110.0	200.0	110.0	10.7	37.6	12.9	27.9	4.074
130.0	200.0	130.0	9.7	38.9	11.8	28.9	3.980
150.0	200.0	150.0	8.7	38.7	10.6	28.7	3.861

VALUES OF Y= .3040E+11 .2933E+11 .3266E+11 .3637E+11 .3929E+11 .4370E+11 .4615E+11

VALUES OF X== .2064E-04 .3440E-04 .4816E-04 .6192E-04 .7568E-04 .6944E-04 .1032E-03

VALUES OF VBAR= .1351E+03 .1716E+03 .2050E+03 .2324E+03 .2553E+03 .2782E+03 .2964E+03

SLOPE= .2144E+15

STANDARD DEVIATION= .2081E+14

INTERCEPT= .2357E+11

STANDARD DEVIATION= .1410E+10

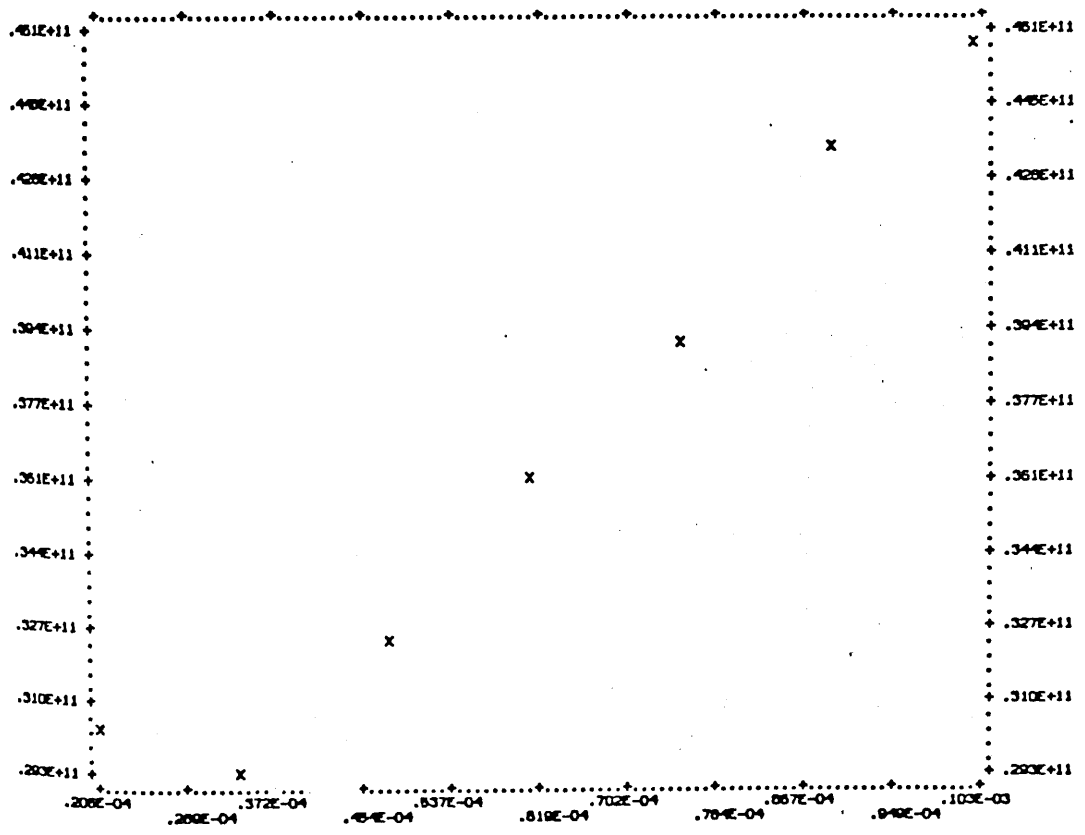

Fig. 8

T	D
400.0	64.4

F1	F2	F3	I01	I1	I02	I2	P
30.0	200.0	30.0	18.7	15.0	20.7	12.8	7.683
50.0	200.0	50.0	35.5	30.3	43.5	26.1	6.548
70.0	200.0	70.0	41.3	38.5	50.1	33.8	5.944
90.0	200.0	90.0	41.3	40.7	49.5	36.0	5.621
110.0	200.0	110.0	37.1	41.7	45.1	36.4	5.496
130.0	200.0	130.0	35.7	42.3	43.1	37.8	5.345
150.0	200.0	150.0	31.5	45.7	38.7	40.3	5.276

VALUES OF Y= .1642E+11 .1837E+11 .2177E+11 .2289E+11 .2668E+11 .2689E+11 .3186E+11

VALUES OF X== .2064E-04 .3440E-04 .4816E-04 .6192E-04 .7568E-04 .8944E-04 .1032E-03

VALUES OF VBAR= .1351E+03 .1725E+03 .2052E+03 .2331E+03 .2548E+03 .2789E+03 .2997E+03

SLOPE= .1720E+15

STANDARD DEVIATION= .1363E+14

INTERCEPT= .1304E+11

STANDARD DEVIATION= .8238E+09

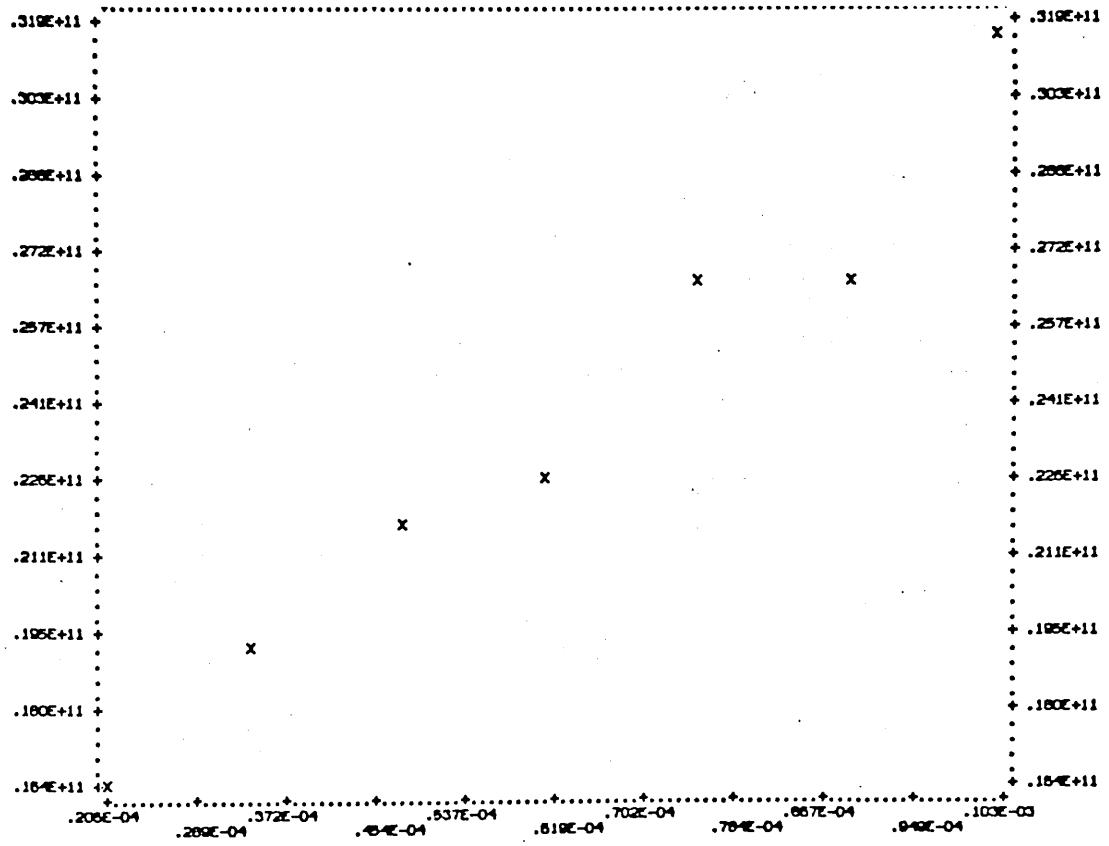

Fig.9

```
  T    D
502.0 64.4
   F1     F2      F3      I01      I1      I02      I2       P
 30.0   200.0    30.0    17.6     22.8     19.8     18.2    9.700
 50.0   200.0    50.0    36.6     35.7     39.8     29.6    8.050
 70.0   200.0    70.0    38.8     34.5     42.7     28.5    7.450
 90.0   200.0    90.0    38.2     31.3     42.5     26.5    7.000
110.0   200.0   110.0    34.7     27.4     38.0     22.8    6.600
130.0   200.0   130.0    32.4     24.0     35.0     20.3    6.550
150.0   200.0   150.0    25.7     20.4     27.8     17.5    6.600

VALUES OF Y=    .1488E+11   .1585E+11   .1718E+11   .1807E+11   .2272E+11   .2348E+11   .2250E+11

VALUES OF X==   .2064E-04   .3440E-04   .4816E-04   .6192E-04   .7568E-04   .8944E-04   .1032E-03

VALUES OF VBAR=   .1344E+03   .1761E+03   .2015E+03   .2349E+03   .2585E+03   .2857E+03   .3007E+03

SLOPE=   .1133E+15


STANDARD DEVIATION=   .1656E+14


INTERCEPT=   .1237E+11


STANDARD DEVIATION=   .1122E+10
```

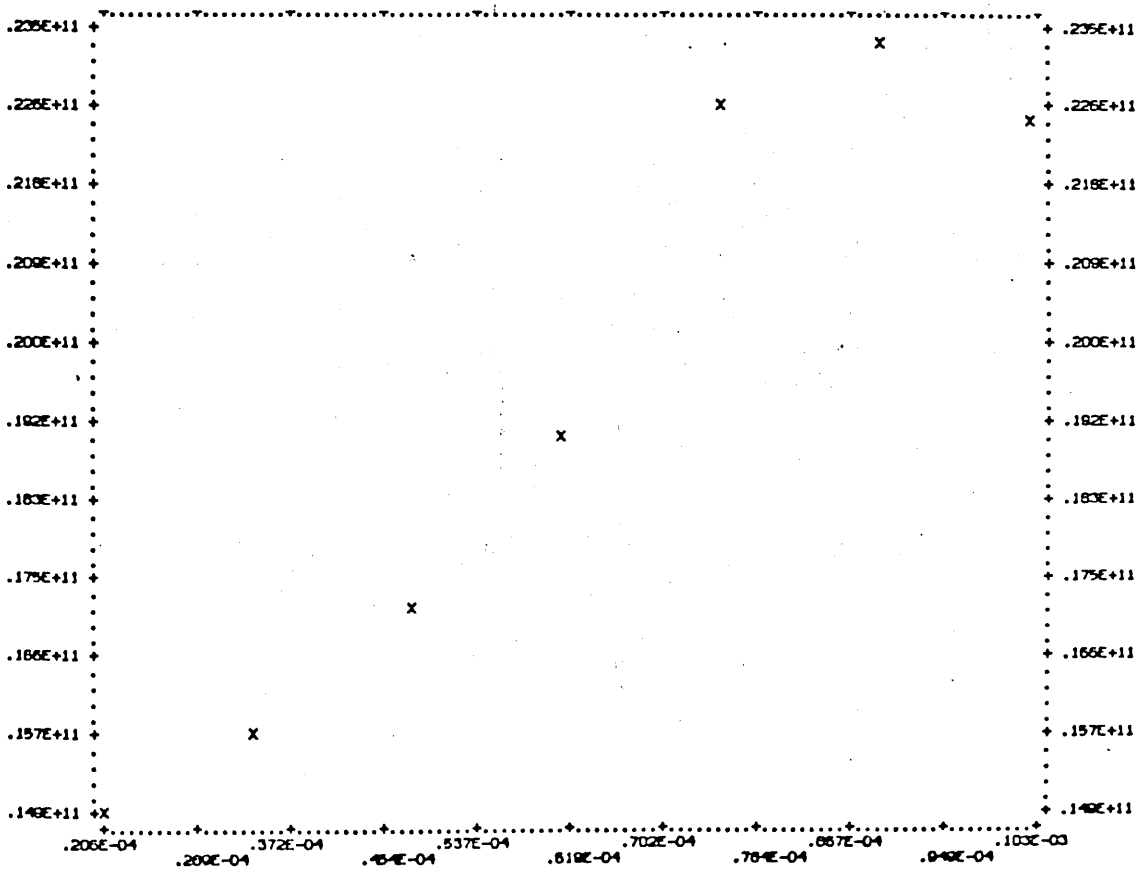

Fig. 10. The experimental points are on a reasonably good straight lines and k_w^* was obtained from the intercept. The slope of the straight line gave the value for 2 F(NO) k_{12}^{Ar} from which values of X_{NO} were calculated using a literature value[128] for k_{12}^{Ar} (= $3.27 \pm 0.42 \times 10^{15} \exp\left\{\frac{594 \pm 35}{T}\right\}$ $cm^6\ mol^{-2}\ s^{-1}$) and

$$X_{NO} = \frac{F\ (NO)}{F\ (NO) + F\ (Ar)}\ \text{discharge}$$

It seems that reference measurements might give some information about the rate of the reaction:

$$O + NO + Ar \longrightarrow NO_2 + Ar \qquad 12$$

This will be discussed again in chapter 7.

The values of the surface recombination efficiency were calculated from $\gamma^* = \frac{2rk_w^*}{\bar{c}}$ and the values of $(\gamma-\gamma^*)$ were calculated from the values of $(k_w - k_w^*)$. Values of all these constants at different temperatures are tabulated (Table 2).

5.4 Experimental Results for the Reaction.

$$O + O_2 + CO_2 \longrightarrow O_3 + CO_2$$

Previous[85] work at 298K showed that for M = CO_2, the surface rate constant is not constant. This may be due to the back diffusion of CO_2 into the discharge to produce various species which are attacked on the surface (e.g. C_2O_3) or to adsorption of CO_2 onto surface. To avoid these difficulties, CO_2 was added as far downstream from the discharge as possible. The principle of the modification was to add CO_2 (0 - 173.6 μ mol s^{-1}) and O_2 (34.4 μ mol s^{-1}) through the inlet jets J_2 and J_5 and to record I_2 and I_1 respectively. The flow line of CO_2 was joined with the O_2 flow line for this purpose. Both CO_2

Legend for Fig. 10

Typical graph of $\frac{Vu}{\Delta V}\frac{V}{V_R}\ln I_2^*/I_1^*$ represented by Y

against $\frac{1}{V^2}\frac{Vu}{\Delta V}\left[\left(\frac{V}{V_u}\right)^3 \sum_M F(M)\, x_{12}^M - \sum_M F(M)\, x_{12}^M\right]$

represented by X (equation 20)

Fig. 10

VALUES OF Y= .7518E+01 .6038E+01 .5357E+01 .4724E+01 .4566E+01 .4345E+01

VALUES OF X= .3084E-15 .2376E-15 .2106E-15 .1857E-15 .1700E-15 .1611E-15

SLOPE= .2181E+17

STANDARD DEVIATION= .6420E+15

INTERCEPT= .7958E+00

STANDARD DEVIATION= .1408E+00

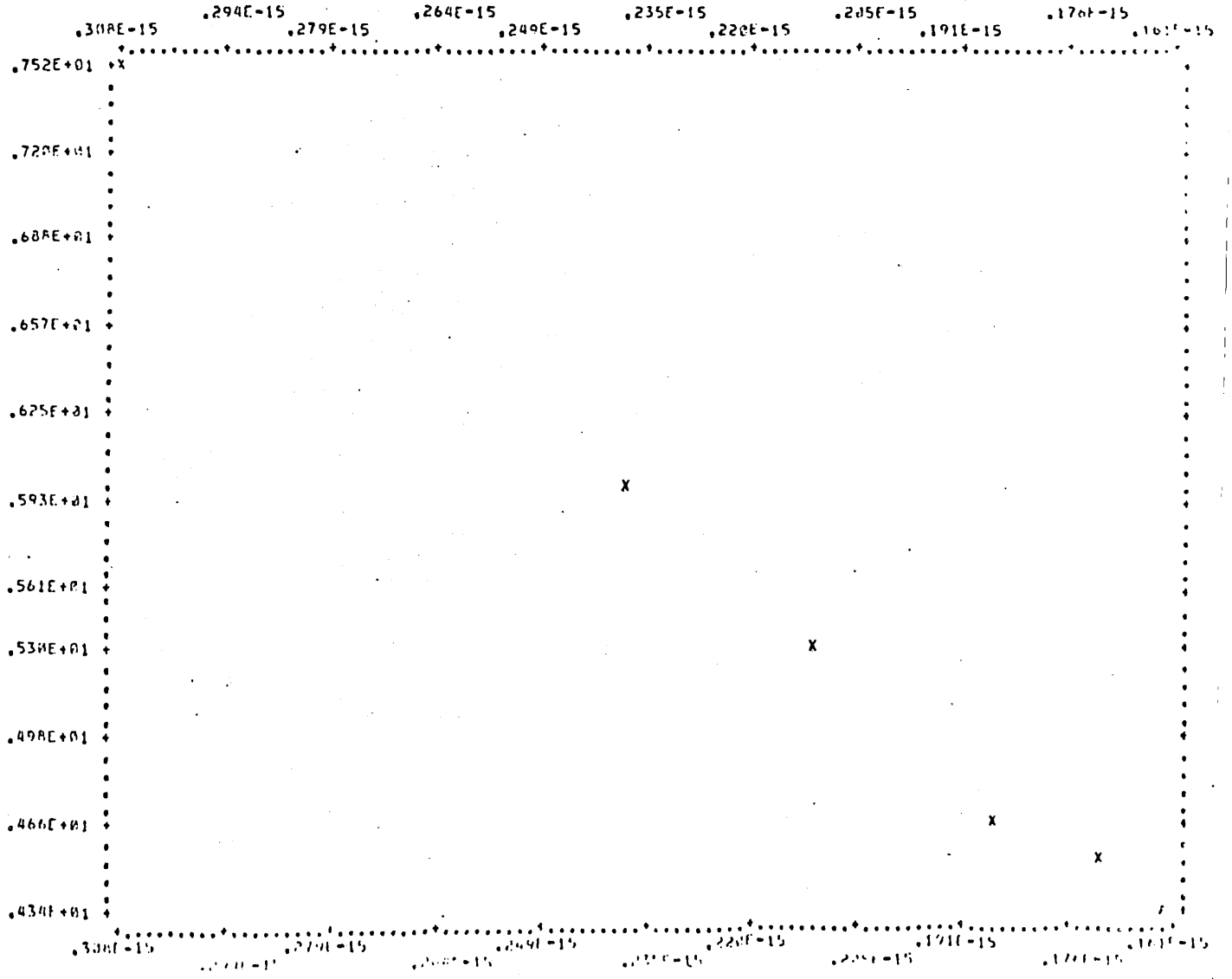

TABLE 2

Values of $k^{O_2}_{1.1}$, $(k_w - k^*_w)$ and k^*_w for the reaction: $O + O_2 + M = O_3 + M$ at Different Temperatures ($M = O_2$)

T/K	$k^{O_2}_{1.1}/10^{14}$ $cm^6\ mol^{-2}\ s^{-1}$	$(k_w - k^*_w)/s^{-1}$	k^*_w/s^{-1}
196	8.162 ± 2.24	-	1.11 ± 0.85
196	9.475 ± 1.27	0.857 ± 0.295	1.11 ± 0.34
196	8.570 ± 0.464	-0.028 ± 0.117	0.796 ± 0.14
196	8.650 ± 0.865	-0.199 ± 0.210	-0.03 ± 0.49
Mean	8.71 ± 1.36	0.210 ± 0.567	-.75 ± 0.45
246	3.440 ± 0.501	0.292 ± 0.13	0.416 ± 0.462
246	4.184 ± 0.439	0.312 ± 0.11	0.540 ± 0.234
Mean	3.81 ± 0.47	0.302 ± 0.018	0.48 ± 0.35
297	2.43 ± 0.55	0.077 ± 0.131	0.227 ± 0.17
297	2.144 ± 0.208	0.166 ± 0.025	0.129 ± 0.13
297	2.374 ± 0.395	-	-
Mean	2.31 ± 0.41	0.122 ± 0.063	0.18 ± 0.15
*406	2.13 ± 0.112	-0.017 ± 0.036	0.111 ± 0.066
400	1.801 ± 0.101	-0.013 ± 0.032	-0.061 ± 0.079
400	1.72 ± 0.136	-0.008 ± 0.044	0.081 ± 0.049
Mean	1.76 ± 0.12	-0.013 ± 0.013	0.044 ± 0.065
500	1.133 ± 0.166	0.145 ± 0.054	-0.21 ± 0.10
500	1.152 ± 0.205	0.036 ± 0.042	-0.11 ± 0.05
Mean	1.14 ± 0.19	0.090 ± 0.077	-0.16 ± 0.08

*Rate constant is not included in the mean value because difference in temperature.

TABLE 2 (Continued)

T/K	$k_{1.1}^{Ar}/10^{14}$ $cm^6\ mol^{-2}\ s^{-1}$	$(\gamma - \gamma^*)$	$\gamma^* \times 10^5$	$X_{NO}\ k_{12}/10^{13}$ $cm^6\ mol^{-2}\ s^{-1}$	$X_{NO} \times 10^4$
196	2.56 ± 0.95	-	5.42 ± 4.16	3.95 ± 0.36	
196	2.52 ± 0.37	-0.97 ± 1.03	0.146 ± 2.39	4.98 ± 0.44	
196	4.67 ± 0.62	4.19 ± 1.44	5.42 ± 1.66	3.54 ± 0.36	
196	2.81 ± 0.20	-0.14 ± 0.57	3.89 ± 0.68	4.36 ± 0.13	
Mean	3.14 ± 0.61	1.03 ± 2.77	3.67 ± 2.2	4.21 ± 0.45	6.22 ± 0.66
246	2.49 ± 0.21	1.27 ± 0.566	1.8 ± 2.014	3.04 ± 0.42	
246	2.52 ± 0.19	1.36 ± 0.48	2.46 ± 1.02	3.08 ± 0.21	
Mean	2.51 ± 0.20	1.31 ± 0.078	2.13 ± 1.52	3.06 ± 0.32	8.36 ± 0.87
295	-	-	-	2.01 ± 0.18	
295	1.62 ± 0.27	0.306 ± 0.522	0.904 ± 0.67	1.21 ± 0.10	
295	-	0.661 ± 0.099	0.514 ± 0.518	-	
295	1.51 ± 0.04	-	-	-	
Mean	1.57 ± 0.20	0.486 ± 0.251	0.71 ± 0.59	1.61 ± 0.14	6.57 ± 0.57
406	-	-0.058 ± 0.12	0.38 ± 0.22	0.703 ± 0.052	
400	0.94 ± 0.05	-0.044 ± 0.11	-0.21 ± 0.27	1.34 ± 0.06	
400	0.948± 0.067	-0.027 ± 0.15	0.277 ± 0.17	1.36 ± 0.04	
Mean	0.944 ± 0.059	-0.044 ± 0.044	0.150 ± 0.222	1.13 ± 0.05	7.85 ± 0.35
500	0.899 ± 0.082	0.44 ± 0.17	-0.64 ± 0.31	0.821 ± 0.079	
500	0.768 ± 0.101	0.11 ± 0.13	-0.336 ± 0.15	1.15 ± 0.064	
500	-	-	-	0.89 ± 0.48	
500	-	-	-	0.661 ± 0.303	
Mean	0.834 ± 0.092	0.275 ± 0.236	-0.49 ± 0.245	0.881 ± 0.071	8.23 ± 0.66

and O_2 were purified in separate molecular sieve traps at 196K before mixing and entering into the flow system. The other requirements were essentially the same as those in the previous experiment. The first measurements of I_1 and I_2 were made when O_2 (34.4 μ mol s^{-1}) with no CO_2 was passed through a stream of O atoms in the reaction tube. The flow rate of O_2 in the subsequent experiments were kept constant while the flow rate of CO_2 was varied. During the experiments the flow velocity $\bar{v}$ was kept constant and the pressures in the system was adjusted accordingly, since $\bar{v} = \frac{\Sigma F_i RT}{\pi r^2 P}$.

Similarly, reference measurements were made to record I_1^* and I_2^* replacing flow of oxygen by argon (34.4 μ mol s^{-1}) and keeping all the other conditions the same. The data so collected at different temperatures were plotted as previously using equation 18 (Figures 11 - 14).

The rate constants $k_{1.1}^{CO_2}$ were calculated from the slopes of the various plots, values of $(k_w - k_w^*)$ were calculated from the intercepts. The graphs were linear in contrast to those obtained previously where the points were found to lie on a curve[85]. Further the surface rate constant calculated by Ball was not constant. He suspected that some molecules of CO_2 might find their way into the discharge by back diffusion to produce various species which are attacked on the surface (e.g. C_2O_3) or some CO_2 itself might adsorb onto the surface. The conditions of the present experiments were adjusted so that CO_2 molecules could not find their way into the discharge by back diffusion. The reference measurements were used with equation 20 to evaluate values

Figs. 11-14

Graphs of $\frac{V^3}{V_R F(O_2)} \ln \frac{I_1 I_2^*}{I_2 I_1^*}$ represented by Y

against $F(CO_2)$ represented by X (equation 18) for the reaction:

$$O + O_2 + CO_2 = O_3 + CO_2 \qquad 1.1$$

In the tabulated data at the head of each graph T, D, I_1, I_2, IO1, IO_2, F_1, VBAR and P represent usual meaning as for figs. 5-9 (P. 74) F_2 and F_3 represent flow rate of argon + F_3 and flow rate of CO_2 respectively.

Fig. 11. $M = CO_2$, $T = 196K$

Fig. 12. $M = CO_2$, $T = 295K$

Fig. 13. $M = CO_2$, $T = 400K$

Fig. 14 $M = CO_2$, $T = 500K$

Fig.11

T	D
196.0	48.8

F1	F2	F3	I01	I1	I02	I2	P
50.0	300.0	50.0	56.5	56.5	57.9	32.8	2.600
50.0	350.0	100.0	45.0	46.5	47.0	25.4	2.900
50.0	400.0	150.0	36.4	38.8	39.2	20.2	3.200
50.0	425.0	175.0	33.4	38.9	36.6	19.3	3.400
50.0	450.0	200.0	30.3	37.8	33.8	18.0	3.600
50.0	475.0	225.0	27.8	36.0	31.6	16.4	3.800
50.0	500.0	250.0	25.2	32.6	29.6	14.4	4.000

VALUES OF Y= .2125E+12 .2608E+12 .3099E+12 .3312E+12 .3496E+12 .3697E+12 .3898E+12

VALUES OF X== .3440E-04 .6880E-04 .1032E-03 .1204E-03 .1376E-03 .1548E-03 .1720E-03

VALUES OF VBAR= .2980E+03 .3054E+03 .3113E+03 .3093E+03 .3075E+03 .3059E+03 .3044E+03

SLOPE= .1287E+16

STANDARD DEVIATION= .3226E+14

INTERCEPT= .1721E+12

STANDARD DEVIATION= .3923E+10

DATA FOR 0+02+C02=03+C02

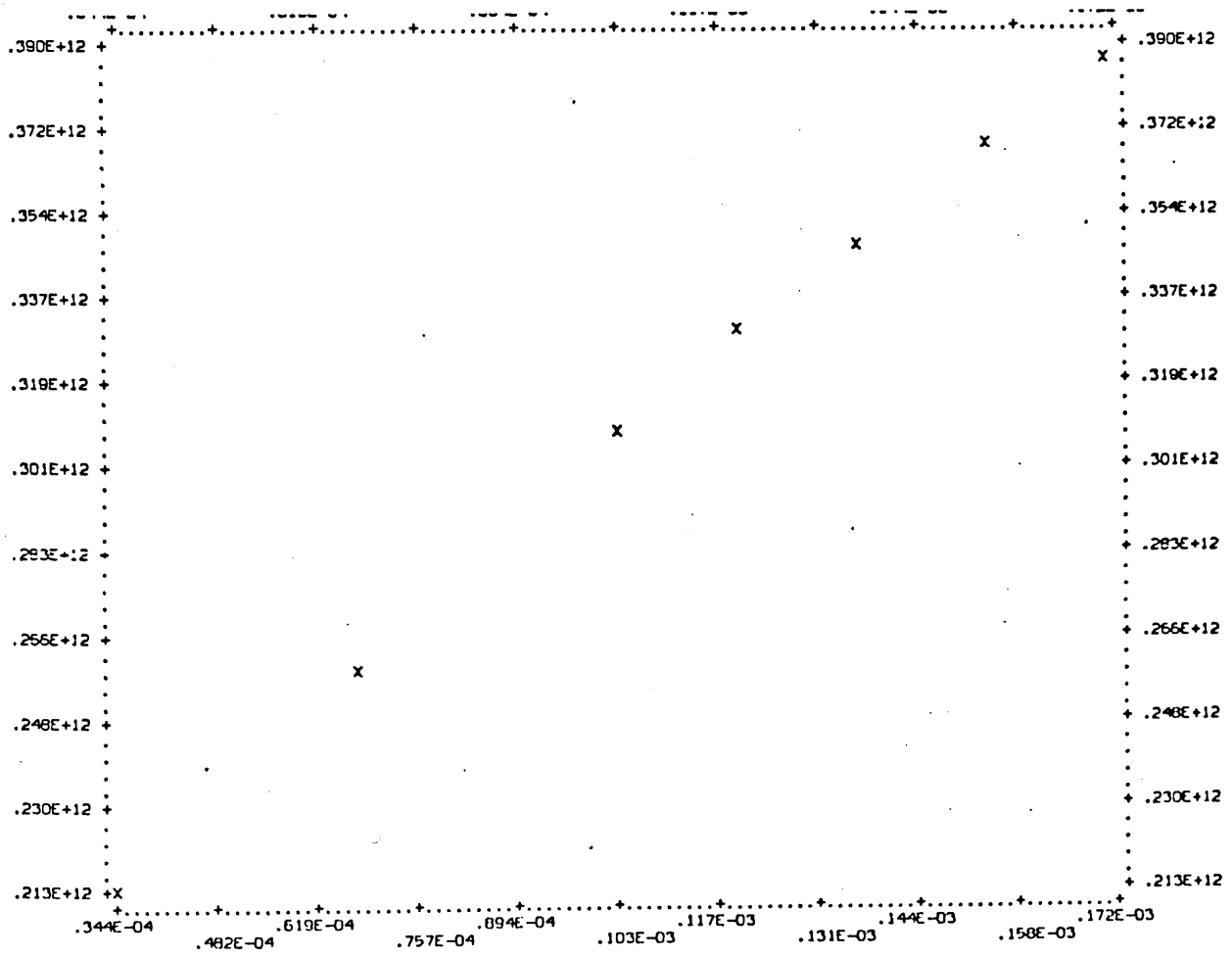

Fig.12

T	D
295.0	48.8

F1	F2	F3	I01	I1	I02	I2	P
50.0	300.0	50.0	21.2	21.5	21.5	17.5	3.800
50.0	350.0	100.0	17.7	18.6	18.1	14.1	4.400
50.0	400.0	150.0	14.4	16.3	15.0	12.1	4.900
50.0	425.0	175.0	13.1	16.2	13.7	11.7	5.200
50.0	450.0	200.0	11.8	16.2	12.6	11.3	5.600
50.0	475.0	225.0	10.7	15.2	11.4	10.6	5.800
50.0	500.0	250.0	9.7	14.6	10.5	10.1	6.000

VALUES OF Y= .8961E+11 .1176E+12 .1372E+12 .1475E+12 .1584E+12 .1643E+12 .1803E+12

VALUES OF X== .3440E-04 .6880E-04 .1032E-03 .1204E-03 .1376E-03 .1548E-03 .1720E-03

VALUES OF VBAR= .3069E+03 .3029E+03 .3060E+03 .3044E+03 .2975E+03 .3016E+03 .3054E+03

SLOPE= .6280E+15

STANDARD DEVIATION= .2361E+14

INTERCEPT= .7117E+11

STANDARD DEVIATION= .2872E+10

DATA FOR 0+02+C02=03+C02

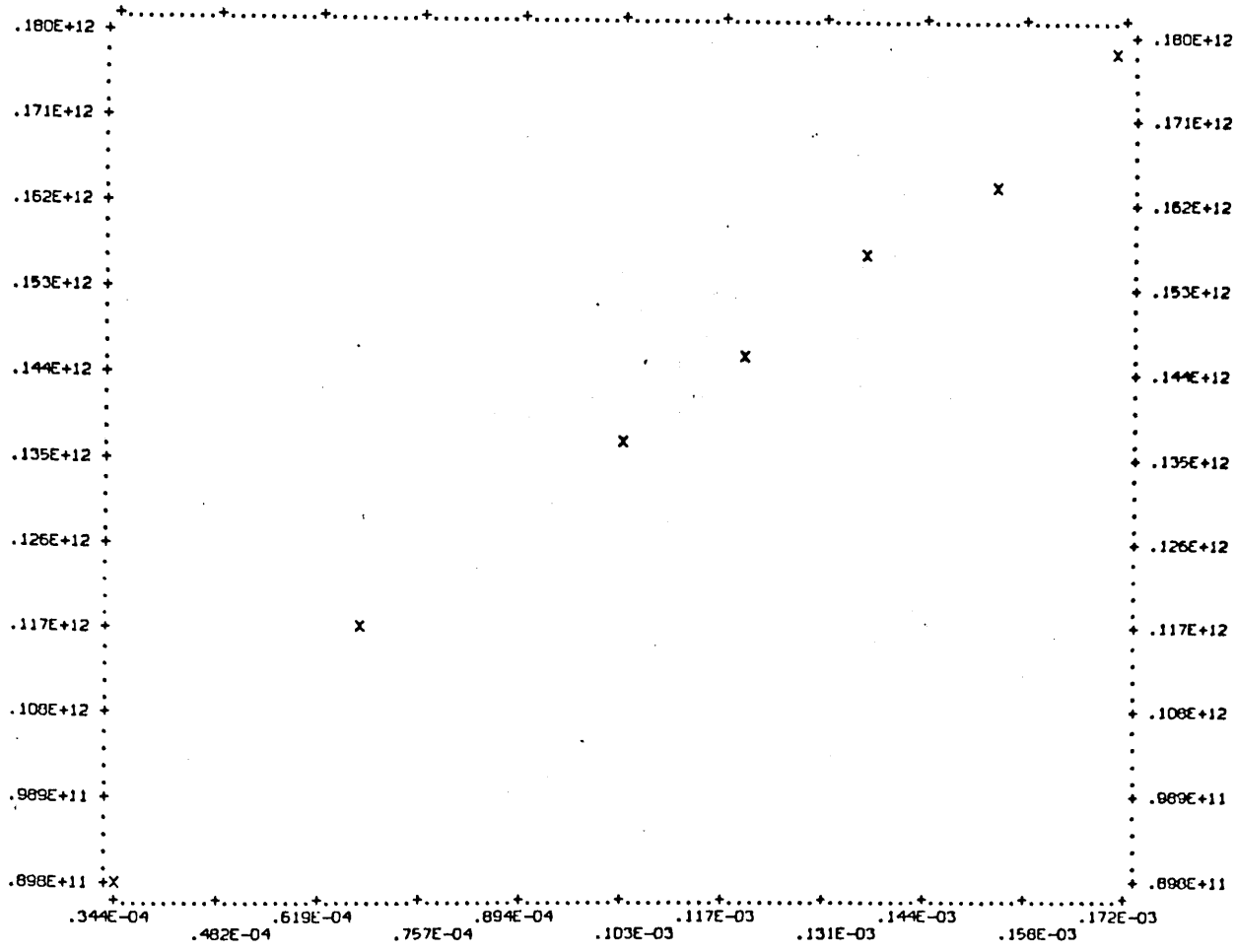

Fig.13

T	D
400.0	48.8

F1	F2	F3	I01	I1	I02	I2	P
50.0	350.0	100.0	74.1	62.5	74.8	53.6	6.000
50.0	400.0	150.0	59.9	49.1	60.7	40.8	6.700
50.0	425.0	175.0	54.1	43.5	55.1	35.3	7.200
50.0	450.0	200.0	48.0	39.2	49.1	31.8	7.500
50.0	475.0	225.0	43.7	35.1	45.1	28.0	7.900
50.0	500.0	250.0	39.7	31.9	41.2	25.5	8.200
50.0	550.0	300.0	32.7	25.7	34.5	20.2	9.000

VALUES OF Y= .6294E+11 .7835E+11 .8501E+11 .8952E+11 .9849E+11 .1026E+12 .1137E+12

VALUES OF X== .6880E-04 .1032E-03 .1204E-03 .1376E-03 .1548E-03 .1720E-03 .2064E-03

VALUES OF VBAR= .3012E+03 .3035E+03 .2981E+03 .3012E+03 .3003E+03 .3030E+03 .3012E+03

SLOPE= .3668E+15

STANDARD DEVIATION= .1468E+14

INTERCEPT= .3962E+11

STANDARD DEVIATION= .2113E+10

DATA FOR O+O2+CO2=O3+CO2

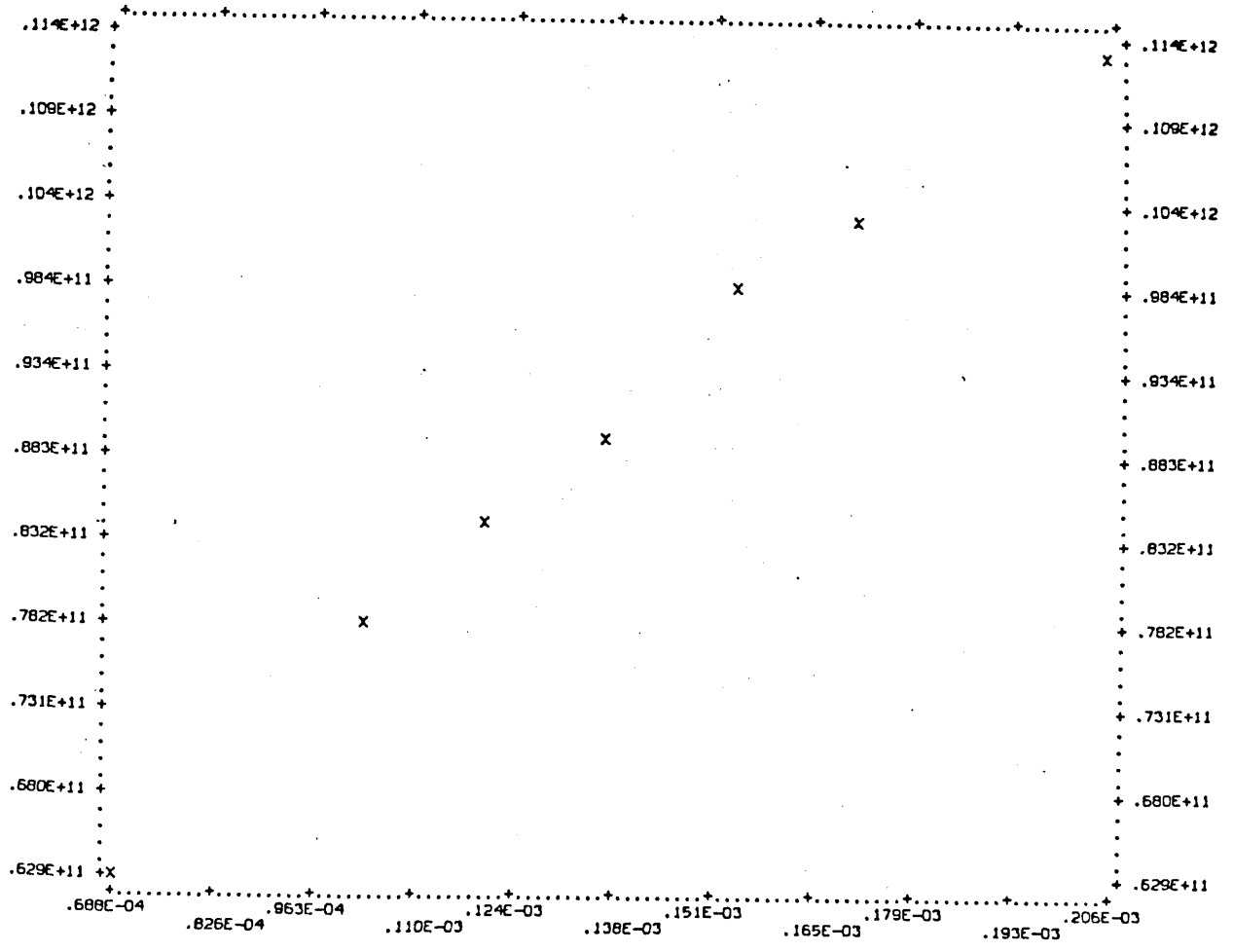

Fig.14

T	D
500.0	48.8

F1	F2	F3	I01	I1	I02	I2	P
50.0	300.0	50.0	102.1	92.1	102.4	85.0	6.500
50.0	350.0	100.0	81.2	71.7	82.0	64.1	7.500
50.0	400.0	150.0	63.0	56.6	63.8	49.9	8.400
50.0	425.0	175.0	55.3	52.2	56.3	45.5	8.900
50.0	450.0	200.0	48.3	48.6	49.7	42.7	9.300
50.0	475.0	225.0	42.9	46.3	44.1	40.5	9.800
50.0	500.0	250.0	37.9	52.8	39.2	45.1	10.300

VALUES OF Y= .3304E+11 .4705E+11 .5424E+11 .6008E+11 .6249E+11 .6317E+11 .7415E+11

VALUES OF X== .3440E-04 .6880E-04 .1032E-03 .1204E-03 .1376E-03 .1548E-03 .1720E-03

VALUES OF VBAR= .3041E+03 .3012E+03 .3026E+03 .3014E+03 .3036E+03 .3026E+03 .3016E+03

SLOPE= .2676E+15

STANDARD DEVIATION= .2327E+14

INTERCEPT= .2607E+11

STANDARD DEVIATION= .2830E+10

DATA FOR 0+02+C02=03+C02

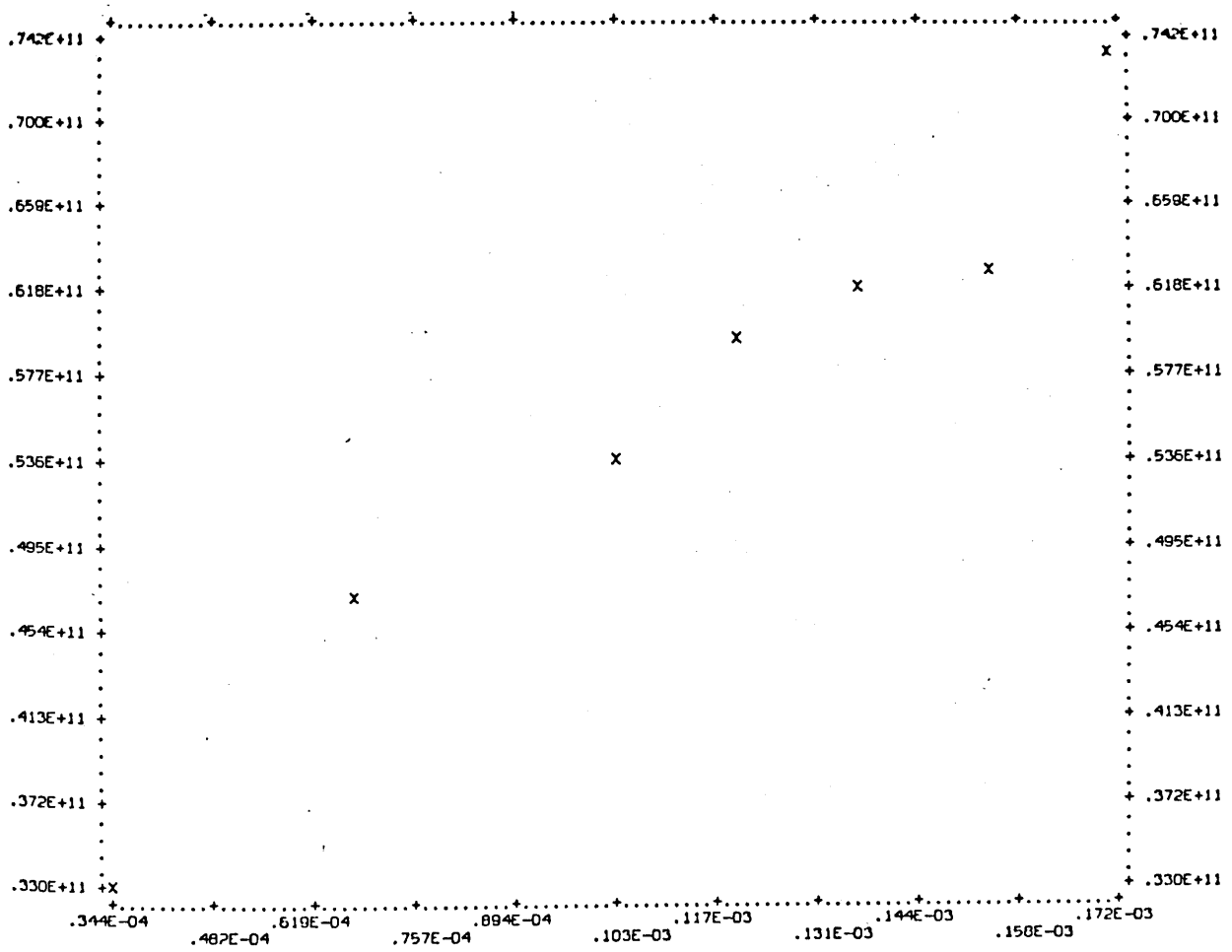

for k_w^* and X_{NO}. The surface poisoning effect of CO_2, the importance of reference measurements and values of the rate constant $k_{1.1}^{CO_2}$ are tabulated (Table 3).

5.5 Experimental Results for the Reaction.

$$O + O_2 + He \longrightarrow O_3 + He$$

These experiments were undertaken to measure the rate constant $k_{1.1}^{He}$ over the temperature range 196 - 500K at total pressures 1.56 - 9.36 torr. $O(^3P)$ atoms were generated by passing an inert carrier gas (106.2 - 173.6 μ mol s^{-1}) containing less than 1000 p.p.m. O_2 and less than 5 p.p.m. N_2 through the microwave discharge. The flow gases were carefully dried as before, and in this case helium was passed through a liquid N_2 trap at 0-1 atmosphere pressure. The first experimental runs at 295K were made under the same conditions as for CO_2. Linear plots of O atom decay rates against F(He) were obtained in four runs. The rate constant obtained using this procedure was approximately 2.3×10^{14} cm^6 mol^{-2} s^{-1}, this is about twice the literature value. The introduction of He, as the third body through the inlet jets was then abandoned.

A new method of adding variable amounts of He gas into the reaction system was devised. Helium, at different flow rates, was passed through the discharge at the same time ensuring a constant trace of O_2 in the discharge. Although the validity of this procedure is questionable, the plots of O atom decay rates against F(He) were linear, the rate constants were again twice the literature value.

TABLE 3

Values of $k_{1.1}^{CO_2}$, $(k_w - k_w^*)$ and k_w^* for the reaction: $O + O_2 + CO_2 = O_3 + CO_2$

at Different Temperatures

T/K	$k_{1.1}^{CO_2}/10^{14}$ $cm^6\ mol^{-2}\ s^{-1}$	$(k_w - k_w^*)/s^{-1}$	k_w^*/s^{-1}
196	10.605 ± 1.047	1.605 ± 0.197	0.20 ± 0.044
196	14.41 ± 0.3485	1.014 ± 0.066	0.10 ± 0.088
196	12.87 ± 0.3226	1.44 ± 0.061	0.093 ± 0.045
196	13.72 ± 0.7526	1.961 ± 0.142	0.11 ± 0.065
Mean	12.90 ± 0.687	1.505 ± 0.393	0.126 ± 0.061
295	6.318 ± 0.1845	0.614 ± 0.035	0.0134 ± 0.064
295	4.513 ± 0.763	0.753 ± 0.090	0.0203 ± 0.028
295	6.280 ± 0.2361	0.588 ± 0.045	0.0784 ± 0.045
295	4.366 ± 0.6973	0.888 ± 0.166	0.0686 ± 0.048
295	6.318 ± 0.18	0.616 ± 0.057	-
Mean	5.559 ± 0.416	0.692 ± 0.121	0.035 ± 0.046
400	2.643 ± 0.791	0.404 ± 0.153	0.0611 ± 0.04
400	3.668 ± 0.1468	0.277 ± 0.034	0.0162 ± 0.022
400	3.459 ± 0.5253	0.583 ± 0.102	0.0659 ± 0.072
400	4.056 ± 0.2111	0.470 ± 0.041	-0.0856 ± 0.016
Mean	3.456 ± 0.492	0.434 ± 0.128	0.014 ± 0.038
500	2.562 ± 1.074	0.221 ± 0.202	-0.011 ± 0.023
500	2.443 ± 0.1707	0.187 ± 0.037	-0.0134 ± 0.015
500	2.676 ± 0.2327	0.166 ± 0.045	-0.0248 ± 0.034
500	3.164 ± 0.5572	0.237 ± 0.108	-0.359 ± 0.021
500	2.841 ± 0.2774	0.234 ± 0.054	-0.0511 ± 0.027
Mean	2.737 ± 0.55	0.209 ± 0.031	-0.027 ± 0.024

TABLE 3 (Continued)

T/K	$(\gamma - \gamma^*) \times 10^5$	$\gamma^* \times 10^5$	$X_{NO} k_{12}^{Ar}/10^{12}$ $cm^6\ mol^{-2}\ s^{-1}$	$X_{NO} \times 10^4$
196	7.838 ± 0.96	0.978 ± 0.215	6.55 ± 0.30	
196	4.96 ± 0.323	0.489 ± 0.43	7.49 ± 0.60	
196	7.04 ± 0.298	0.455 ± 0.22	6.37 ± 0.031	
196	9.59 ± 0.69	0.538 ± 0.318	6.51 ± 0.45	
Mean	7.36 ± 1.92	0.62 ± 0.030	6.73 ± 0.35	0.99 ± 0.06
295	2.446 ± 0.14	0.053 ± 0.26	3.09 ± 0.42	
295	3.000 ± 0.358	-0.0809 ± 0.11	3.33 ± 0.16	
295	2.34 ± 0.179	0.312 ± 0.179	2.52 ± 0.30	
295	3.538 ± 0.662	0.273 ± 0.19	2.80 ± 0.28	
295	2.455 ± 0.277	-	-	
Mean	2.76 ± 0.48	0.14 ± 0.18	2.93 ± 0.29	1.20 ± 0.12
400	1.38 ± 0.523	0.209 ± 0.137	0.822 ± 0.267	
400	0.95 ± 0.116	0.055 ± 0.075	1.70 ± 0.128	
400	1.994 ± 0.349	0.225 ± 0.246	1.01 ± 0.48	
400	1.607 ± 0.14	-0.293 ± 0.055	2.10 ± 0.11	
Mean	1.48 ± 0.436	0.05 ± 0.13	1.41 ± 0.25	0.98 ± 0.17
500	0.676 ± 0.618	-0.034 ± 0.07	1.36 ± 0.15	
500	0.572 ± 0.113	-0.041 ± 0.046	1.26 ± 0.095	
500	0.508 ± 0.138	-0.076 ± 0.104	1.61 ± 0.224	
500	0.725 ± 0.33	-0.11 ± 0.064	1.25 ± 0.14	
500	0.716 ± 0.165	-0.156 ± 0.08	1.455 ± 0.178	
Mean	0.64 ± 0.095	-0.08 ± 0.07	1.39 ± 0.16	1.30 ± 0.15

A convenient way of adding variable amounts of He was through the third body inlets jets D (Fig. 3). The experiments were commenced by adding a constant flow of oxygen (34.7 μ mol s^{-1}) to a stream of O (^3P) atoms. The flow of helium was then admitted at varying flow rates (0 - 208.3 μ moles s^{-1}) through the third body inlet jets in successive measurements; either by adjusting the total pressure or the flow velocities. In all runs, the measured decay rates were a linear function of the concentration of added He. This indicated that equation 18 was obeyed and rate constants were derived accordingly from the slopes of graphs of the decay rate against the helium flow, F(He). The rate constants under all conditions at room temperature was about 2.3×10^{14} cm^6 mol^{-2} s^{-1}.

There are two possibilities which could account for the observed higher rate constant, as compared with the literature value; either there are some impurities in the discharge or there is some wall loss. In consequence the reaction tube was dismantled, cleaned and washed with surface active agents. This reaction system was then fitted to the other parts of the flow tube and checked carefully to ensure there were no leaks. The discharge inert gases were purified by a rare gas purifier which reduced impurities to a level of less than 1 part in 10^7. Measurements under these improved conditions (in the temperature range 196-500K) yielded rate constants of the same value as before.

To test the system, two runs were made at 295K with argon as the third body keeping all the other conditions exactly the same as for helium. The value of the rate constant $k_{1.1}^{Ar}$, 1.5×10^{14} cm^6 mol^{-2} s^{-1}, was in agreement with the literature value and the value obtained

previously in this work (Table 2). Further experiments were commenced by passing an excess of oxygen (69.4 μ mol s^{-1}) into the stream of oxygen atoms. The flow velocities were then decreased about 200 cm s^{-1} to increase the residence time. The rate constant obtained under these conditions were now comparable to the literature value. The measured rate constant was 1.1 x 10^{14} cm^6 mol^{-2} s^{-1}. These results implied that some excited ozone, most likely triplet[127], might approach steady state concentration during the reaction 1.1. Previous tests ruled out the possibility of ground state ozone reaching steady state, therefore it is most probably an excited state which approaches a steady state value. In this case reaction 1.1 will be followed by two competitive reactions

$$O + O_3^{*3} \longrightarrow 2\ O_2 \qquad 1.3b$$

$$O_3^{*3} + M \longrightarrow O_3^1 + M \qquad 1.5$$

In presence of the less efficient quenching agent helium, process 1.5 can be neglected, and with the fast reaction 1.3b following 1.1, a steady state concentration of O_3^{*3} would be quickly set up leading to:

$$-d[O]/dt = 2k_{1.1}^{He}\ [O_2]\ [O]\ [M]$$

as the gas phase rate equation for O atom decay. Thus the measured rate constant should be identified with $2k_{1.1}$ and this was done in deriving the values summarized in Table 4. Since the rate of reaction 1.1 decreases and that of 1.3 increases with the rise of temperature, reaction 1.3 presumably becomes more important at higher temperatures. The curvature observed at higher temperatures in the Arrhenius plot might explain this behaviour. However, the plot of log $k_{1.1}^{He}$ against

log T is reasonably linear and its slope is similar to that obtained using argon as third body.

Typical results for the reaction 1.1 in which helium is the third body (Figures 15-19) are summarized in Table 4.

Figs. 15-19

Graphs of $\frac{V^3}{V_R F (O_2)} \ln \frac{I_1 I_2^*}{I_2 I_1^*}$ represented by Y

against F(He) represented by X (equation 18) for the reaction:

$$O + O_2 + He = O_3 + He \qquad 1.1$$

In the tabulated data at the head of each graph T, D, I_1, I_2, IO1, IO_2, F_1, VBAR and P represent usual meaning as for figs. 5-9 (P. 74). For figs 15-18, F_2 and F_3 represent flow rate of argon + F_3 and flow rate of Helium (cm^3 min^{-1}) respectively. For fig. 19, F_2 and F_3 represent flow rate of Helium (cm^3 min^{-1}).

Fig. 15. M = He, T = 196K

Fig. 16. M = He, T = 300K

Fig. 17. M = He, T = 293K

Fig. 18. M = He, T = 400K

Fig. 19. M = He, T = 500K

Fig.15

T	D
196.0	48.8

F1	F2	F3	I01	I1	I02	I2	P
50.0	250.0	0.0	19.2	29.8	19.6	19.4	2.650
50.0	300.0	50.0	14.5	33.0	14.9	20.5	3.100
50.0	350.0	100.0	12.0	42.5	12.4	25.2	3.500
50.0	400.0	150.0	11.0	53.1	11.3	29.2	4.000
50.0	425.0	175.0	10.5	55.7	10.7	29.7	4.200
50.0	450.0	200.0	9.9	64.2	10.1	33.4	4.400
50.0	475.0	225.0	9.2	63.5	9.4	32.6	4.600
50.0	500.0	250.0	8.9	62.6	9.1	29.6	4.900

VALUES OF Y= .1001E+12 .1110E+12 .1271E+12 .1364E+12 .1436E+12 .1515E+12 .1569E+12 .1672E+12

VALUES OF X== 0. .3440E-04 .6880E-04 .1032E-03 .1204E-03 .1376E-03 .1548E-03 .1720E-03

VALUES OF VBAR= .2506E+03 .2500E+03 .2530E+03 .2491E+03 .2504E+03 .2516E+03 .2527E+03 .2485E+03

SLOPE= .3813E+15

STANDARD DEVIATION= .1130E+14

INTERCEPT= .9902E+11

STANDARD DEVIATION= .1286E+10

DATA FOR O+O2+HE=O3+HE

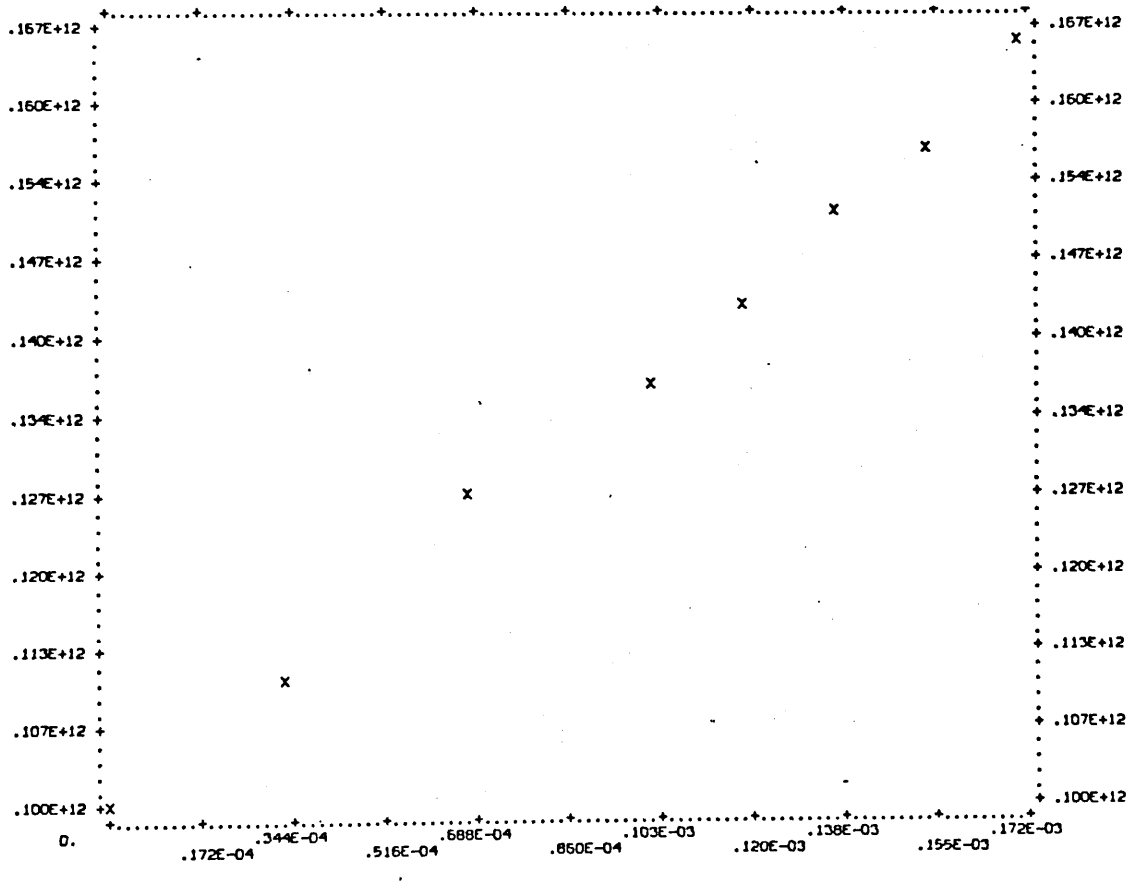

Fig.16

T	D
300.0	48.8

F1	F2	F3	I01	I1	I02	I2	P
50.0	250.0	0.0	100.0	107.7	100.0	86.8	4.100
50.0	300.0	50.0	100.0	101.4	100.0	79.2	4.700
50.0	350.0	100.0	100.0	99.5	100.0	75.2	5.300
50.0	400.0	150.0	100.0	98.4	100.0	70.0	6.100
50.0	425.0	175.0	100.0	97.5	100.0	68.0	6.400
50.0	450.0	200.0	100.0	95.9	100.0	66.7	6.700
50.0	475.0	225.0	100.0	95.2	100.0	64.7	7.000
50.0	500.0	250.0	100.0	96.6	100.0	62.2	7.500

VALUES OF Y= .4646E+11 .5610E+11 .6617E+11 .7516E+11 .8099E+11 .8296E+11 .8957E+11 .9544E+11

VALUES OF X== 0. .3440E-04 .6880E-04 .1032E-03 .1204E-03 .1376E-03 .1548E-03 .1720E-03

VALUES OF VBAR= .2479E+03 .2523E+03 .2557E+03 .2500E+03 .2515E+03 .2529E+03 .2541E+03 .2485E+03

SLOPE= .2789E+15

STANDARD DEVIATION= .6125E+13

INTERCEPT= .4653E+11

STANDARD DEVIATION= .6969E+09

DATA FOR 0+02+HE=03+HE

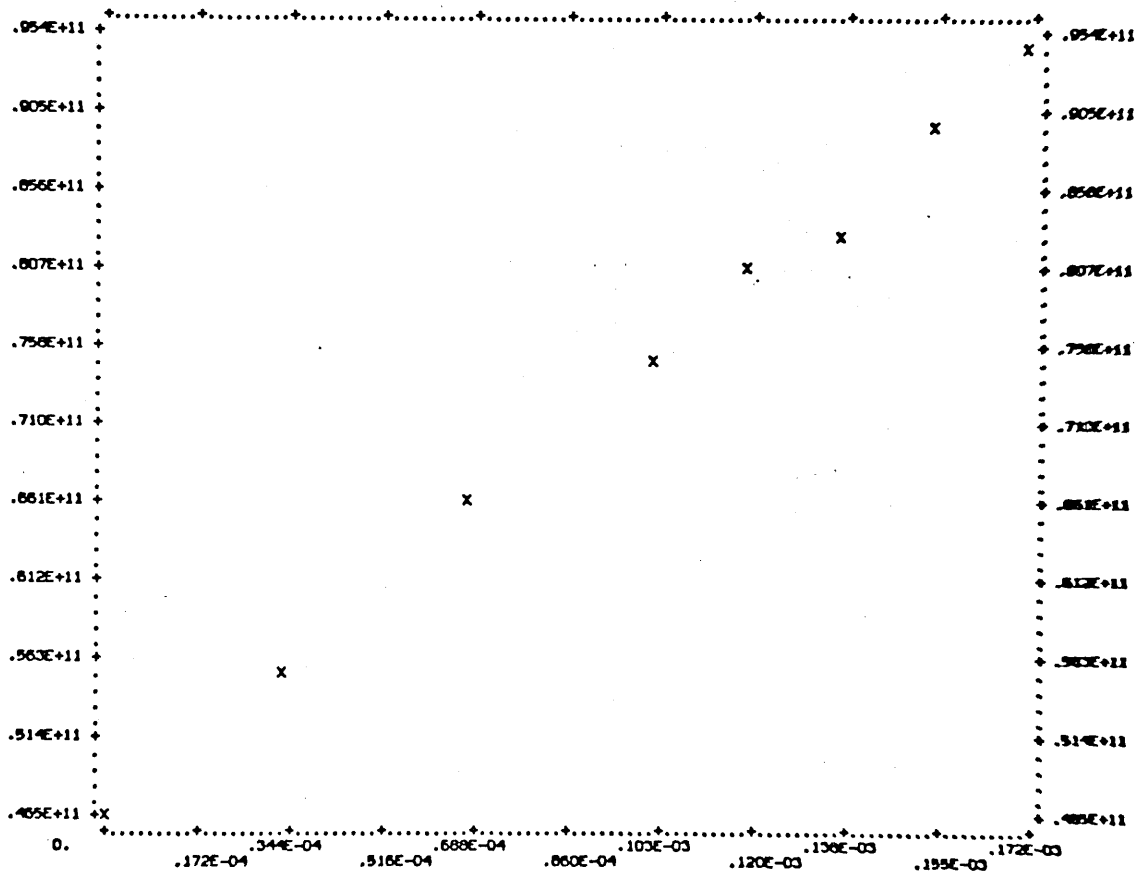

Fig.17

T	D						
293.0	64.4						
F1	F2	F3	I01	I1	I02	I2	P
100.0	350.0	100.0	54.2	47.5	61.8	24.5	6.000
100.0	400.0	150.0	41.7	39.2	50.4	20.8	6.600
100.0	425.0	175.0	35.5	36.0	44.3	19.0	6.900
100.0	450.0	200.0	30.6	32.9	39.9	17.5	7.300
100.0	475.0	225.0	26.4	31.9	36.2	17.3	7.600
100.0	500.0	250.0	22.6	31.4	32.3	17.4	8.000

VALUES OF Y= .6494E+11 .6945E+11 .7355E+11 .7441E+11 .7795E+11 .7756E+11

VALUES OF X== .6880E-04 .1032E-03 .1204E-03 .1376E-03 .1548E-03 .1720E-03

VALUES OF VBAR= .2482E+03 .2507E+03 .2518E+03 .2493E+03 .2504E+03 .2482E+03

SLOPE= .1315E+15

STANDARD DEVIATION= .1452E+14

INTERCEPT= .5639E+11

STANDARD DEVIATION= .1897E+10

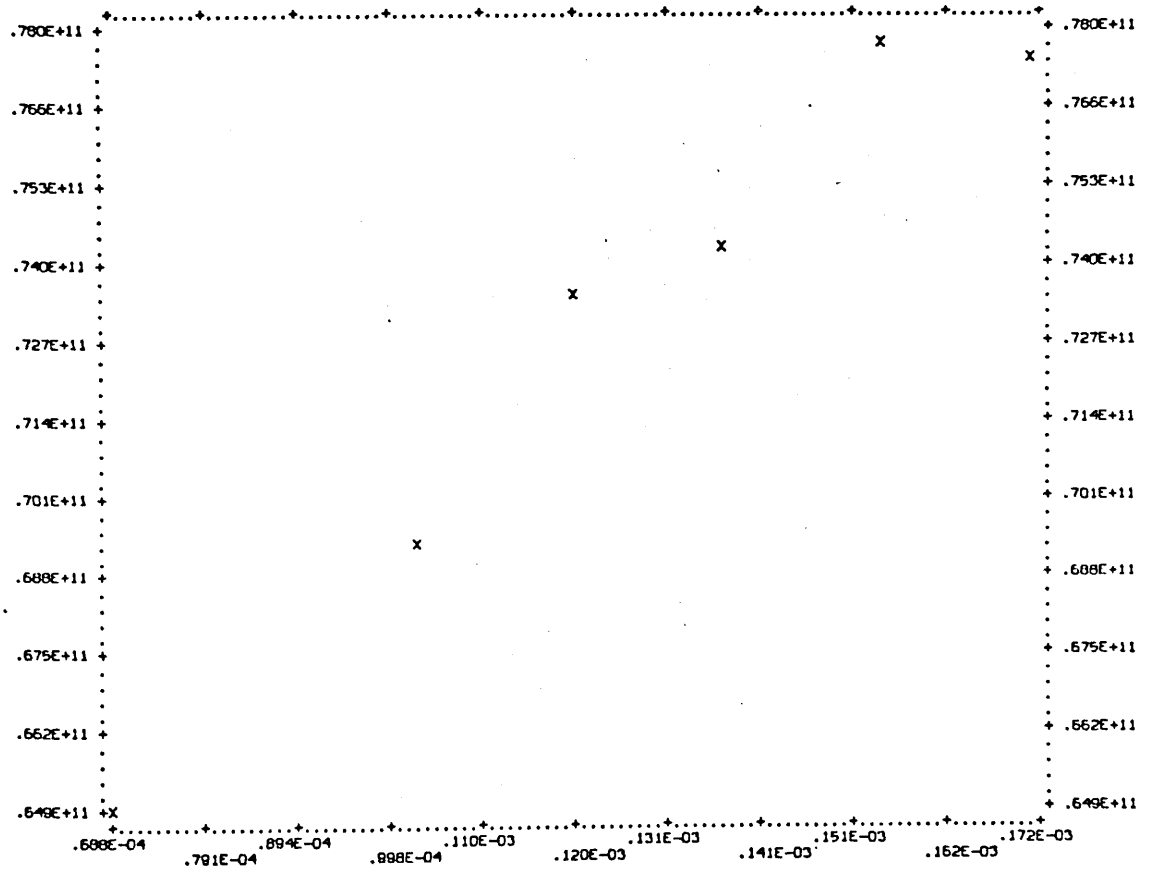

Fig.18

T	D
400.0	48.8

F1	F2	F3	I01	I1	I02	I2	P
50.0	250.0	0.0	100.0	72.3	100.0	59.6	5.400
50.0	300.0	50.0	100.0	59.9	100.0	48.6	6.300
50.0	350.0	100.0	100.0	51.6	100.0	41.1	7.100
50.0	400.0	150.0	100.0	45.1	100.0	34.7	8.100
50.0	425.0	175.0	100.0	42.3	100.0	32.2	8.600
50.0	450.0	200.0	100.0	39.9	100.0	29.9	9.000
50.0	475.0	225.0	100.0	37.9	100.0	28.2	9.400
50.0	500.0	250.0	100.0	35.0	100.0	25.6	10.000

VALUES OF Y= .4316E+11 .4671E+11 .5301E+11 .5857E+11 .5990E+11 .6447E+11 .6711E+11 .6781E+11

VALUES OF X== 0. .3440E-04 .6880E-04 .1032E-03 .1204E-03 .1376E-03 .1548E-03 .1720E-03

VALUES OF VBAR= .2510E+03 .2510E+03 .2545E+03 .2510E+03 .2495E+03 .2510E+03 .2523E+03 .2485E+03

SLOPE= .1528E+15

STANDARD DEVIATION= .5950E+13

INTERCEPT= .4248E+11

STANDARD DEVIATION= .6769E+09

DATA FOR 0+02+HE=03+HE

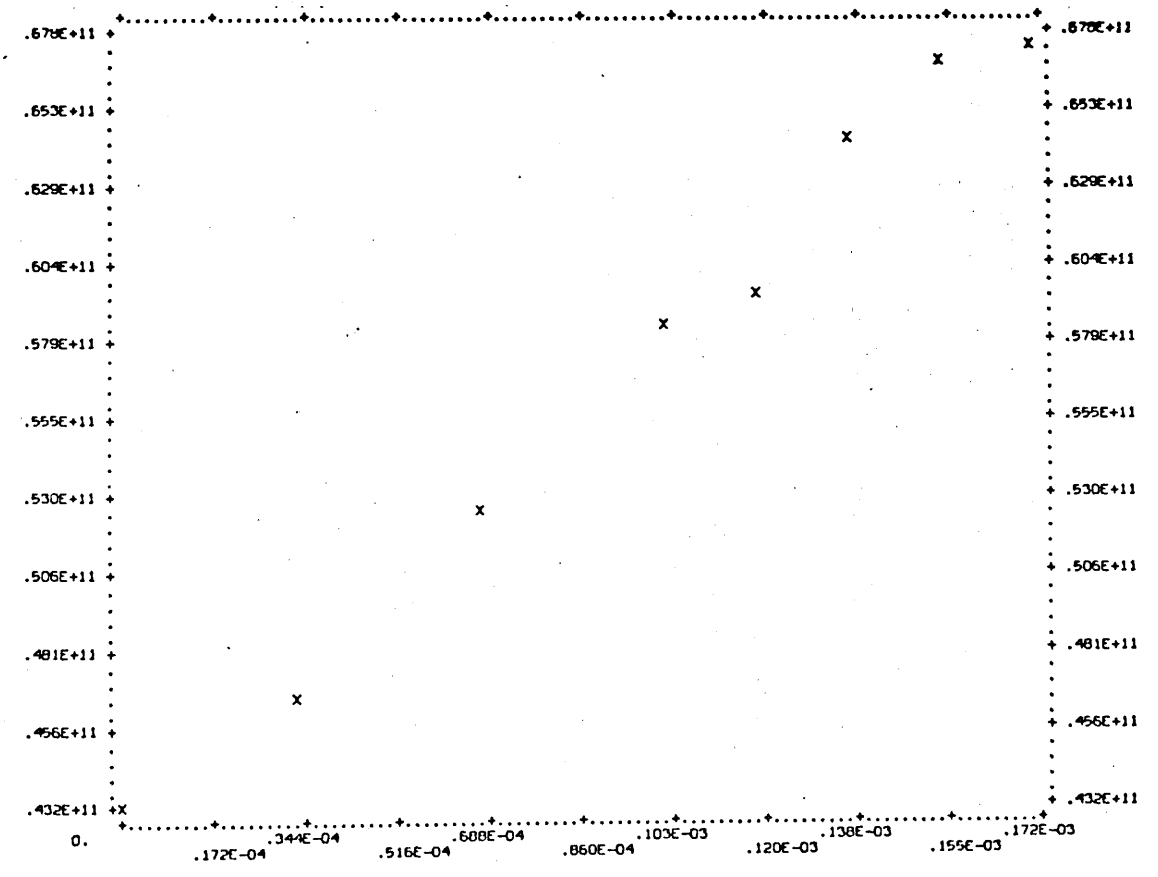

Fig.19

500.0 64.4

F1	F2	F3	I01	I1	I02	I2	P
50.0	100.0	100.0	10.4	22.1	11.3	20.1	4.200
50.0	150.0	150.0	13.5	21.4	14.4	18.2	5.600
50.0	200.0	200.0	15.1	19.7	16.0	15.8	7.100
50.0	250.0	250.0	16.7	17.1	17.6	13.1	8.400
50.0	300.0	300.0	54.5	46.5	56.9	33.3	9.900
50.0	350.0	350.0	58.5	43.8	60.9	30.7	11.200
50.0	400.0	400.0	62.8	35.9	64.8	23.8	12.500

VALUES OF Y= .1563E+11 .1990E+11 .2345E+11 .2802E+11 .3213E+11 .3475E+11 .3981E+11

VALUES OF X== .6880E-04 .1032E-03 .1376E-03 .1720E-03 .2064E-03 .2408E-03 .2752E-03

VALUES OF VBAR= .2017E+03 .2017E+03 .1989E+03 .2017E+03 .1997E+03 .2017E+03 .2033E+03

SLOPE= .1152E+15

STANDARD DEVIATION= .2752E+13

INTERCEPT= .7860E+10

STANDARD DEVIATION= .5098E+09

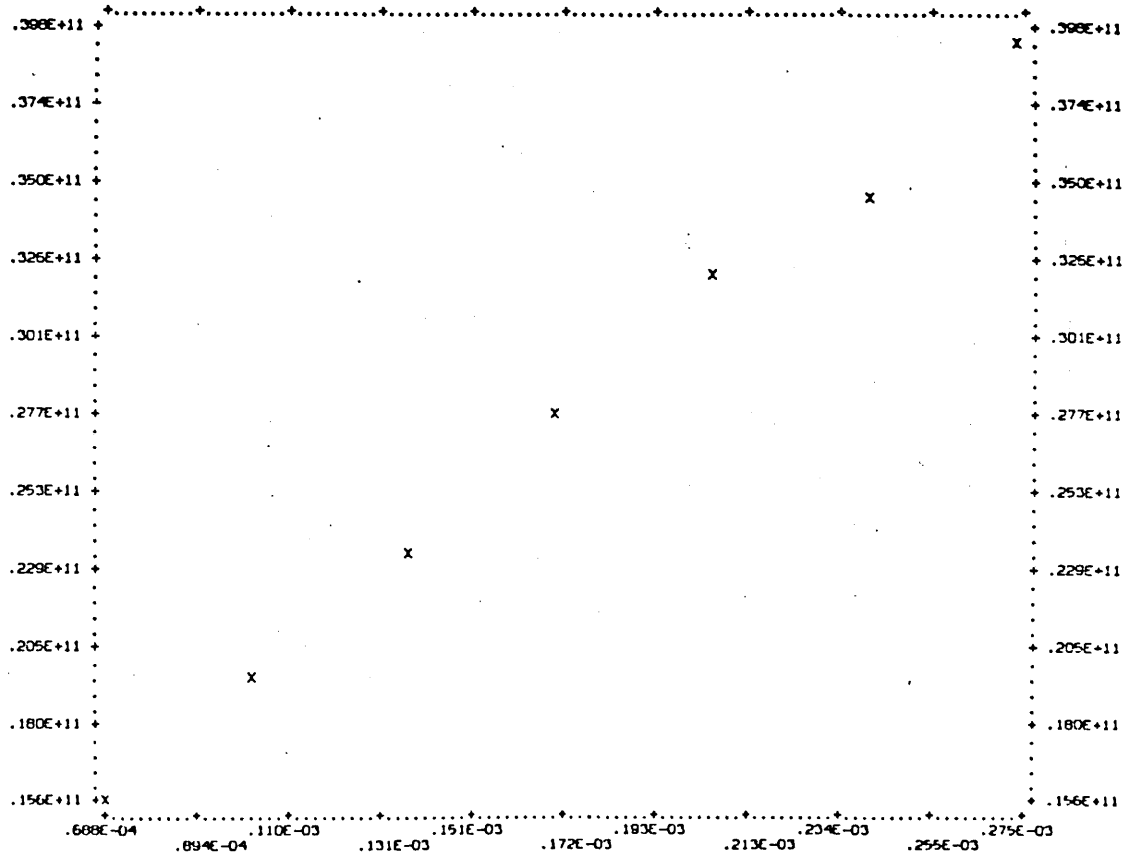

TABLE 4

Values of $k^{He}_{1.1}$, $(k_w - k^*_w)$, k^*_w, $(\gamma - \gamma^*)$ and γ^* for the reaction $0 + 0_2 + He$ at different temperatures

T/K	$k^{He}_{1.1}/10^{14}$ $cm^6\ mol^{-2}\ s^{-1}$	$(k_w - k^*_w)/s^{-1}$	$(\gamma - \gamma^*)x10^5$	k^*_w/s^{-1}	$\gamma^* x10^5$
196	(3.813 ± 0.113)x1/2	0.458 ± 0.030	2.24 ± 0.15		
196	(3.543 ± 0.1316)x1/2	0.277 ± 0.034	1.35 ± 0.166		
196	(3.875 ± 0.2235)x1/2	0.822 ± 0.059	4.02 ± 0.29		
196	(3.126 ± 0.2664)x1/2	0.092 ± 0.141	0.45 ± 0.69	0.161 ± 0.034	0.787 ± 0.1
196	(3.571 ± 0.2715)x1/2	0.192 ± 0.098	0.94 ± 0.48	0.073 ± 0.048	0.357 ± 0.23
196	(3.385 ± 0.2042)x1/2	2.330 ± 0.135	11.39 ± 0.6		
196	(3.775 ± 0.1616)x1/2	0.927 ± 0.107	4.53 ± 0.52		
Mean	1.792 ± 0.198	0.728 ± 0.773	3.56 ± 3.78	0.117 ± 0.062	0.572 ± 0.3
295	1.164 ± 0.1078	0.671 ± 0.055	2.674 ± 0.22	0.289 ± 0.033	1.15 ± 0.132
295	1.057 ± 0.1772	0.733 ± 0.100	2.92 ± 0.398	0.103 ± 0.095	0.41 ± 0.38
295	1.315 ± 0.1452	0.723 ± 0.088	2.88 ± 0.351	0.052 ± 0.043	0.21 ± 0.17
295	1.029 ± 0.0678	0.292 ± 0.045	1.16 ± 0.18		
295	(2.338 ± 0.2056)x1/2	0.781 ± 0.053	3.11 ± 0.21		
295	(2.621 ± 0.0734)x1/2	0.638 ± 0.019	2.54 ± 0.075		
295	(2.359 ± 0.3631)x1/2	1.087 ± 0.094	4.332 ± 0.0375		
295	(2.809 ± 0.3774)x1/2	1.388 ± 0.098	5.53 ± 0.39		
295	(2.236 ± 0.0765)x1/2	0.695 ± 0.050	2.77 ± 0.199		

TABLE 4 (Continued)

T/K	$k_{1.1}^{He}/10^{14}$ $cm^6\ mol^{-2}\ s^{-1}$	$(k_w - k_w^*)/s^{-1}$	$(\gamma - \gamma^*)x10^5$	k_w^*/s^{-1}	$\gamma^* x10^5$
295	(2.052 ± 0.1284)x1/2	0.758 ± 0.086	3.021 ± 0.343		
295	(2.198 ± 0.04135)x1/2	0.103 ± 0.027	0.41 ± 0.11		
295	(2.219 ± 0.0843)x1/2	0.776 ± 0.022	2.89 ± 0.088		
Mean	1.169 ± 0.108	0.720 ± 0.325	2.85 ± 1.295	0.148 ± 0.125	0.59 ± 0.5
400	(1.282 ± 0.0877)x1/2	0.429 ± 0.023	1.47 ± 0.0786		
400	(1.698 ± 0.0779)x1/2	0.421 ± 0.020	1.44 ± 0.068		
400	(1.528 ± 0.0595)x1/2	0.458 ± 0.016	1.566 ± 0.055		
400	(1.805 ± 0.1253)x1/2	0.414 ± 0.033	1.416 ± 0.113		
Mean	0.789 ± 0.045	0.43 ± 0.019	1.471 ± 0.065		
500	(1.031 ± 0.123)x1/2	0.472 ± 0.081	1.44 ± 0.095		
500	(1.251 ± 0.0627)x1/2	0.228 ± 0.041	0.697 ± 0.125		
500	(1.115 ± 0.0275)x1/2	0.141 ± 0.018	0.431 ± 0.055		
500	(1.095 ± 0.0359)x1/2	0.055 ± 0.010	0.168 ± 0.031		
500	(1.163 ± 0.045)x1/2	0.045 ± 0.012	0.1377 ± 0.038		
500	(1.089 ± 0.124)x1/2	0.031 ± 0.034	0.095 ± 0.104		
Mean	0.562 ± 0.040	0.162 ± 0.169	0.496 ± 0.517		

CHAPTER 6

A STUDY OF THE REACTION $O + SO_2 + M \longrightarrow SO_3 + M$

6.1 Introduction.

The homogeneous rate of recombination of $O(^3P)$ atoms with SO_2 has been studied at temperatures between 240-500K. Rates of recombination by the reaction:

$$O + SO_2 + M \longrightarrow SO_3 + M \qquad 2.1$$

were measured for four third bodies, viz: M = SO_2, N_2, He and Ar; the temperature range 240-500K was covered only for M = SO_2. The rate constant for M = SO_2 at 298K is the subject of great controversy in the literature and the measurement of the temperature coefficient of this is attempted for the first time.

When SO_2 is added to a stream of O atoms in a carrier gas M, the possible reactions are:

$O + Wall$	=	$\frac{1}{2} O_2 + Wall$	W
$O + SO_2 + M$	=	$SO_3 + M$	2.1
$O + NO + M$	=	$NO_2 + O_2$	
$O + NO_2$	=	$NO + O_2$	12
$O + O + M$	=	$O_2 + M$	1.4

When reaction 1.4 can be neglected (provided $k_{1.4}[O] \ll k_{2.1}[SO_2]$), all the reaction steps are first order with respect to O atoms. A rate equation was developed similar to the equation 18 only replacing O_2 by SO_2 (Chapter 4). The rate equation for reaction 2.1 thus becomes:

$$\frac{V^3}{F(SO_2)V_R} \ln\left(\frac{I_1 I_2^*}{I_2 I_1^*}\right) = \frac{V^2}{F(SO_2)}\left(k_w - k_w^*\right) + k_{2.1}^{SO_2} F(SO_2) + \Sigma k_{2.1}^{M} F(M)$$

$$+ 2 F(NO)\left\{k_{12}^{SO_2} - k_{12}^{M}\right\} \qquad 18'$$

6.2 Preliminary Investigations.

The reaction system used to study the reaction is similar to that described previously (Chapter 2). The discharge gases were purified by passing through a "deoxo" unit and a molecular sieve trap at 77K. Oxygen atoms were generated in excess argon by a microwave discharge. The argon fed to the discharge contained 0.05 to 0.25% oxygen. The concentration of oxygen atoms was allowed to increase to a reasonably extent so that a sufficient intensity signal was produced to record. The SO_2 was metered by a calibrated MeteRate flow meter tubes (Glass Precision Engineering Ltd). Sulphur dioxide caused no special problems in this regard and metering was reproducible to better than 1% at a given setting. Sulphur dioxide was used directly from a cylinder and passed through a trap containing glass beads.

The decay of 0 atoms was monitored at a fixed position downstream from the reactor. When SO_2 was added to the reaction system, the intensity signal decreased considerably. Sulphur dioxide was then injected through another inlet jet further upstream from the first one. The surprising observation was that most of the NO- afterglow was consumed by the addition of SO_2 through inlet jet J1. It was realized in the first instance that the reaction might be faster than that reported by other investigators.

The intensity signal, recorded by the digital voltmeter, usually, approached a constant value within a few seconds. But in this case, the signal intensity decayed continuously and never reached a constant value. Some measurements were made at the inlet jets J5 and J4 (Fig. 3) where it was possible to record an intensity signal, although it was realized that 0 atoms were decaying slowly. These measurements were made only to assess the apparent reasons of discrepancies in the literature. A series of experiments were commenced for M = SO_2 and Ar at 295K. The rate constants for these experiments are summarized in Table 5. For M = SO_2, flow rate of argon through the discharge was 137.6 μmol s^{-1} and the flow rate of SO_2 was varied from 20.64-90 μ mol s^{-1}. Flow velocity was varied between 156 to 333.2 cm s^{-1} in a typical experiment. For M = Ar, the flow rate of argon through the discharge was 172 μ mol s^{-1}, and the flow rate of argon through the third body inlet jets varied from 0-172 μ mol s^{-1} at constant flow velocity between 250-300 cm s^{-1}. The plots of decay rate of 0 atoms against F(M) were generally linear, however, for M = SO_2, a smooth curve was obtained. The values obtained were not reproducible within the range of existing data at 295K. This irreproducibility could be due to the catalytic effect of the surface; this could also be a cause of instability of the 0 atom decay signal. It was observed that the instability of the intensity signal increased with the increasing concentration of $O(^3P)$ atoms. The SO_3 produced in the reaction might increase the catalytic action of the walls on the recombination of 0 atoms (Kaufman[32]). Some oily deposit was found in the reactor, this was presumed to be H_2 SO_4 since it could not be removed by pumping. Its presence might be one of the reasons for non-reproducible

TABLE 5

Preliminary Results for $O + SO_2 + M \longrightarrow SO_3 + M$ at 295K

M	$10^{-15} k_{2.1}^{Ar}$ $cm^6\ mol^{-2}\ s^{-1}$
Ar	2.08 ± 0.13
	1.4 ± 0.09
	0.78 ± 0.007
SO_2	7.511 ± 0.43
	6.023 ± 0.71
	4.32 ± 0.43

results[90]. The results obtained in these preliminary investigations, therefore, add general support to the conclusion of Kaufman, and Mulcahy that SO_3-poisoned surfaces give rise to non-reproducible results due to a variable catalytic efficiency.

6.3 Detailed Study of the Reaction.

$$O + SO_2 + SO_2 \longrightarrow SO_3 + SO_2$$

In the preliminary investigations it was difficult to obtain stable rates of disappearance of O after SO_2 had been introduced into the reaction system. It was possible, however, to obtain stable decay signal using comparatively low concentrations of oxygen atoms. After the preliminary investigations the whole reaction system was dismantled and cleaned with surface active agents (Decon 90) and washed with distilled water. The surface was not poisoned with syrupy phosphoric acid. The reaction tube was then dried in an oven at about 400K and after drying, it was fitted in the flow line and pumped for two or three days.

The first experiments performed in the newly cleaned tube used SO_2 as third body. The general experimental and data collection procedure was the same as that adopted previously (5.2). It was found to be very important to dry all the reagents before admitting them into the reactor. The Ar-O_2 mixture was passed through a molecular sieve trap at liquid nitrogen temperature. The SO_2 gas (about 98.98% pure) was passed through a trap containing Drierite to remove water from the system. The experiments were performed under Pseudo-first order conditions with SO_2 in large excess over atomic oxygen. Some NO was added through the inlet jet J6 just before the photomultiplier to facilitate detection of low concentrations

of oxygen atoms. The flow of Ar through the discharge was 173.6 μ mol s^{-1}. The oxygen fed into the discharge was less than 0.02% of the total flow in the discharge. The flow rate of SO_2 (20.64-90 μ mol s^{-1}) was varied through the inlet jets keeping $\frac{V^2}{F(SO_2)}$ constant in successive measurements. The intensity measured at inlet jet J5 and J2 approached a constant value within a few seconds and was steady enough to record. The data obtained in this way in a series of measurements was used to calculate the L.H.S. of the equation 18′ and this was plotted against $F(SO_2)$. The results of representative experiments at temperatures 240-500K are presented in Figures 20-23. The measurements at lower temperatures were more convenient than those at higher temperatures; at higher temperatures the surface of the reaction tube became increasingly catalytic possibly due to the enhanced formation of SO_3. The flow velocity was changed to a maximum of 500 cm s^{-1} to achieve reproducibility. As before, the rate constant $k_{2.1}^{SO_2}$ was evaluated from the slope of each line at each temperature and values of $(k_w - k_w^*)$ and k_w^* from the intercepts (Table 6). The graph of $\lg k_{2.1}^{SO_2}$ against $10^3/T$ (Fig. 24) is linear over the temperature range 240-500K. The precision of each measurement is indicated by the attached error bars. The values of $k_{2.1}^{SO_2}$ vary approximately as $T^{2.5}$ (Fig. 25). The value of the absolute rate constants for SO_2 as third body at 295K is $30.5125 \pm 1.852 \times 10^{14}$ cm^6 mol^{-2} s^{-1} (Table 6), this is significantly lower than the literature value. This value supports the view of Westenberg and Dettaas[98] regarding the stoichiometry of the reaction 2.1 (Chapter 7).

Figs. 20-23

Graphs of $\frac{V^3}{V_R F(SO_2)} \ln \frac{I_1 I_2^*}{I_2 I_1^*}$ represented by Y

against $F(SO_2)$ represented by X (equation 18') for the reaction:

$$O + SO_2 + SO_2 = SO_3 + SO_2 \qquad 2.1$$

In the tabulated data at the head of each graph

F_1 is the flow rate of sulphur dioxide ($cm^3\ min^{-1}$);

F_3 the flow rate of sulphur dioxide ($cm^3\ min^{-1}$);

I_1 the intensity when sulphur dioxide was passed through jet J5;

I_2 the intensity when sulphur dioxide was passed through jet J2;

T, D, F_2, I01, IO_2, VBAR and P represent usual meaning as for figs. 5-9 (P. 74).

Fig. 20. M = SO_2, T = 240K

Fig. 21. M = SO_2, T = 295K

Fig. 22. M = SO_2, T = 400K

Fig. 23. M = SO_2, T = 500K

Fig.20

T	D
240.0	48.8

F1	F2	F3	I01	I1	I02	I2	P
30.0	200.0	30.0	100.4	72.4	102.0	9.7	4.000
50.0	200.0	50.0	63.0	45.5	64.0	8.5	3.300
70.0	200.0	70.0	48.4	35.6	49.2	6.9	3.100
90.0	200.0	90.0	40.0	26.8	40.8	5.7	2.900
110.0	200.0	110.0	32.6	20.2	33.6	4.3	2.800
130.0	200.0	130.0	27.8	17.3	28.4	4.0	2.700

VALUES OF Y= .1807E+12 .2072E+12 .2201E+12 .2451E+12 .2739E+12 .2937E+12

VALUES OF X== .2064E-04 .3440E-04 .4816E-04 .6192E-04 .7568E-04 .8944E-04

VALUES OF VBAR= .1559E+03 .2054E+03 .2361E+03 .2711E+03 .3001E+03 .3313E+03

SLOPE= .1640E+16

STANDARD DEVIATION= .7085E+14

INTERCEPT= .1465E+12

STANDARD DEVIATION= .4240E+10

DATA FOR 0+S02+S02=S03+S02

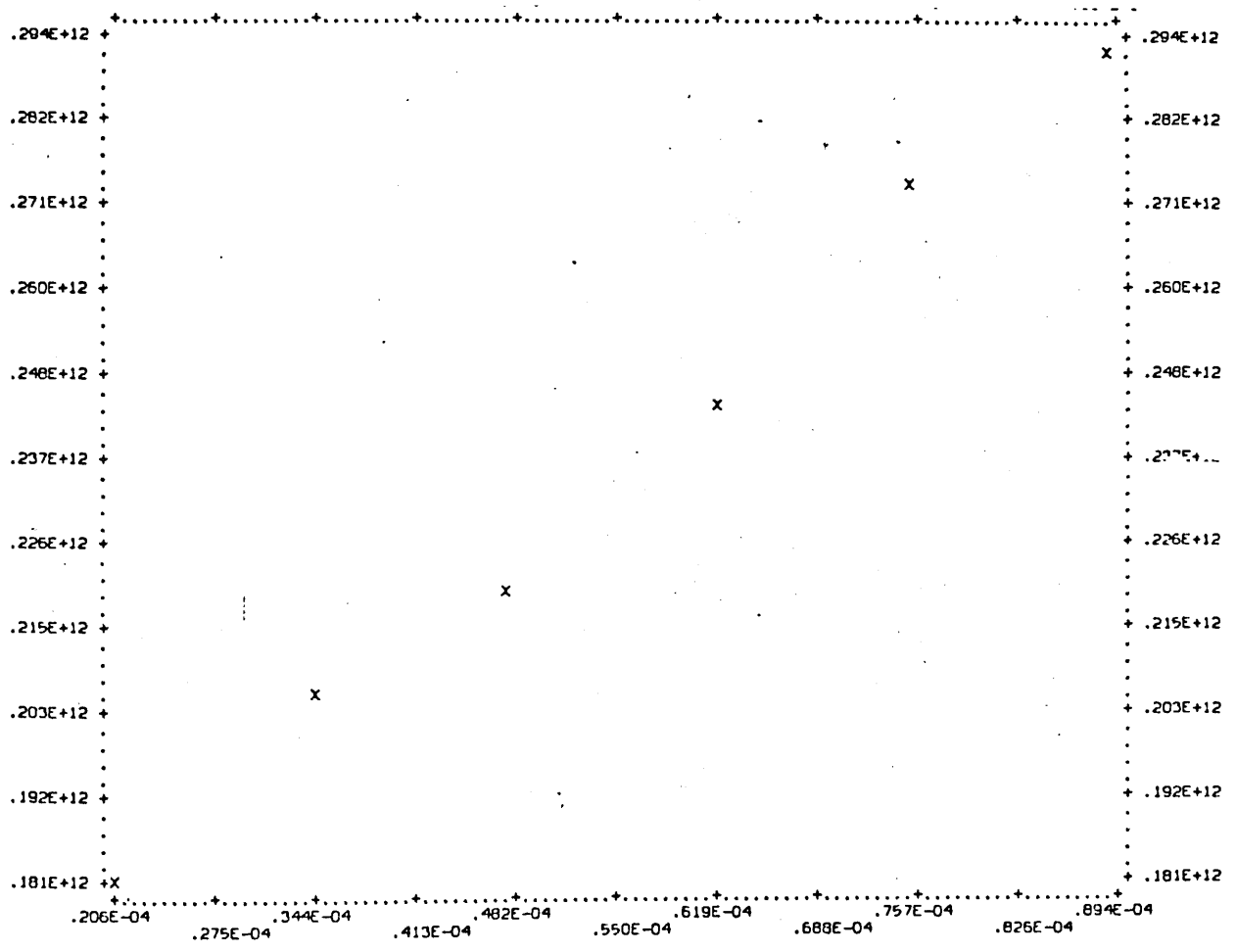

Fig.21

T	D
295.0	48.8

F1	F2	F3	I01	I1	I02	I2	P
30.0	200.0	30.0	98.0	77.4	100.8	4.8	4.900
50.0	200.0	50.0	69.6	58.6	70.8	4.4	4.100
70.0	200.0	70.0	52.8	51.9	54.0	4.2	3.800
90.0	200.0	90.0	43.6	42.9	44.4	3.6	3.600
110.0	200.0	110.0	35.6	34.0	36.8	3.3	3.400
130.0	200.0	130.0	31.6	30.0	32.4	3.0	3.300

VALUES OF Y= .2530E+12 .3088E+12 .3397E+12 .3789E+12 .4260E+12 .4679E+12

VALUES OF X== .2064E-04 .3440E-04 .4816E-04 .6192E-04 .7568E-04 .8944E-04

VALUES OF VBAR= .1564E+03 .2032E+03 .2368E+03 .2684E+03 .3038E+03 .3332E+03

SLOPE= .3042E+16

STANDARD DEVIATION= .9960E+14

INTERCEPT= .1950E+12

STANDARD DEVIATION= .5961E+10

DATA FOR 0+S02+S02=S03+S02

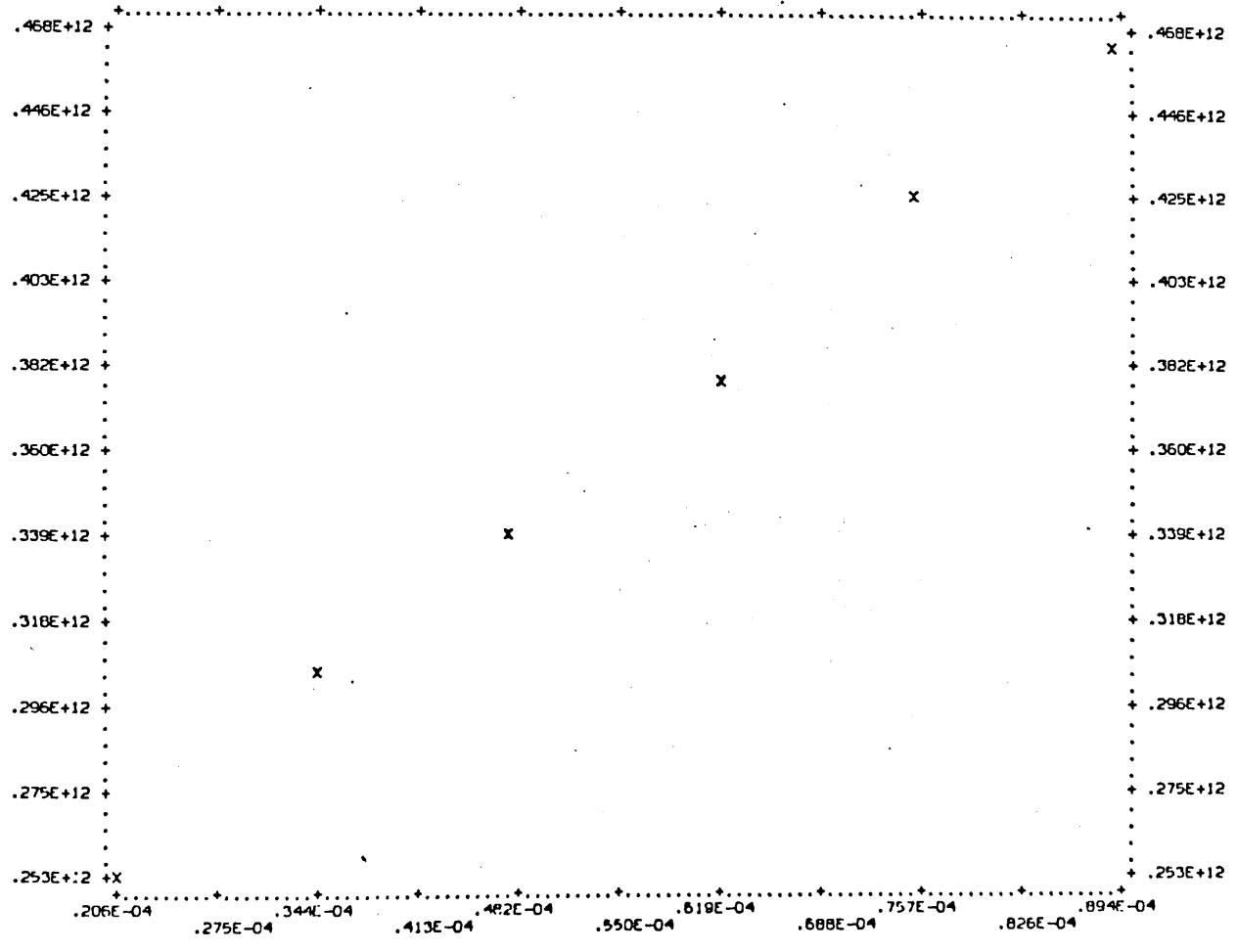

Fig.22

T	D
400.0	48.8

F1	F2	F3	I01	I1	I02	I2	P
30.0	200.0	30.0	88.6	42.0	89.2	4.6	4.000
50.0	200.0	50.0	62.5	20.9	63.9	2.6	3.400
70.0	200.0	70.0	46.6	15.4	47.7	2.7	3.100
90.0	200.0	90.0	36.6	11.3	37.3	2.3	2.900
110.0	200.0	110.0	31.2	6.9	32.2	1.4	2.800
130.0	200.0	130.0	26.8	5.3	27.6	1.2	2.700

VALUES OF Y= .9159E+12 .1091E+13 .1085E+13 .1166E+13 .1308E+13 .1386E+13

VALUES OF X== .2064E-04 .3440E-04 .4816E-04 .6192E-04 .7568E-04 .8944E-04

VALUES OF VBAR= .2598E+03 .3322E+03 .3935E+03 .4518E+03 .5002E+03 .5522E+03

SLOPE= .6398E+16

STANDARD DEVIATION= .7385E+15

INTERCEPT= .8065E+12

STANDARD DEVIATION= .4419E+11

DATA FOR 0+S02+S02=S03+S02

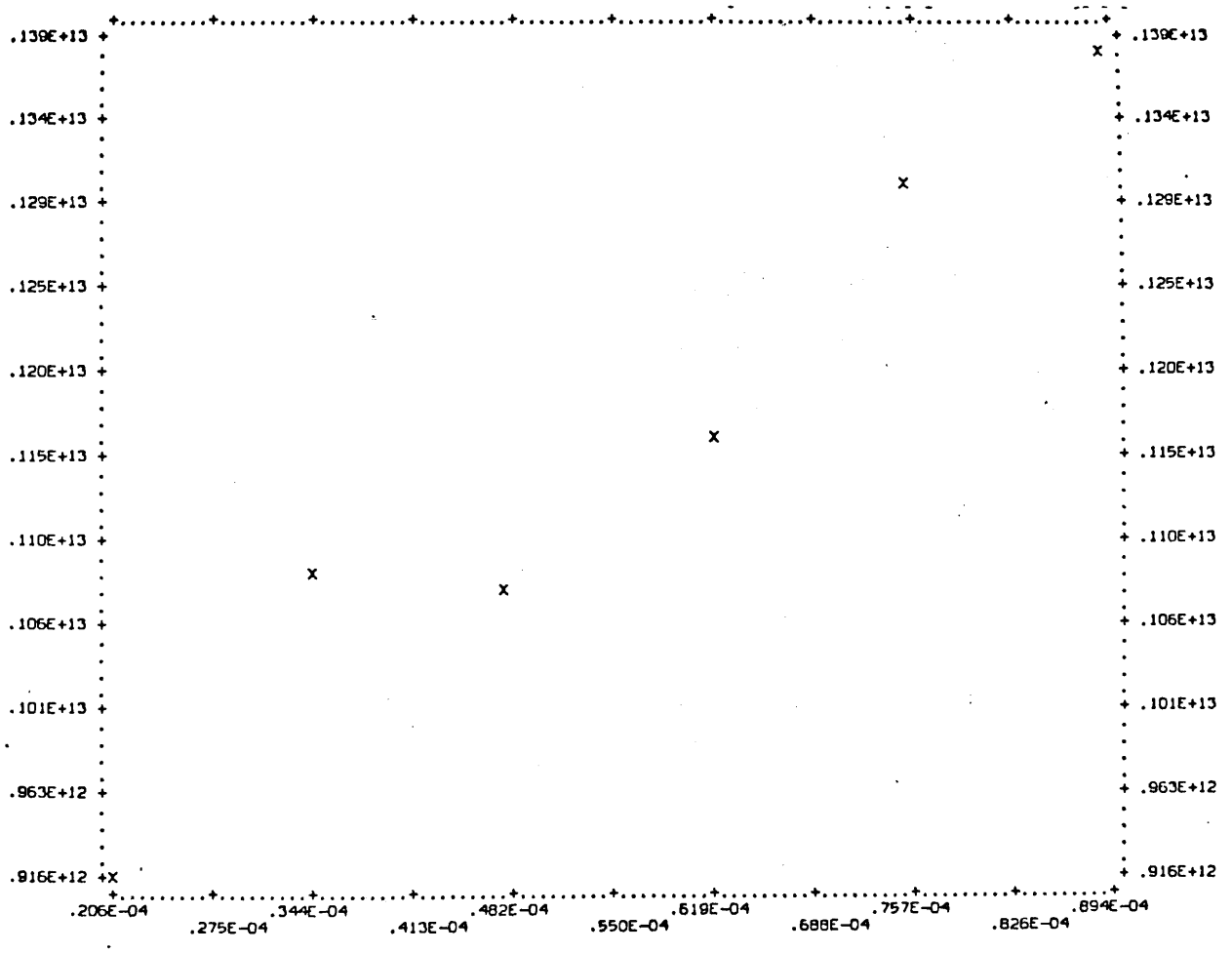

Fig.23

T	D
500.0	48.8

F1	F2	F3	I01	I1	I02	I2	P
30.0	200.0	30.0	74.1	66.6	75.7	8.8	4.300
50.0	200.0	50.0	54.5	47.2	55.9	8.0	3.600
70.0	200.0	70.0	42.8	42.6	44.1	8.7	3.300
90.0	200.0	90.0	37.5	33.5	39.0	6.7	3.200
110.0	200.0	110.0	31.5	27.2	33.1	5.7	3.100
130.0	200.0	130.0	28.5	24.5	29.6	5.5	3.000

VALUES OF Y= .1328E+13 .1534E+13 .1611E+13 .1735E+13 .1865E+13 .1996E+13

VALUES OF X== .2064E-04 .3440E-04 .4816E-04 .6192E-04 .7568E-04 .8944E-04

VALUES OF VBAR= .3021E+03 .3922E+03 .4621E+03 .5118E+03 .5648E+03 .6212E+03

SLOPE= .9253E+16

STANDARD DEVIATION= .5024E+15

INTERCEPT= .1169E+13

STANDARD DEVIATION= .3007E+11

DATA FOR 0+S02+S02=S03+S02

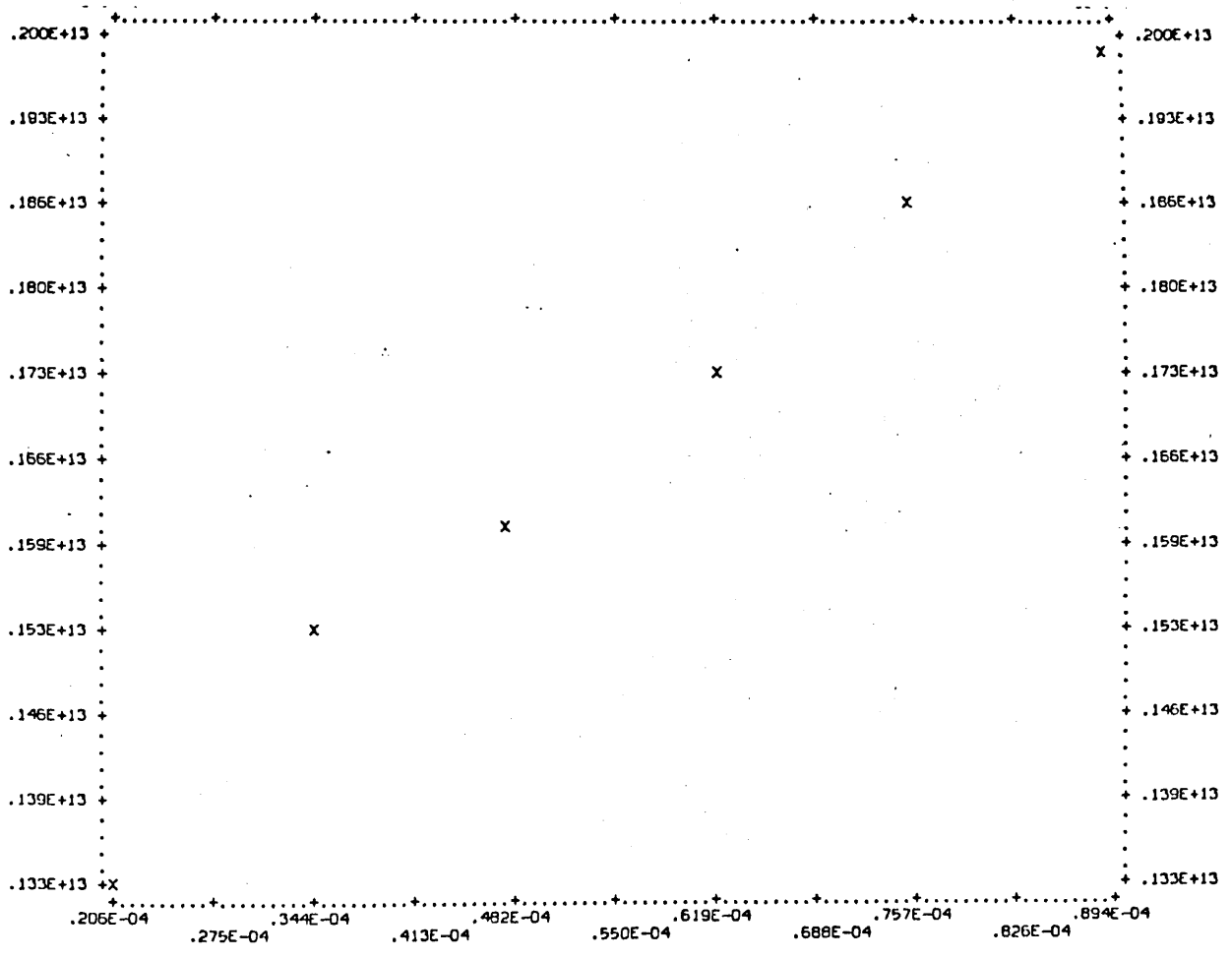

TABLE 6

Values of $k_{2.1}^{SO_2}$, $k_w - k_w^*$ and k_w^* for the reaction: $O + SO_2 + SO_2 = SO_3 + SO_2$ at Different Temperatures

T/K	$k_{2.1}/10^{14}$ $cm^6\ mol^{-2}\ s^{-1}$	$(k_w - k_w^*)/s^{-1}$	$(\gamma - \gamma^*) \times 10^4$
240	16.74 ± 0.948	4.624 ± 0.2004	2.04 ± 0.0885
240	16.4 ± 0.708	4.3096 ± 0.1498	1.9042 ± 0.0662
240	16.23 ± 1.486	4.55 ± 0.3142	2.01 ± 0.1388
Mean	16.456 ± 1.047	4.4945 ± 0.2215	1.986 ± 0.0978
295	30.42 ± 0.996	4.096 ± 0.21	1.63 ± 0.0835
295	31.69 ± 1.971	4.297 ± 0.417	1.71 ± 0.166
295	28.98 ± 2.33	-	-
295	30.96 ± 2.15	4.35 ± 0.4589	1.35 ± 0.075
Mean	30.5125 ± 1.862	4.2476 ± 0.3619	1.69 ± 0.144
400	63.98 ± 7.385	7.18 ± 0.568	2.455 ± 0.194
400	66.25 ± 5.485	7.1245 ± 0.422	2.436 ± 0.144
Mean	65.115 ± 6.435	7.15225 ± 0.495	2.455 ± 0.169
500	109.7 ± 6.83	5.658 ± 0.3969	1.731 ± 0.1245
500	99.18 ± 7.622	6.066 ± 0.443	1.856 ± 0.1355
500	92.53 ± 5.024	6.47 ± 0.296	1.9798 ± 0.0906
Mean	100.47 ± 6.492	6.0647 ± 0.379	1.856 ± 0.1168

TABLE 6 (Continued)

T/K	k_w^*/s^{-1}	$\gamma^* \times 10^5$
240	0.1874 ± 0.0508	0.8280456 ± 0.224
240	0.2026 ± 0.0626	0.8952 ± 0.2766
240	0.2026 ± .06256	0.8952 ± 0.2764
Mean	0.1975 ± 0.0586	0.872815 ± 0.259
298	0.0528 ± 0.11	0.210 ± 0.4378
298	0.024 ± 0.0517	0.0955 ± 0.2057
298	0.21 ± 0.2828	0.8358 ± 1.125
Mean	0.0956 ± 0.148	0.3804 ± 0.589
400	0.7089 ± 0.1487	2.424 ± 0.5085
400	0.7117 ± 0.1386	2.434 ± 0.474
Mean	0.7103 ± 0.1436	2.429 ± 0.491
500	1.148 ± 0.2297	3.513 ± 0.7855
500	0.8726 ± 0.1537	2.670 ± 0.4703
500	0.873 ± 0.154	2.671 ± 0.471
Mean	0.9645 ± 0.179	2.95 ± 0.5756

FIGURE 24: PLOT OF Log $k_{2.1}^{SO_2}$ AGAINST (1/T) X 10^3

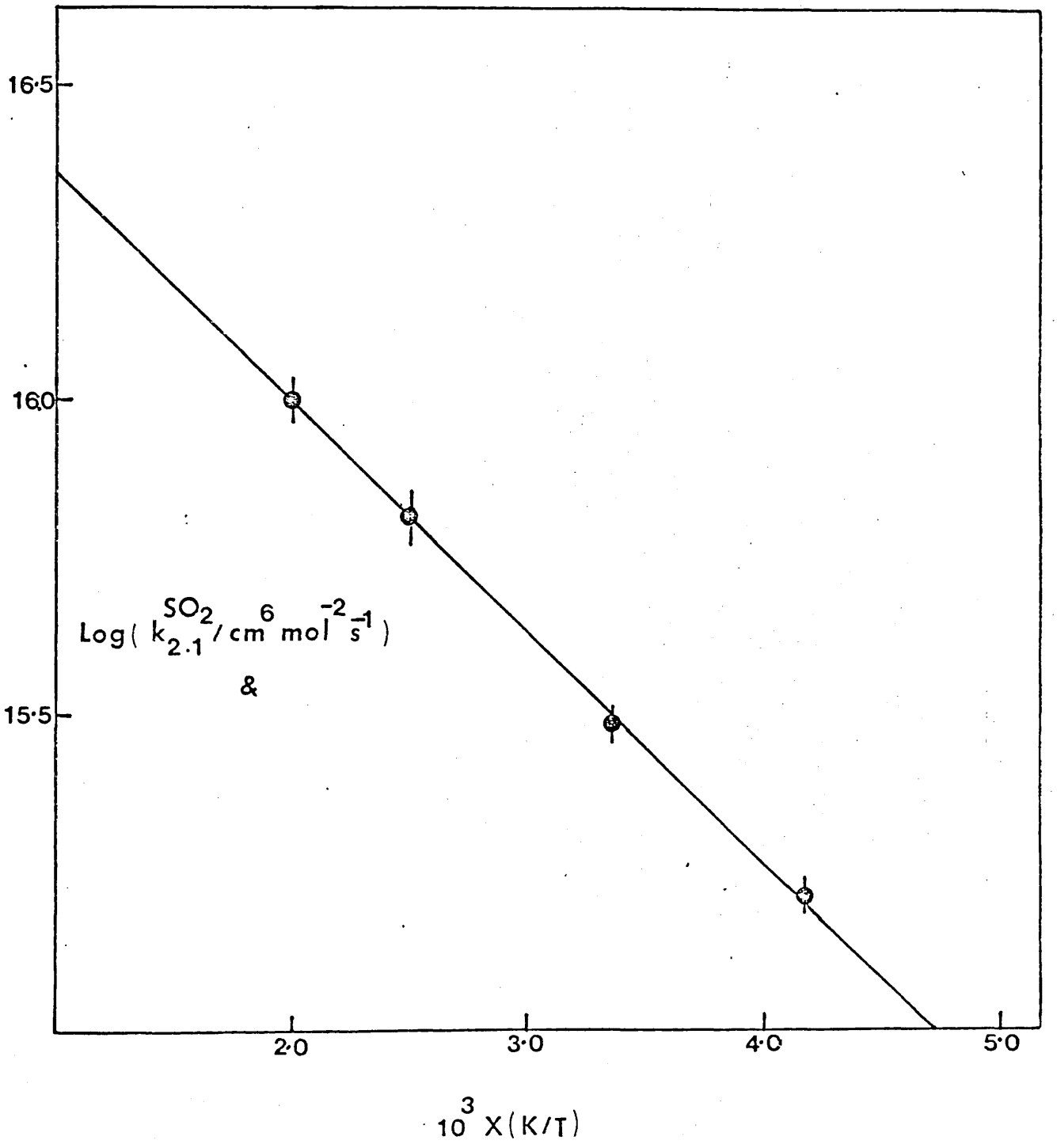

FIG 25: PLOT OF Log $k_{2.1}^{SO_2}$ AGAINST Log T

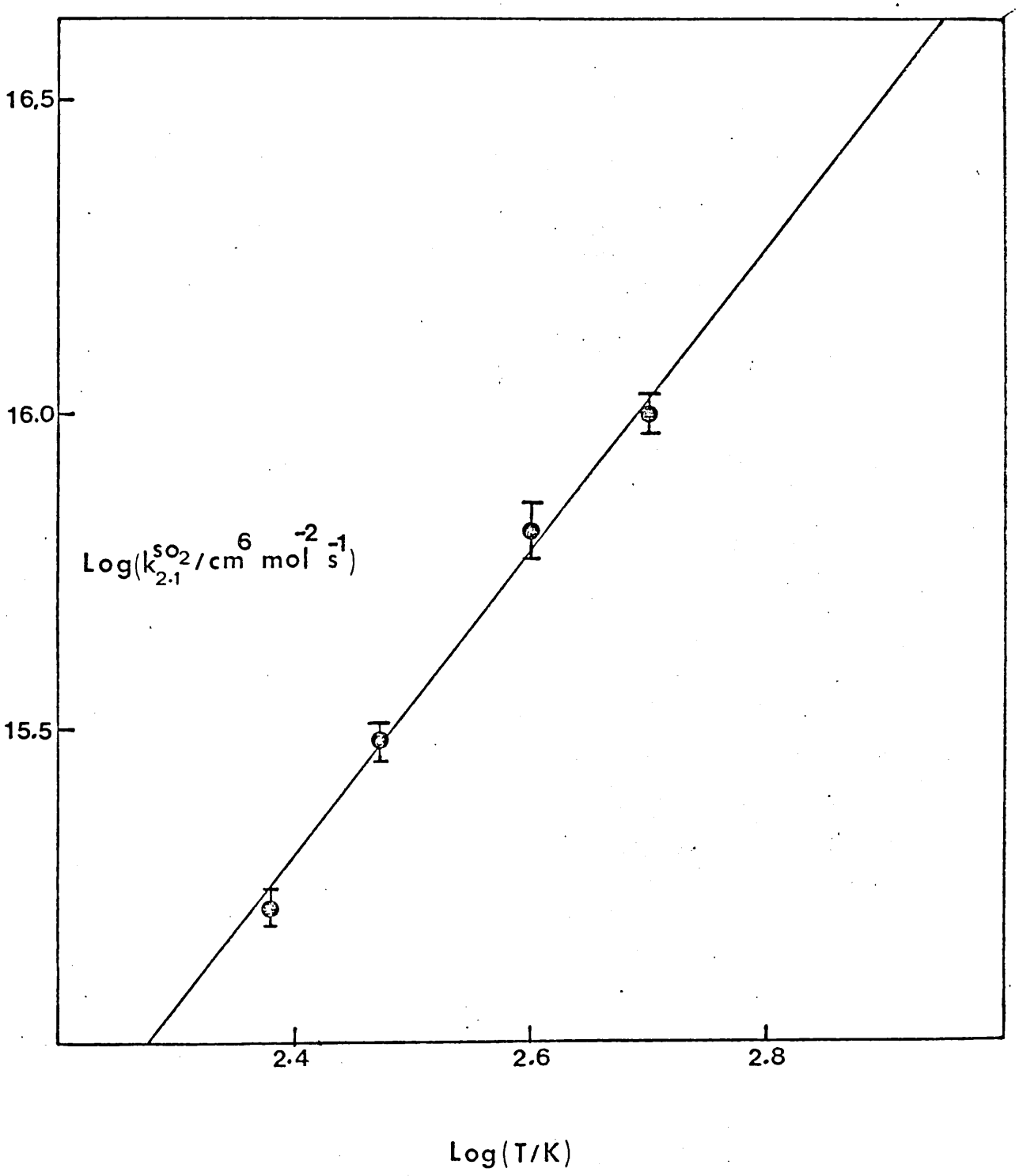

6.4 Detailed Study of the Reaction.

$O + SO_2 + M \longrightarrow SO_3 + M$ where M = N_2, He and Ar at 298 $\pm$ 2K

The reaction 2.1 was studied at 298 $\pm$ 2K using N_2, He and Ar as the third body. The general experimental technique (Chapter 2) was followed. All the flow gases were purified as described (6.3). $O(^3P)$ atoms were generated by microwave discharge in a trace of O_2 (<0.25%) carried in Ar (173.6 μ mol s^{-1}). The gas used as third body (flow rate 0-275 μ mol s^{-1}) was introduced through the third body inlet jets. The rate constants for each third body were measured at two different flow rate of SO_2 (Figures 26-31). The rate constant obtained from the slopes of this lines for M = N_2, He and Ar are summarized in Tables 7, 8, 9 respectively. Except for Ar, there is a considerable decrease in the rate constant when excess SO_2 is introduced into the reaction system. The results obtained ~~is~~ are discussed and compared with those of other investigators in Chapter 7.

Figs. 26-31

Graphs of $\frac{V^3}{V_R F(SO_2)} \ln \frac{I_1 I_2^*}{I_2 I_1^*}$ represented by Y

against F(M) represented by X (equation 18') for the reaction:

$$O + SO_2 + M \rightleftharpoons SO_3 + M \qquad 2.1$$

In the tabulated data at the head of each graph

F_1 is the flow rate of sulphur dioxide ($cm^3\ min^{-1}$);

F_3 the flow rate of M ($cm^3\ min^{-1}$);

I_1 the intensity when sulphur dioxide was passed through jet J5;

I_2 the intensity when sulphur dioxide was passed through jet J2;

T, D, F_2, I01, IO_2, VBAR and P represent usual meaning as for figs. 5-9 (P. 74).

Fig. 26. M = N_2, Flow of SO_2: 34.4 μ mole s^{-1}

Fig. 27. M = N_2, " 68.8 μ mole s^{-1}

Fig. 28. M = He, " 34.4 μ mole s^{-1}

Fig. 29. M = He, " 68.8 μ mole s^{-1}

Fig. 30. M = Ar, " 34.4 μ mole s^{-1}

Fig. 31. M = Ar, " 68.8 μ mole s^{-1}

RN2

Fig. 26

T	D
298.0	48.8

F1	F2	F3	I01	I1	I02	I2	P
50.0	250.0	0.0	100.0	81.0	100.0	6.1	3.900
50.0	300.0	50.0	100.0	75.8	100.0	4.3	4.600
50.0	350.0	100.0	100.0	71.0	100.0	3.5	5.200
50.0	400.0	150.0	100.0	61.8	100.0	2.2	5.900
50.0	450.0	200.0	100.0	56.4	100.0	1.7	6.500
50.0	500.0	250.0	100.0	48.6	100.0	1.2	7.200
50.0	550.0	300.0	100.0	40.8	100.0	.7	7.900
50.0	600.0	350.0	100.0	35.2	100.0	.5	8.600
50.0	650.0	400.0	100.0	29.3	100.0	.3	9.300

VALUES OF Y= .6343E+12 .6810E+12 .7382E+12 .7974E+12 .8588E+12 .8890E+12 .9597E+12 .9897E+12 .1053E+13

VALUES OF X== 0. .3440E-04 .6880E-04 .1032E-03 .1376E-03 .1720E-03 .2064E-03 .2408E-03 .2752E-03

VALUES OF VBAR= .2589E+03 .2561E+03 .2589E+03 .2567E+03 .2589E+03 .2571E+03 .2556E+03 .2544E+03 .2534E+03

SLOPE= .1519E+16

STANDARD DEVIATION= .3445E+14

INTERCEPT= .6356E+12

STANDARD DEVIATION= .5641E+10

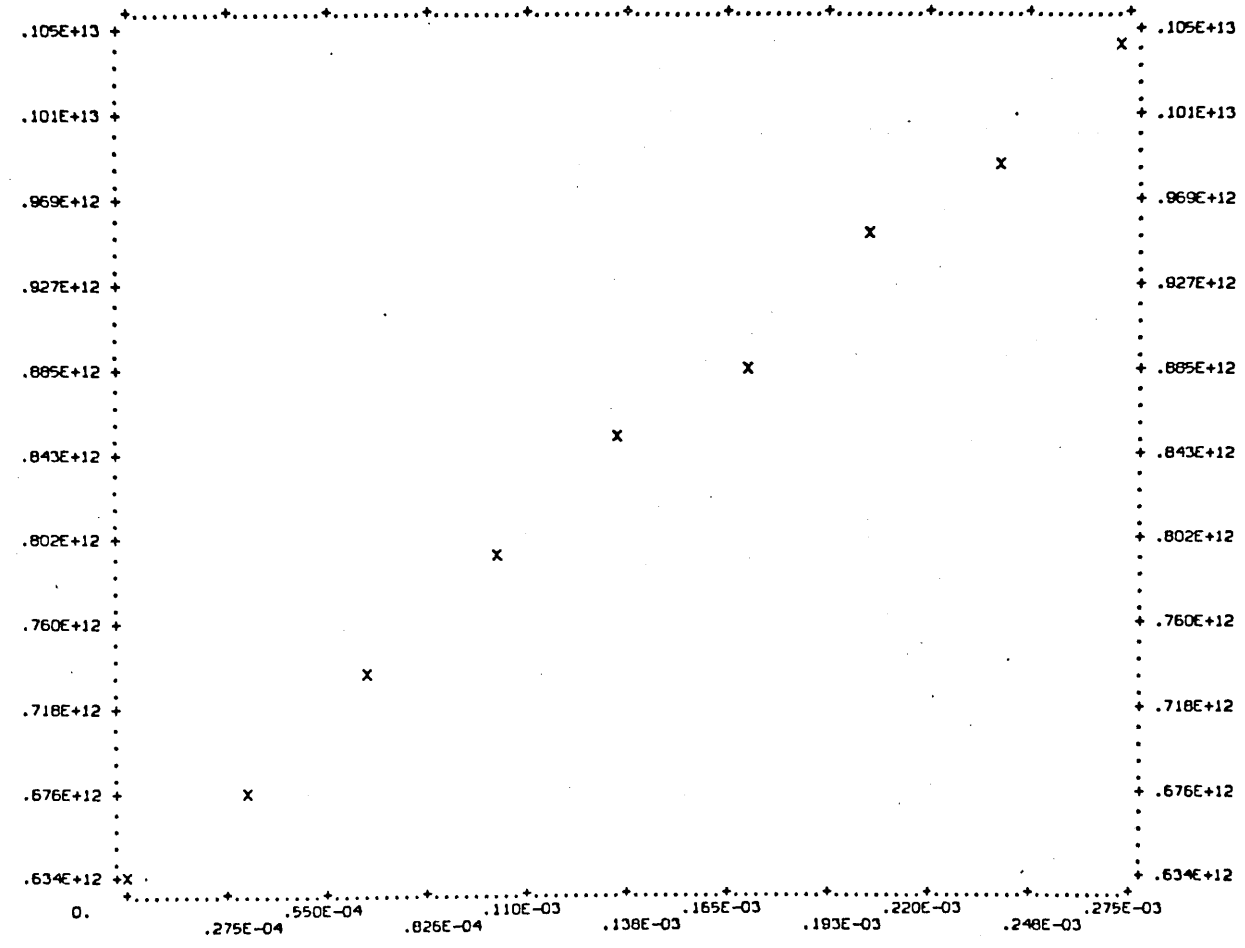

T	D						
288.0	30.0						
F1	F2	F3	I01	I1	I02	I2	P
100.0	250.0	0.0	100.0	70.4	100.0	2.9	4.700
100.0	300.0	50.0	100.0	52.0	100.0	1.8	5.400
100.0	350.0	100.0	100.0	36.6	100.0	1.0	6.100
100.0	400.0	150.0	100.0	27.5	100.0	.7	6.700
100.0	450.0	200.0	100.0	20.6	100.0	.4	7.400
100.0	500.0	250.0	100.0	11.5	100.0	.2	8.100

VALUES OF Y= .5772E+12 .5991E+12 .6334E+12 .6686E+12 .7092E+12 .7217E+12

VALUES OF X== 0. .3440E-04 .6880E-04 .1032E-03 .1376E-03 .1720E-03

VALUES OF VBAR= .2507E+03 .2493E+03 .2483E+03 .2512E+03 .2502E+03 .2493E+03

SLOPE= .9036E+15

STANDARD DEVIATION= .5308E+14

INTERCEPT= .5738E+12

STANDARD DEVIATION= .5529E+10

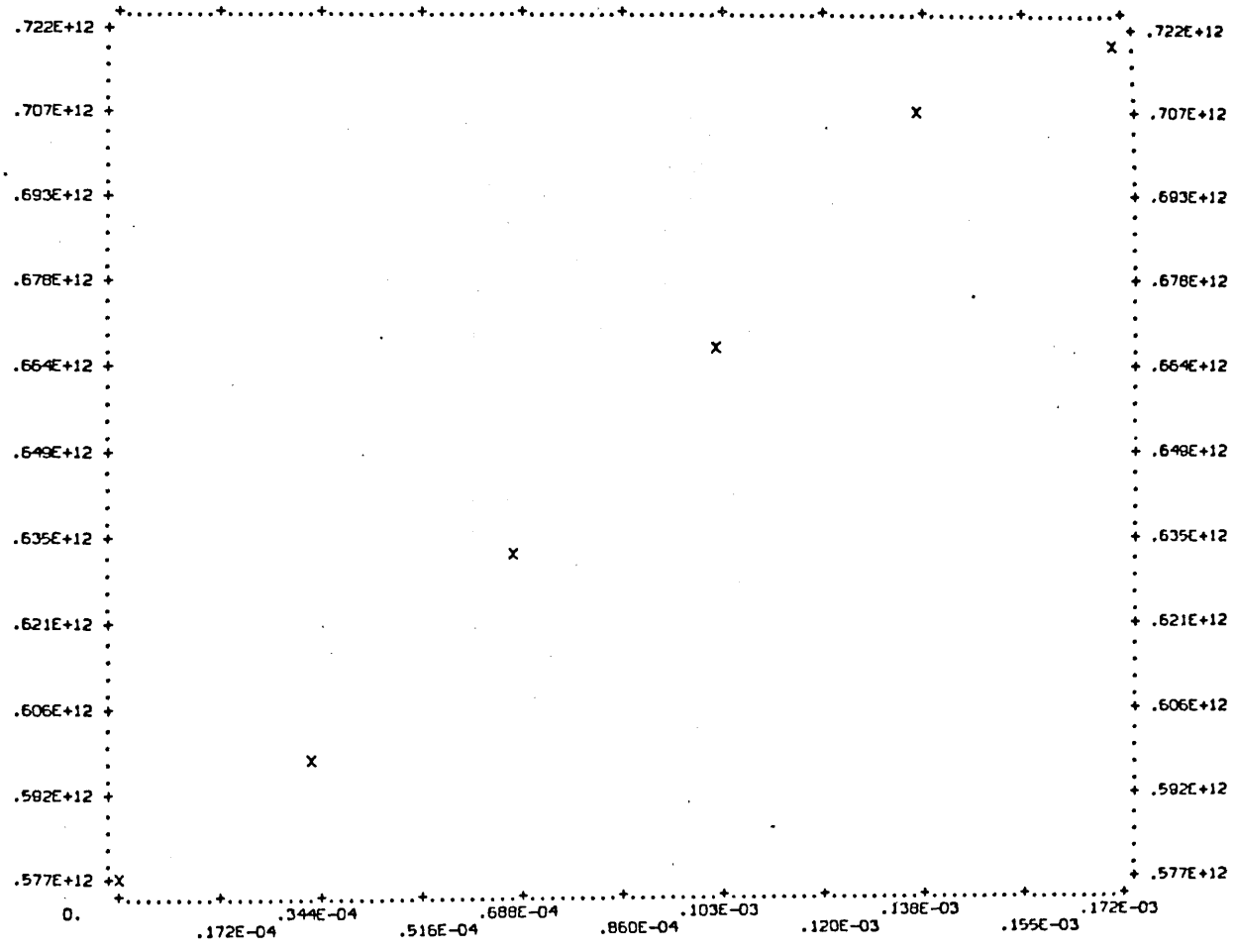

Fig.28

T	D
295.0	48.8

F1	F2	F3	I01	I1	I02	I2	P
50.0	250.0	0.0	100.0	30.4	100.0	4.1	3.900
50.0	300.0	50.0	100.0	22.6	100.0	2.5	4.600
50.0	350.0	100.0	100.0	19.0	100.0	2.0	5.200
50.0	400.0	150.0	100.0	13.0	100.0	1.1	5.900
50.0	450.0	200.0	100.0	9.0	100.0	.7	6.500
50.0	500.0	250.0	100.0	6.0	100.0	.4	7.200

VALUES OF Y= .4767E+12 .5069E+12 .5356E+12 .5728E+12 .6076E+12 .6310E+12

VALUES OF X== 0. .3440E-04 .6880E-04 .1032E-03 .1376E-03 .1720E-03

VALUES OF VBAR= .2563E+03 .2535E+03 .2563E+03 .2541E+03 .2563E+03 .2545E+03

SLOPE= .9226E+15

STANDARD DEVIATION= .2544E+14

INTERCEPT= .4758E+12

STANDARD DEVIATION= .2650E+10

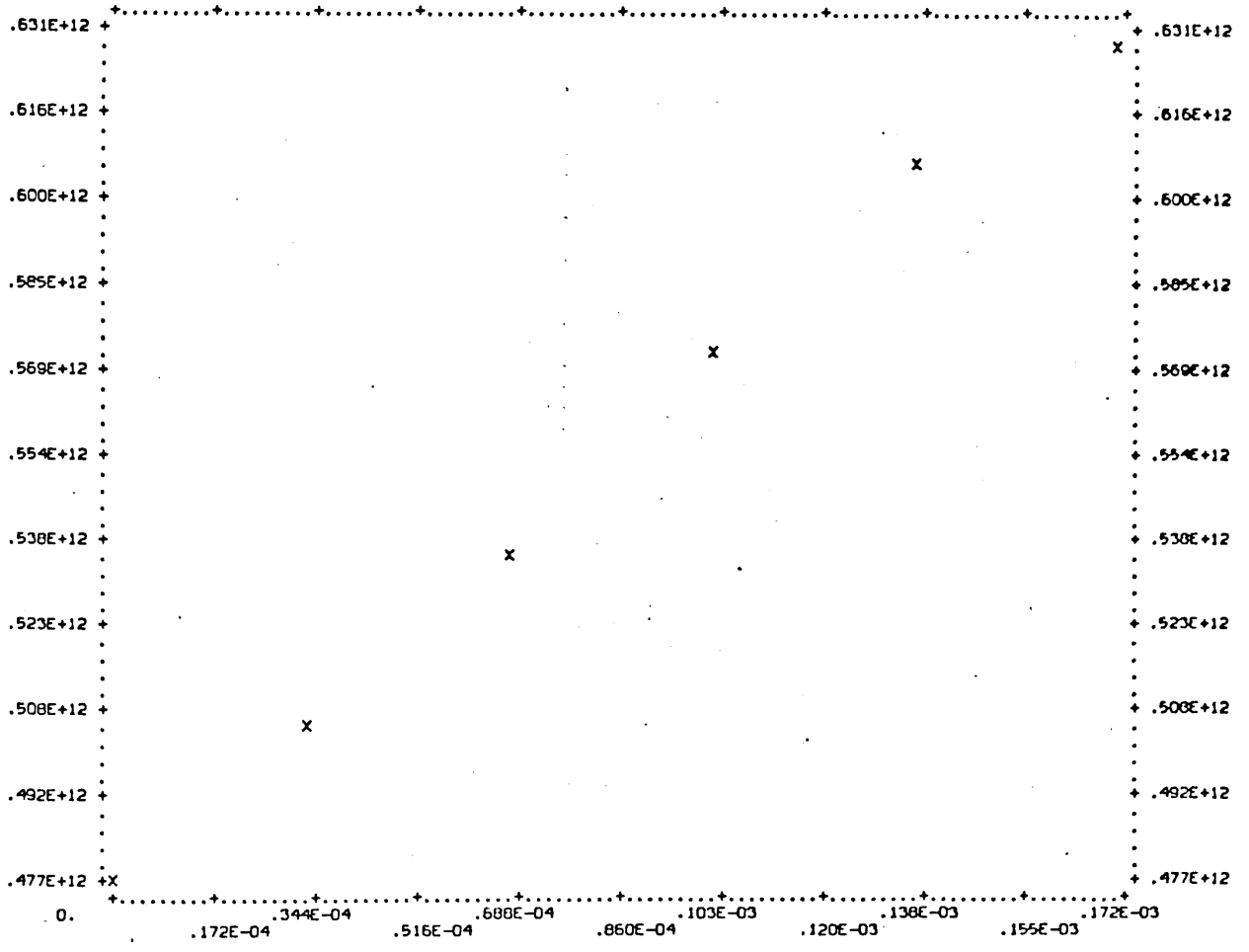

Fig.29

T	D
294.0	15.0

F1	F2	F3	I01	I1	I02	I2	P
100.0	250.0	0.0	100.0	39.4	100.0	9.4	4.700
100.0	300.0	50.0	100.0	29.8	100.0	6.7	5.400
100.0	350.0	100.0	100.0	27.4	100.0	5.8	6.100
100.0	400.0	150.0	100.0	26.2	100.0	5.5	6.700
100.0	450.0	200.0	100.0	25.7	100.0	5.2	7.400
100.0	500.0	250.0	100.0	12.5	100.0	2.4	8.100
100.0	550.0	300.0	100.0	11.1	100.0	2.1	8.700

VALUES OF Y= .4981E+12 .5105E+12 .5246E+12 .5460E+12 .5522E+12 .5645E+12 .5844E+12

VALUES OF X== 0. .3440E-04 .6880E-04 .1032E-03 .1376E-03 .1720E-03 .2064E-03

VALUES OF VBAR= .2473E+03 .2460E+03 .2450E+03 .2478E+03 .2468E+03 .2460E+03 .2481E+03

SLOPE= .4096E+15

STANDARD DEVIATION= .1929E+14

INTERCEPT= .4978E+12

STANDARD DEVIATION= .2393E+10

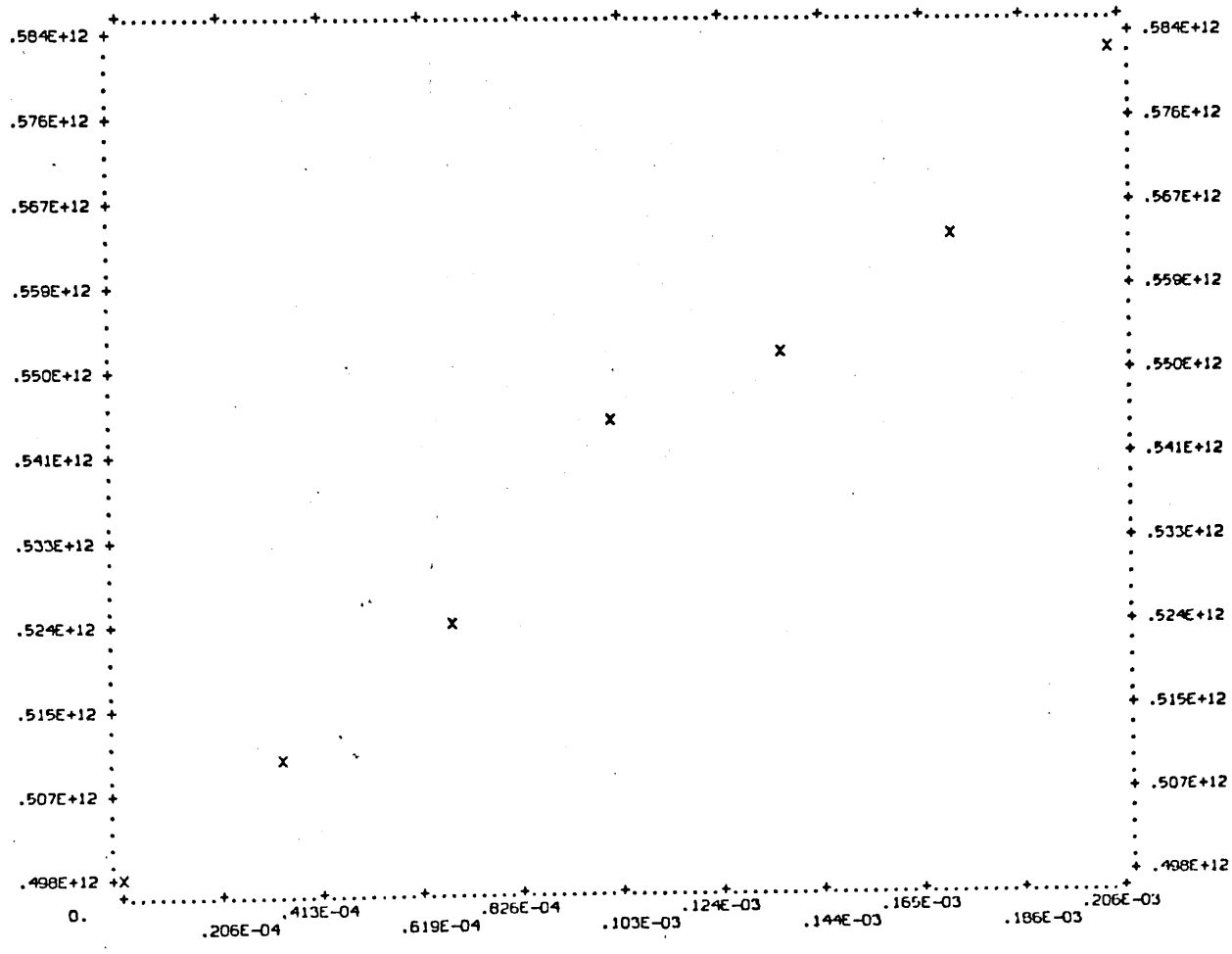

R1AR

Fig. 30

T	D
298.0	48.8

F1	F2	F3	I01	I1	I02	I2	P
50.0	250.0	0.0	100.0	76.6	100.0	7.7	3.900
50.0	300.0	50.0	100.0	68.5	100.0	5.5	4.600
50.0	350.0	100.0	100.0	67.2	100.0	4.8	5.200
50.0	400.0	150.0	100.0	62.0	100.0	3.3	5.900
50.0	425.0	175.0	100.0	59.5	100.0	3.0	6.200
50.0	450.0	200.0	100.0	57.8	100.0	2.7	6.500
50.0	475.0	225.0	100.0	55.6	100.0	2.5	6.800
50.0	500.0	250.0	100.0	52.8	100.0	2.0	7.200
50.0	550.0	300.0	100.0	45.2	100.0	1.3	7.900

VALUES OF Y= .5634E+12 .5986E+12 .6472E+12 .7012E+12 .7238E+12 .7514E+12 .7692E+12 .7862E+12 .8377E+12

VALUES OF X== 0. .3440E-04 .6880E-04 .1032E-03 .1204E-03 .1376E-03 .1548E-03 .1720E-03 .2064E-03

VALUES OF YEAR= .2589E+03 .2561E+03 .2589E+03 .2567E+03 .2579E+03 .2589E+03 .2599E+03 .2571E+03 .2556E+03

SLOPE= .1354E+16

STANDARD DEVIATION= .2625E+14

INTERCEPT= .5586E+12

STANDARD DEVIATION= .3345E+10

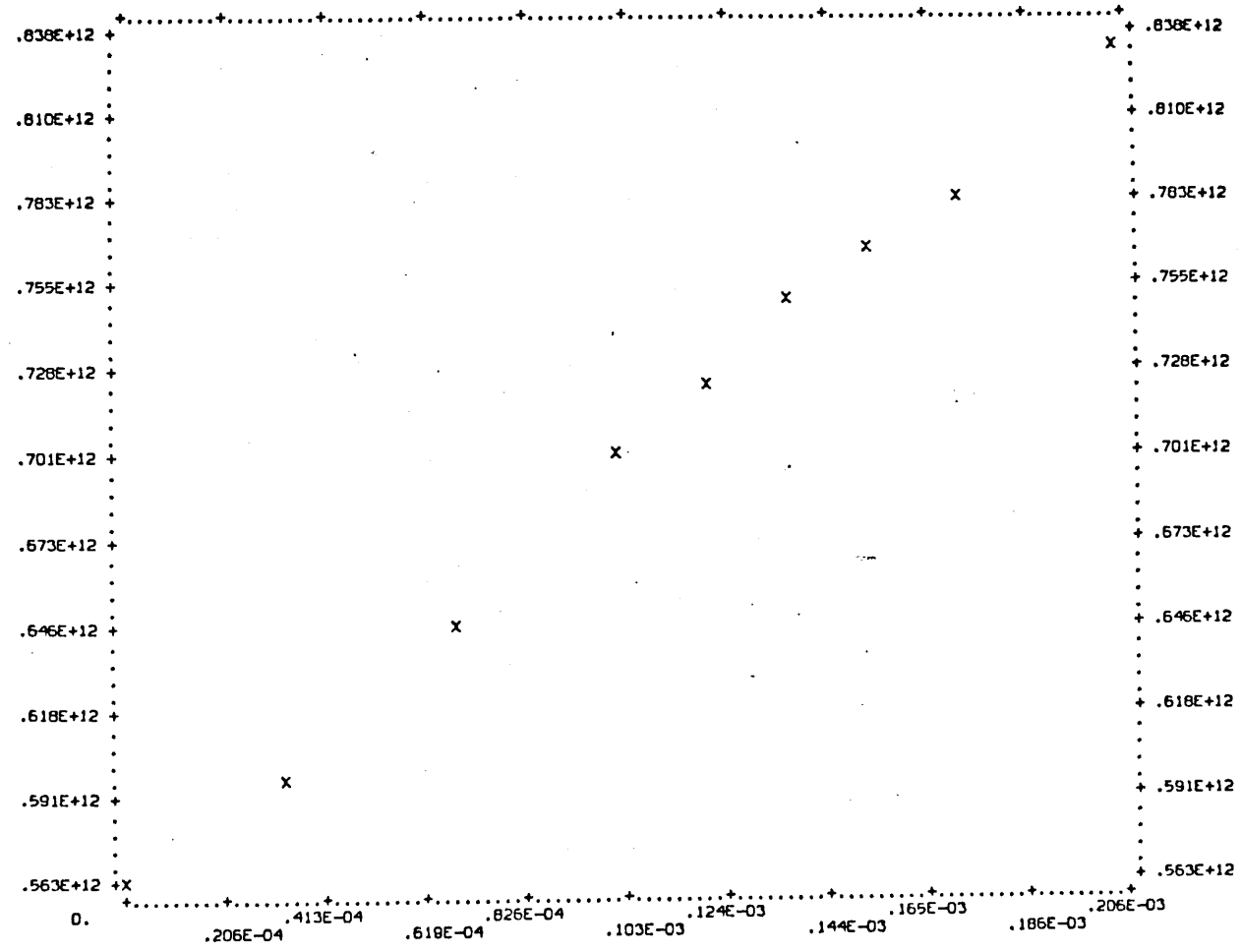

Fig.31

T	D
294.0	30.0

F1	F2	F3	IB1	I1	IB2	I2	P
100.0	250.0	0.0	100.0	48.5	100.0	2.6	4.700
100.0	300.0	50.0	100.0	37.6	100.0	1.6	5.400
100.0	350.0	100.0	100.0	31.2	100.0	1.2	6.100
100.0	400.0	150.0	100.0	20.4	100.0	.7	6.700
100.0	450.0	200.0	100.0	16.5	100.0	.5	7.400
100.0	500.0	250.0	100.0	13.1	100.0	.3	8.100
100.0	550.0	300.0	100.0	9.4	100.0	.2	8.700

VALUES OF Y= .5085E+12 .5400E+12 .5504E+12 .5898E+12 .6041E+12 .6460E+12 .6757E+12

VALUES OF X== 0. .3440E-04 .6880E-04 .1032E-03 .1376E-03 .1720E-03 .2064E-03

VALUES OF VBAR= .2473E+03 .2460E+03 .2450E+03 .2478E+03 .2468E+03 .2460E+03 .2481E+03

SLOPE= .7966E+15

STANDARD DEVIATION= .4440E+14

INTERCEPT= .5056E+12

STANDARD DEVIATION= .5507E+10

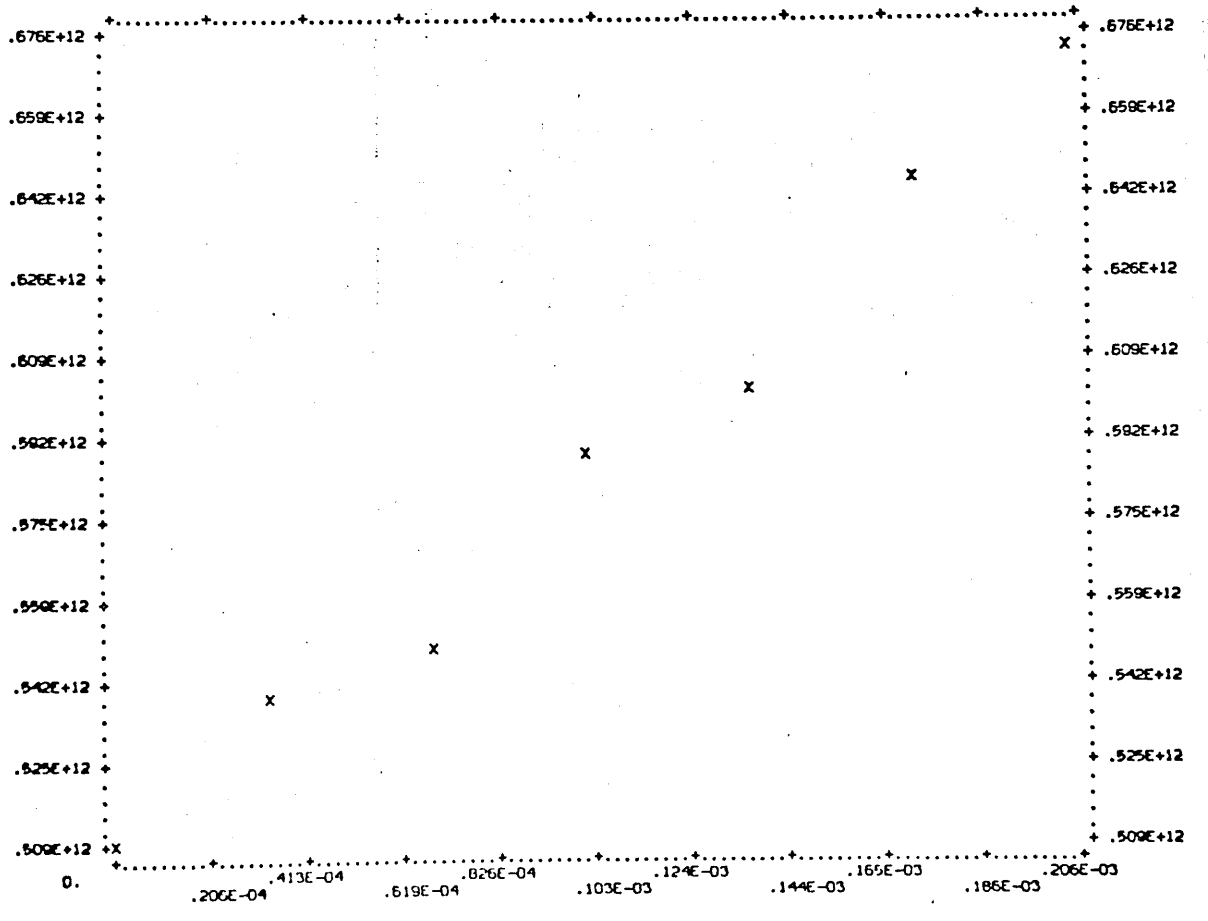

TABLE 7

Summary of Results for the Reaction: $O + SO_2 + N_2 = SO_3 + N_2$ at 298 ± 2K

$k^{N_2}_{2.1}/10^{14}$ $cm^6\ mol^{-2}\ s^{-1}$	$(k_w - k_w^*)/s^{-1}$	$(\gamma - \gamma^*)x10^4$	Conditions
16.62 ± 0.9304	3.1997 ± 0.2942	1.24 ± 0.117	Flow of N_2:
18.31 ± 0.7142	2.9909 ± 0.2259	1.19 ± 0.0899	0-208 μ moles/sec
15.19 ± 0.3445	5.0257 ± 0.1239	2.0 ± 0.049	Flow of SO2:
			34.4 μ moles/sec
Mean: 16.71 ± 0.663 .. 3.7387 ± 0.215 .. 1.4867 ± 0.085			
8.503 ± 1.037	12.089 ± 0.501	4.81 ± 0.199	Flow of SO2:
8.567 ± 0.371	-	-	68.8 μ moles/sec
9.036 ± 0.5309	12.29 ± 0.26	4.89 ± 0.103	Flow of N2:
			0-208 μ moles/sec
Mean: 8.702 ± 0.6463 .. 12.189 ± 0.38 .. 4.85 ± 0.151			

TABLE 8

Summary of Results for the Reaction: $O + SO_2 + He = SO_3 + He$ at 298 ± 2K

$k^{He}_{2.1,}/10^{14}$ $cm^6\ mol^{-2}\ s^{-1}$	$(k_w - k_w^*)/s^{-1}$	$(\gamma - \gamma^*)x10^{14}$	Conditions
9.226 ± 0.2544	1.514 ± 0.0585	0.6026 ± 0.02328	Flow of SO2:
8.02 ± 0.577			34.4 μ moles/sec
	2.2328 ± 0.1321	0.8886 ± 0.0557	Flow of He:
6.518 ± 0.7527	2.0549 ± 0.1713	0.8178 ± 0.068	0-208 μ moles/sec
7.496 ± 0.7124	1.5934 ± 0.1942	0.634 ± 0.07729	
Mean: 7.815 ± 0.574 ..	1.8487 ± 0.139 ..	0.73578 ± 0.0553	
4.644 ± 0.401	9.7195 ± 0.238	3.868 ± 0.0947	Flow of SO2:
2.96 ± 0.411	-	-	68.8 μ moles/sec
4.096 ± 0.1929	9.0646 ± 0.1144	3.607 ± 0.0455	Flow of He:
			0-208 μ moles/sec
Mean: 3.9 ± 0.3349 ..	9.392 ± 0.1762 ..	3.737 ± 0.0701	

TABLE 9

Summary of Results for the Reaction: $O + SO_2 + Ar = SO_3 + Ar$ at 298 ± 2K

$k^{Ar}_{2.1}/10^{14}$ $cm^6\ mol^{-2}\ s^{-1}$	$(k_w - k_w)/s^{-1}$	$(\gamma - \gamma^*)x10^4$	Conditions
11.27 ± 0.9089	8.508 ± 0.2858	3.386 ± 0.114	Flow of SO2:
12.53 ± 0.6843	10.507 ± 0.217	4.18 ± 0.086	34.4 μ moles/sec
11.15 ± 0.4686	8.618 ± 0.148	3.43 ± 0.059	Flow of Ar:
10.2 ± 0.908	8.42 ± 0.2874	3.35 ± 0.114	0-208 μ moles/sec
10.1 ± 0.8858	6.849 ± 0.2415	2.73 ± 0.096	
13.5 ± 0.2625	7.664 ± 0.0729	3.05 ± 0.029	
Mean: 11.458 ± 0.686 ... 8.428 ± 0.2088 .. 3.3543 ± 0.083			
8.276 ± 0.5107	6.7967 ± 0.3002	2.71 ± 0.119	Flow of SO2:
7.966 ± 0.44			34.4 μ moles/sec
			Flow of Ar:
			0.208 μ moles/sec
Mean: 8.121 ± 0.475			

CHAPTER 7

DISCUSSION

7.1 Discussion.

As discussed previously (Chapter 1), the results of the combination reaction:

$$O + O_2 + M \longrightarrow O_3 + M \qquad 1.1$$

might be affected by the presence of extraneous active species from discharge unless they are rigorously excluded. In the present work these active species arising from the discharge, were eliminated by rigorous purification of the gases and the great dilution of the oxygen with argon before passing through the discharge. The mean rate constants determined at 295K for four third bodies are compared with rate constants of those investigators who also excluded contaminants (Table 10). The measured values of $k_{1.1}^{O_2}$, $k_{1.1}^{Ar}$, $k_{1.1}^{CO_2}$ and $k_{1.1}^{He}$ with an estimated absolute accuracy of between 5 and 17% lie in the middle of the range of extreme values and are in good agreement (5-15%) with the values obtained by Huie et al[80] Stuhl and Niki[79] and Kaufman and Kelso[71]. The other values, such as those from stirred flow measurements[72] and the pulse radiolysis[74,75,77] are respectively 30-100% higher and 0-50% lower than those reported here. Bevan and Johnson[77] have shown that the UV absorption bands of ozone are distorted by vibrational excitation of ozone; this may cause errors in the latter method.

The very high value reported by Mulcahy and Williams[72] is probably due to the fact that it was assumed that the ozone concentration was zero when the flow speed was adjusted for a minimum, while in fact it

TABLE 10

Summary of Rate Constants $k^{M}_{1.1}$ at 295-300K

$10^{-14} \times k^{M}_{1.1}/cm^{6}\ mol^{-2}\ s^{-1}$ when M is					
O_2	Ar	CO_2	He	Method	Reference
2.31	1.57	5.56	1.17	Discharge flow	This work
-	1.86	-	-	"	68
3.18	2.85	9.7	2.3	Pyrolysis/stirred flow	72
2.35	1.45	5.45	1.45	Pyrolysis/flow	71
-	1.34	-	1.21	Flash photolysis/ resonance fluorescence	80
-	1.6	-	-	"	78
-	1.81	-	1.67	Flash photolysis/absorption	1.34
2.32	-	-	-	Flash photolysis/ chemiluminescence	79
-	1.0	4.2	0.7	Pulse radiolysis	74
1.5	-	3.7	-	"	75
2.0	1.0	4.8	-	"	77

was at a steady state value determined by the initial ozone concentration.

Stuhl and Niki[79], using the photodissociation-CO chemiluminescence technique, neglected the ozone reaction with atomic oxygen entirely and obtained a value of $k_{1.1}^{O_2}$ of 2.32×10^{14} cm^6 mol^{-2} s^{-1}. The neglect is justified on the ground that at least half the gas in the reaction vessel is CO.

Benson and Axworthy[69] reconsidered their previously published results[45] on the thermal decomposition of ozone, and gave a value for $k_{1.1}$ of $2.97 \times 10^{13} \exp \frac{447.9}{T}$ cm^6 mol^{-2} s^{-1} at 300K $k_{1.1} = 1.3 \times 10^{14}$ cm^6 mol^{-2} s^{-1}. In experiments similar to those of Benson and Axworthy, Zaslowski et al.[81] reported a value of $k_{1.2}^{O_3} = 7.8 \times 10^{15} \exp \frac{-12,229.49}{T}$ cm^3 mol^{-1} s^{-1}.

To determine $k_{1.2}^{O_2}$, for O_2 as third body, the efficiency ratio $k_{1.2}^{O_2} / k_{1.2}^{O_3}$ is required, according to Benson and Axworthy this has a value of 0.44, a value which leads to $k_{1.2}^{O_2}$ at 300K of 9.034×10^{-3} cm^3 mol^{-1} s^{-1}. The rate constant of reaction 1.1 can now be calculated[128] from the equilibrium constant $K = \frac{k_{1.1}\ (cm^6\ mol^{-2}\ s^{-1})}{k_{1.2}\ (cm^3\ mol^{-1}\ s^{-1})} = 19.75 \times 10^{15}$ cm^3 mol^{-1} which gives a value of 1.78×10^{14} cm^6 mol^{-2} s^{-1} for $k_{1.1}$. Furthermore, a shock tube study of the thermal decomposition of ozone[82] in nitrogen gave a value of $k_{1.2}^{N_2} = 5.78 \times 10^{16} \exp \frac{-11,650.7}{T}$ cm^3 mol^{-1} s^{-1} when the data of Benson and Axworthy are included. The relative efficiency of O_2 compared to N_2 is 1.07 which leads to $k_{1.2}^{O_2} = 9.034 \times 10^{-3}$ cm^3 mol^{-1} s^{-1} at 300K. When $k_{1.2}$ is multiplied by K the equilibrium constant, the result is 1.74×10^{14} cm^6 mol^{-2} s^{-1}.

It is thus apparent that the results of studies of the thermal decomposition of ozone leads to values of $k_{1.1}$ which are low: 1.3, 1.78 and 1.74 x 10^{14} cm^6 mol^{-2} s^{-1}. All these values were obtained from the inverse reaction rate constants and the equilibrium constant K. The standard heat of formation of ozone ΔH_f^Θ at 0 K is known to an accuracy of $\pm$ 0.4 k cal. mol^{-1}; this results in an uncertainty of a factor of 2 in the value of the equilibrium constant[69]. Thus the results reported here are also in agreement with those obtained from measurement of the thermal decomposition of ozone, within the experimental limits of accuracy.

The value of $k_{1.1}^{Ar}$ (Table 2) was evaluated from the intercept of equation 18 assuming negligible surface reaction and is in agreement with Ball's[85] directly measured data within $\pm$ 15%. The temperature dependence of $k_{1.1}^{Ar}$ is compared with the values reported by other workers (including studies on the thermal decomposition of ozone[81], in Figs 32 and 33.) The results of the present work are in agreement with those obtained from static measurements by Huie, Herron and Davis (HHD). The results from earlier flow studies of Clyne, McKenney and Thrush[68] (CMT) and Mulcahy and Williams[72] (MW) diverge to a significant extent from the present results. The specific reasons for the discrepancies between the various results is difficult to explain on the basis of wall recombination since this has a positive temperature dependence. The agreement of the present results with those from the static measurements, where the reaction time is much shorter than the time for diffusion to the walls, is a clear evidence that wall reactions are not a serious problem in measurements involving flow techniques.

FIGURE 32: PLOT OF Log $k^{Ar}_{1.1}$ AGAINST (1/T) X 10^3

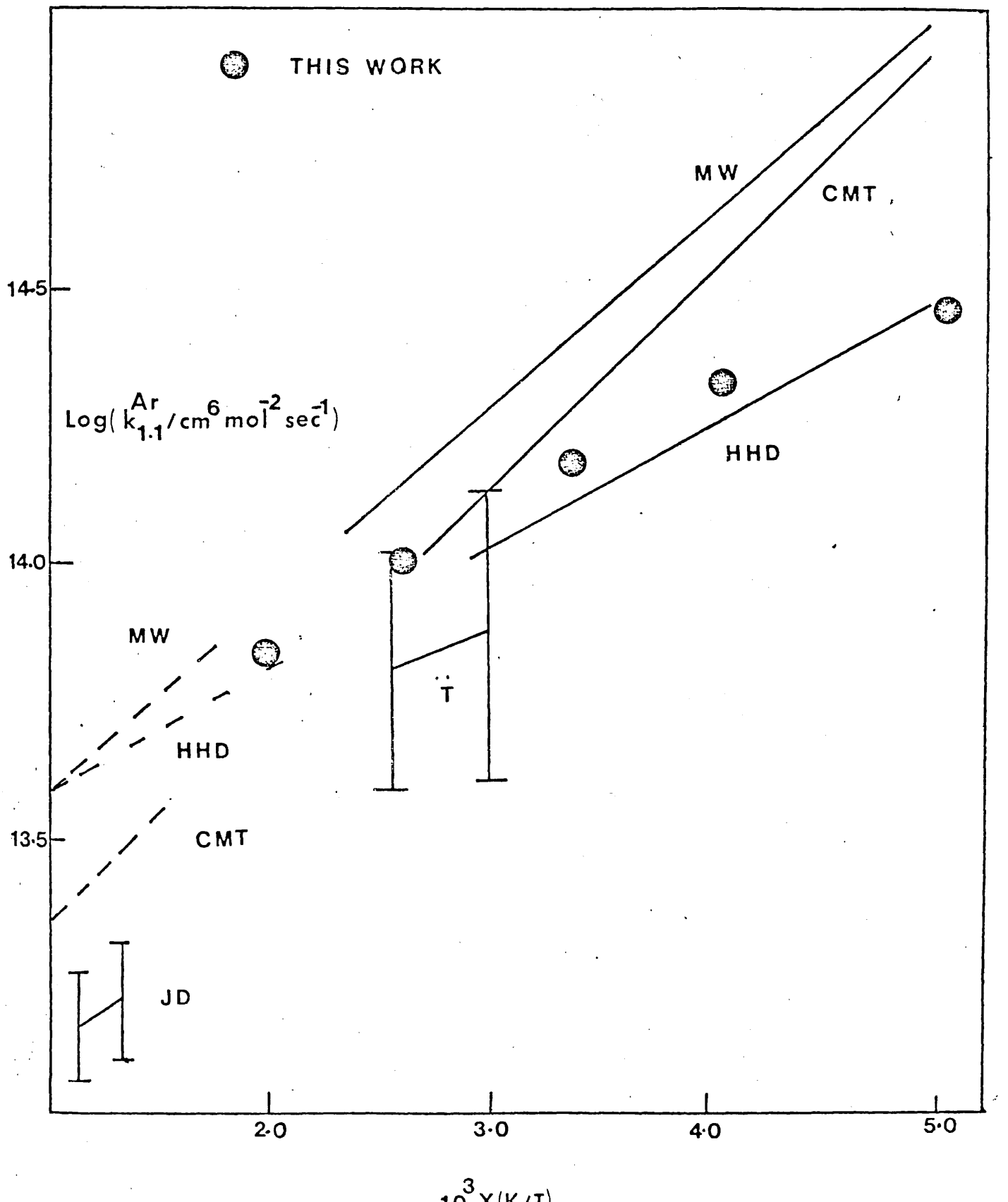

FIGURE 33 : PLOT OF Log $k_{1.1}^{Ar}$ AGAINST Log T

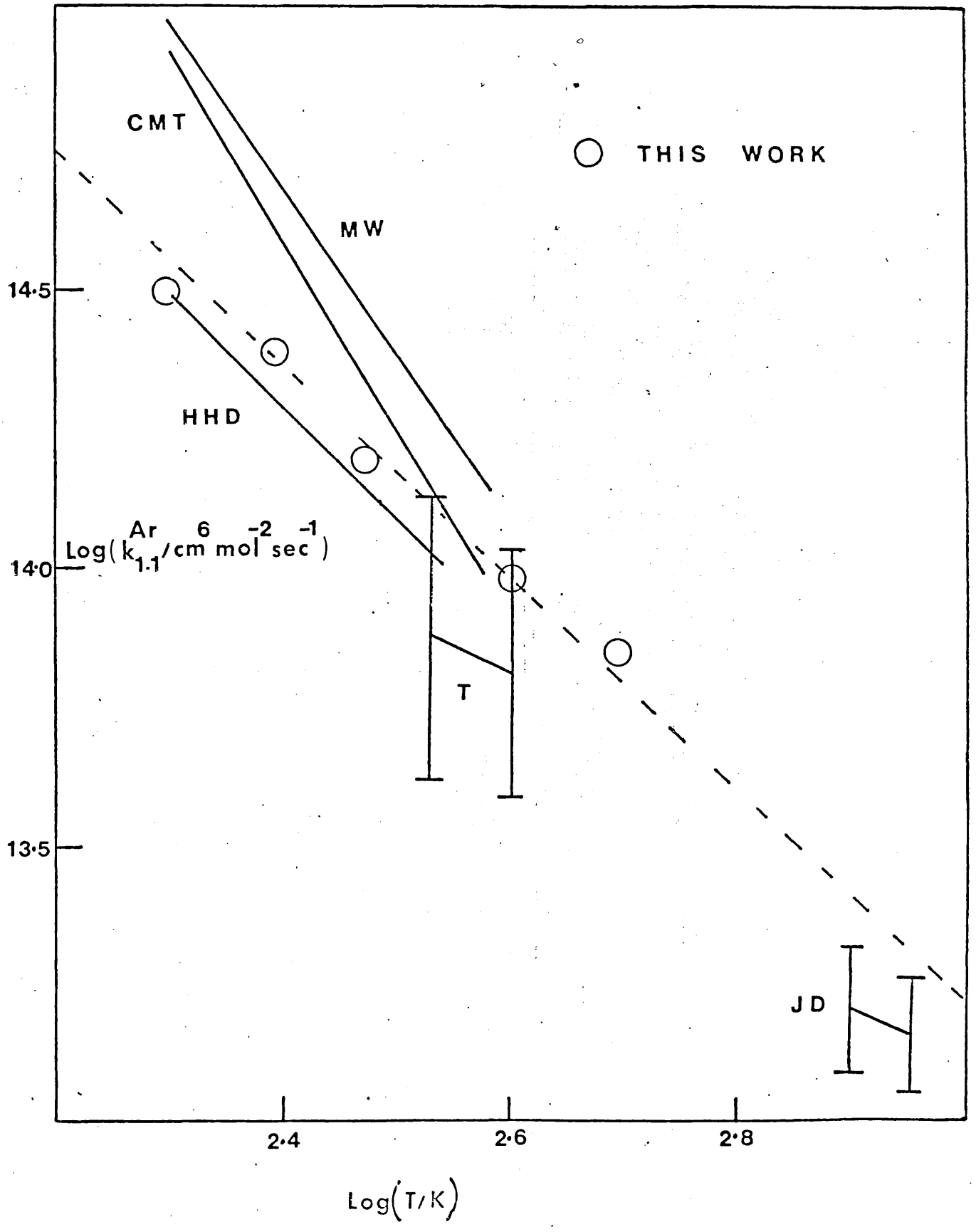

The temperature dependence for the reaction where M = O_2 is shown in the form of plots of log $k_{1.1}^{O_2}$ against 1/T and against log T (Figs. 34 and 35). Neither of these graphs is linear over the range of temperatures studied, it is possible to draw a smooth curve through the points. The temperature coefficient measured here for the first time is significantly dependent on the temperature of measurement. Previous estimates of stratospheric ozone generated by reaction 1.1 are based on the temperature coefficients for M = Ar or N_2. Present results show that efficiency of O_2:Ar is different at lower temperatures (typical atmospheric temperature 300 and 220K) from that at room temperature. The results suggest that estimates of stratospheric ozone generated by reaction 1.1 could be in error if one considers the temperature coefficient of Ar and the room temperature efficiency of O_2 with respect to Ar as a basis of estimation for O_2 as third body.

In Figs. 36 and 37, the temperature dependence of $k_{1.1}^{He}$ is shown in the normal Arrhenius form and as the graph of log $k_{1.1}^{He}$ against log T form respectively, again it is apparent that log $k_{1.1}^{He}$ is not a linear function of 1/T. The corresponding data for $k_{1.1}^{CO_2}$ over the temperature range 196-500K is shown in Fig. 38 in the Arrhenius form and in Fig. 39 as log $k_{1.1}^{CO_2}$ against log T. Also plotted in Fig. 39 is the data of Mulcahy and Williams[72] for M = CO_2. These authors used the O + NO chemiluminescence to follow the atom concentration, but used thermal decomposition of ozone as an atom source and carried out the study in a bulb reactor. Their result for $k_{1.1}^{CO_2}$ is a factor of 1.8 higher than the present results at 295K and a factor of 2.23 higher at 220K. The results of Mulcahy and Williams depend on the assumption of perfect mixing in

FIGURE 34: PLOT OF Log $k_{1.1}^{O_2}$ AGAINST $(1/T) \times 10^3$

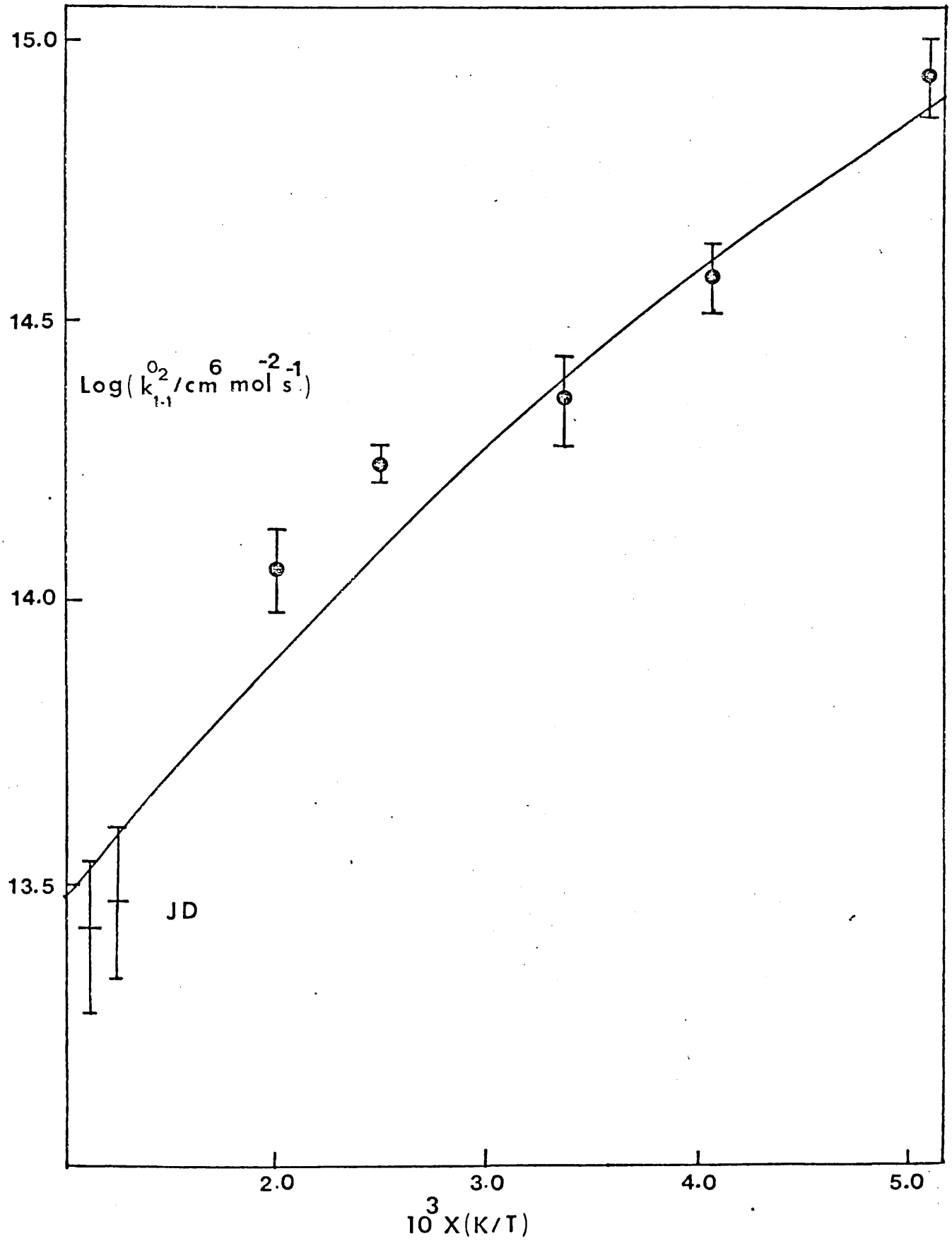

FIGURE 35: PLOT OF Log $k_{1.1}^{O_2}$ AGAINST Log T

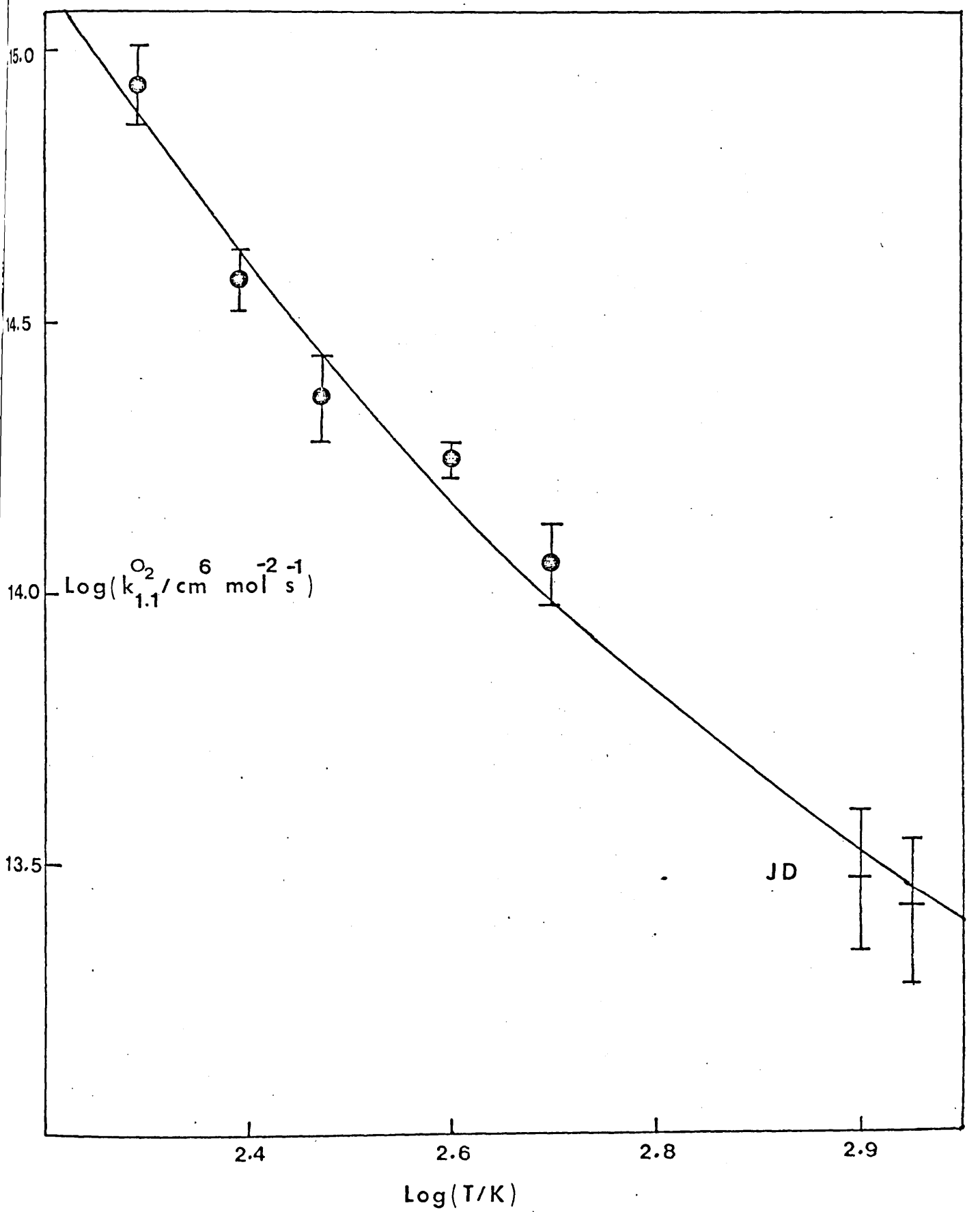

FIGURE 36: PLOT OF Log $k_{1.1}^{He}$ AGAINST $(1/T) \times 10^3$

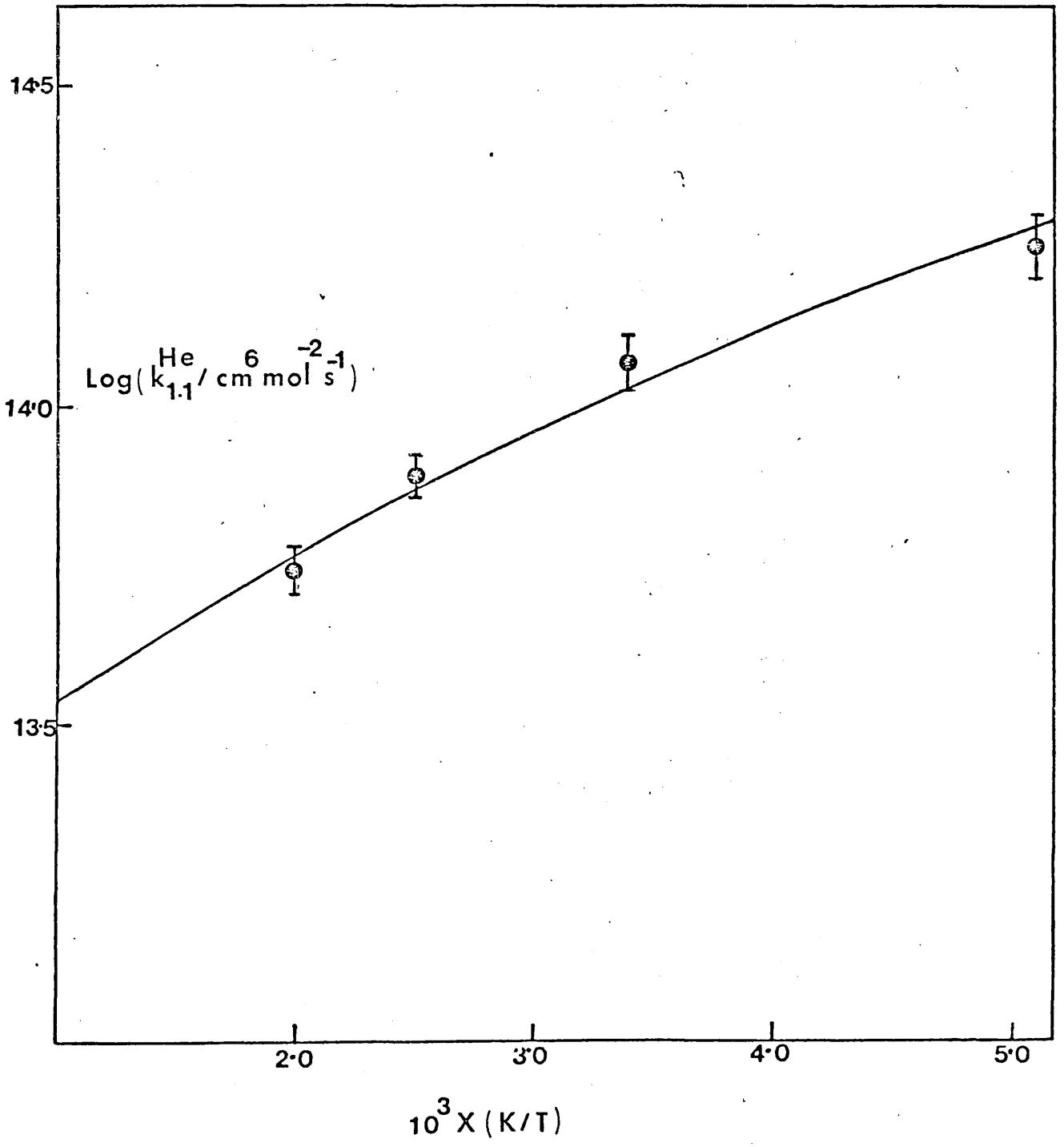

FIG 37: PLOT OF $\log k_{1.1}^{He}$ AGAINST $\log T$

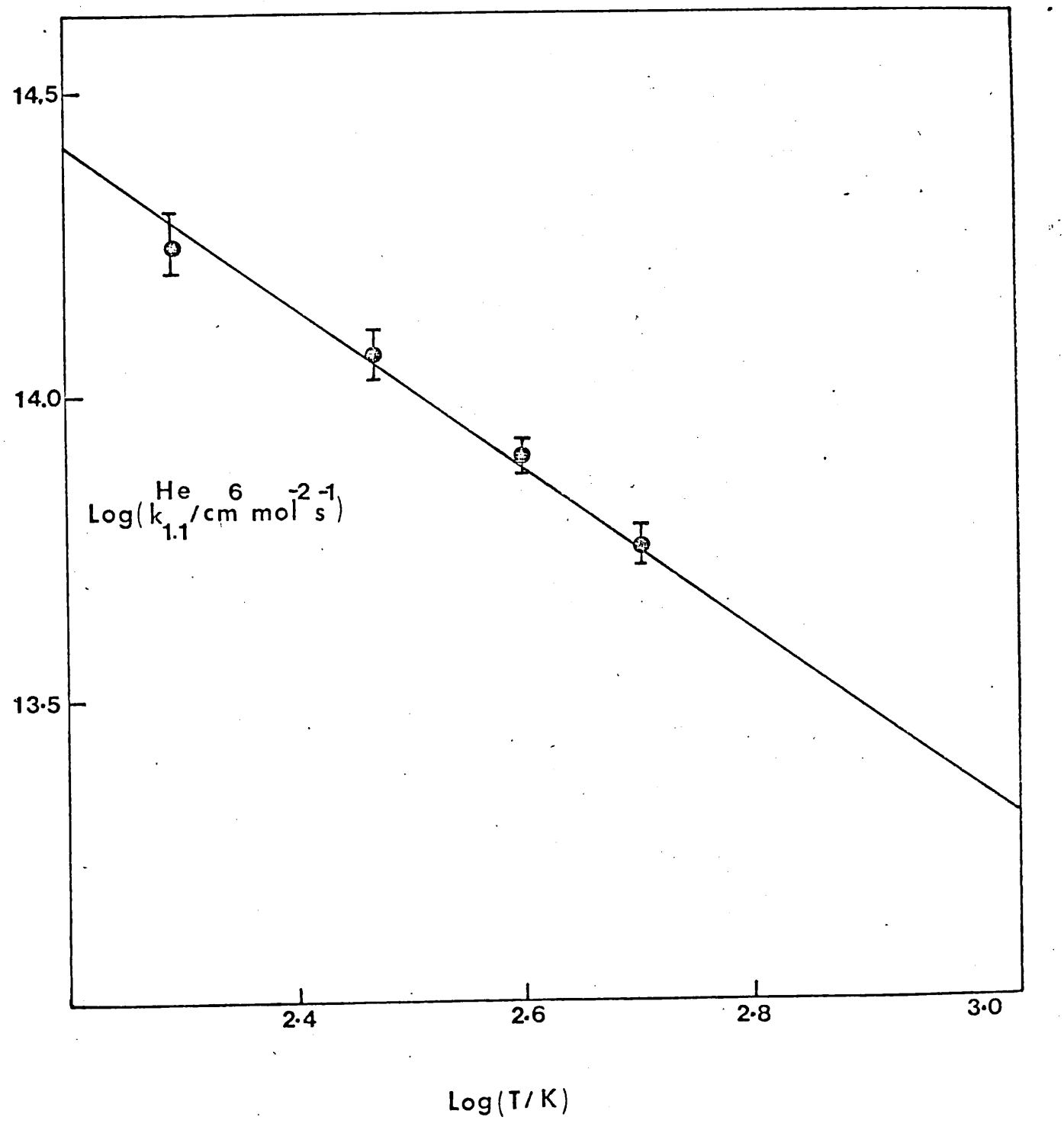

FIGURE 38: PLOT OF Log $k_{1.1}^{CO_2}$ AGAINST(1/T) X 10^3

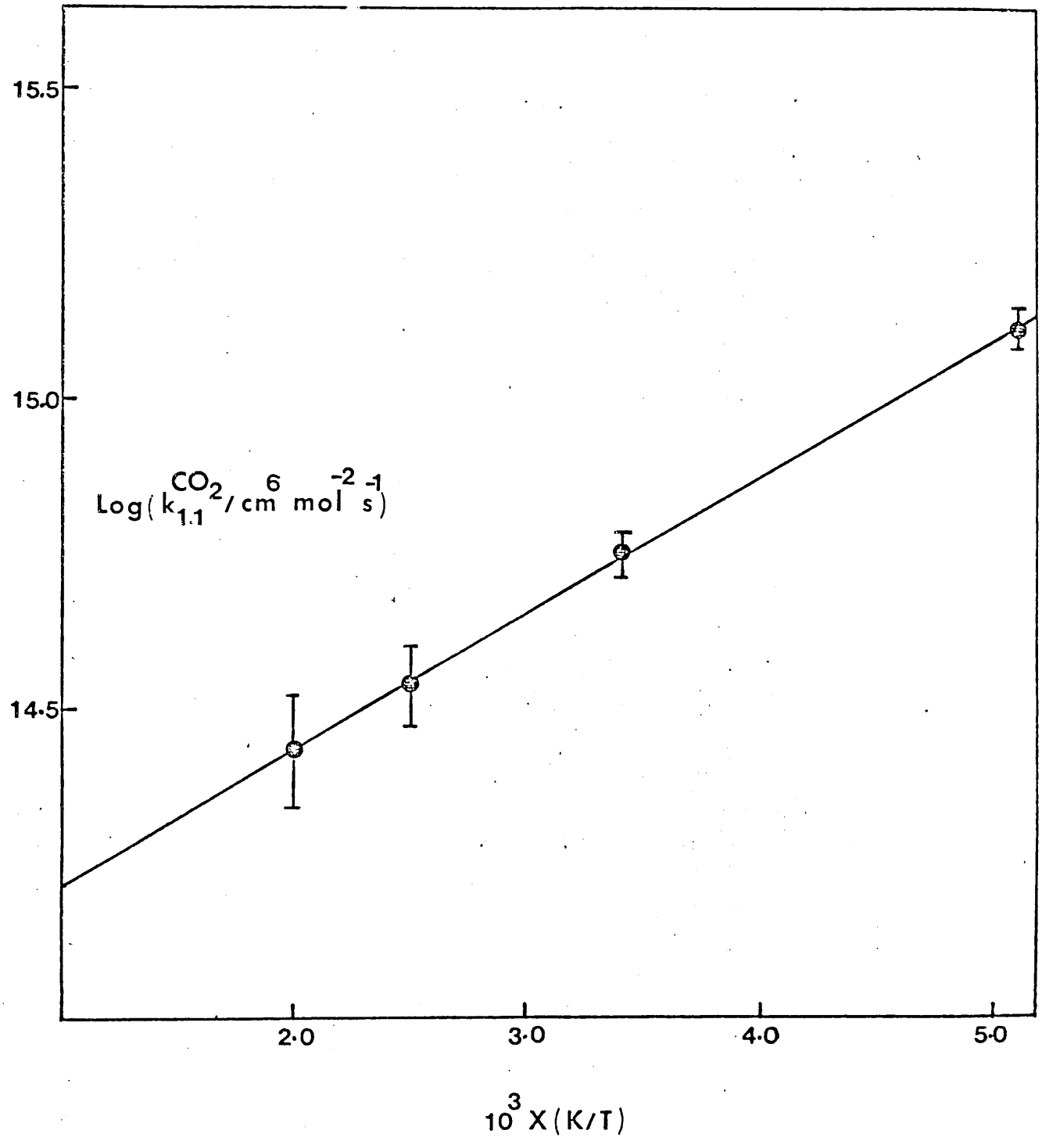

FIGURE 39 : PLOT OF $\log k_{1.1}^{CO_2}$ AGAINST $\log T$

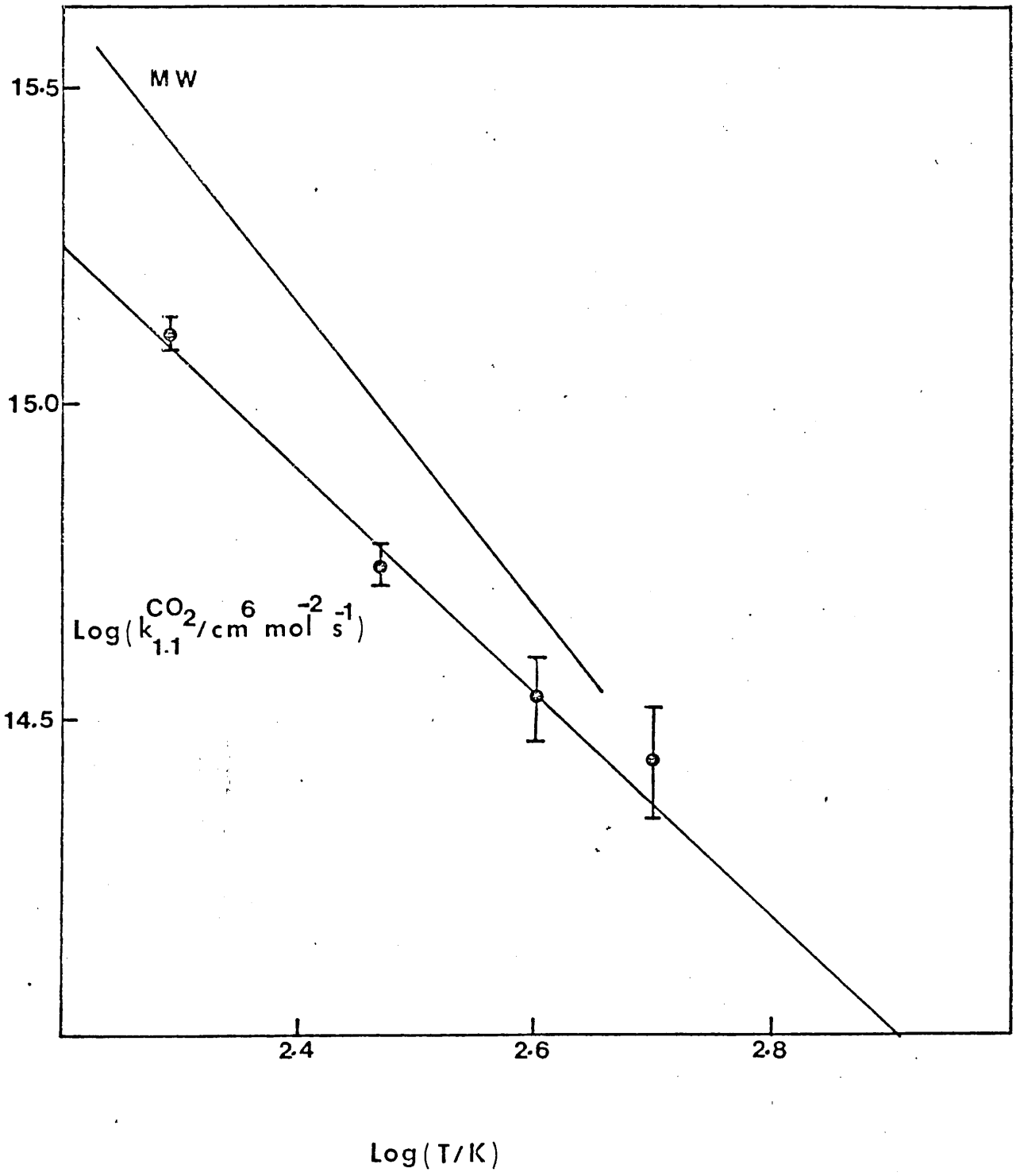

their bulb, which if in error could possibly explain why their results for Ar were also higher than those of Clyne et al.[68]

The Arrhenius activation energies and temperature coefficients for O_2, Ar, CO_2 and He ~~is~~ are presented in Table 11.

TABLE 11. Temperature Dependence of $k^M_{1.1}$ from 196-500K.

$k^M_{1.1} = A \exp(-E/RT)$			$k^M_{1.1} = B\left(\frac{T}{295}\right)^{-n}$	
M	A (10^{13} cm^6 mol^{-2} s^{-1})	$-E/R$	B (10^{14} cm^6 mol^{-2} s^{-1})	n
Ar	3.21 ± 0.519	465.88 ± 42.17	1.57 ± 0.2	1.53 ± 0.16
O_2	4.74 ± 1.22	535.48 ± 82.84	2.31 ± 0.41	2.025 ± 0.31
CO_2	10.00 ± 0.21	502.05 ± 6.089	5.559 ± 0.416	1.65 ± 0.16
He	3.056 ± 0.54	359.03 ± 56.16	1.177 ± 0.11	1.26 ± 0.24

It is interesting to compare the Arrhenius plots for M = O_2 (Fig. 34), He (Fig. 36), CO_2 (Fig. 38) and for Ar (Fig. 32). It appears that for most efficient third body CO_2 the graph of log K against $1/T$ is truly linear and for less efficient third body He a curvature is more prominent especially at higher temperatures. Curvature in such plots may suggest that two or more competitive reactions with different energies of activation are occurring in the system.

For all third bodies, a negative temperature coefficient is observed; this means that the reaction has a rate constant which decreases with increasing temperature. The termolecular combination process is usually considered in terms of an energy-transfer mechanism where the atom A combines with a diatomic molecule B to form an

energy rich complex, AB*. This complex can either dissociate back to reactants or be stabilized by collision with a third body M:

$$A + B \underset{k_b}{\overset{k_a}{\rightleftharpoons}} AB^* \qquad \text{combination dissociation}$$

$$AB^* + M \xrightarrow{k_c} AB + M \qquad \text{stabilization}$$

Applying the steady state approximation to AB* the rate of loss of A is given by

$$-\frac{d[A]}{dt} = \frac{k_a k_c [A][B][M]}{k_b + k_c [M]}$$

Under low pressure conditions i.e. $k_b >> k_c [M]$, the kinetics are termolecular with

$$k_{experimental} = \frac{k_a k_c}{k_b} = K \cdot k_c$$

where K is the equilibrium constant of the combination/dissociation process.

The rate decreases as the temperature is raised because the amount of excess kinetic energy which must be removed increases, reducing the efficiency of the deactivating collisions. Complex molecules prove to be more efficient third bodies than simple molecules since they can soak up excess energy in their internal degrees of freedom.

An alternative bound complex mechanism for atom recombination is that atom A first combines with the third body M to form a complex AM*.

$$A + M \underset{}{\overset{}{\rightleftharpoons}} AM^*$$

$$AM^* + M \underset{}{\overset{}{\rightleftharpoons}} AM + M \quad \text{or} \quad AM^* + B \longrightarrow AB + M$$

$$AM + B \longrightarrow AB + M$$

Davidson[16], and Porter[25] adopted this mechanism to interpret iodine atom recombinations, this is justified by the large observed rate constants and negative temperature coefficients for such third bodies as methyl and ethyl iodides, benzene, mesitylene and iodine.

In the present investigation, the temperature dependence for different third bodies does not differ markedly from one to another; this suggests that energy transfer mechanism is dominant, since substantially different temperature dependences for the different third bodies would be expected for the alternative bound complex mechanism to be important. There is no evidence that $O(^3P)$ reacts with CO_2 to form a CO_3 complex and the experimental data presented here argues strongly against the importance of such a complex in the reaction sequence leading to the formation of ozone. However, the formation of CO_3 from the reaction of $O(^1D)$ with CO_2 has been postulated in several studies[131, 133] although there is disagreement as to the lifetime of the complex. There is also doubt as to whether the atomic $O(^1D)$ is deactivated to $O(^3P)$ when and if the complex dissociates.

Pulse radiolysis experiments[76] have shown a transient absorption which is attributed to vibrationally excited ozone. Riley and Cahil[136] confirmed the absorption spectrum and suggested that some "transient species", which is not vibrationally excited ozone, may be responsible for the time dependence of the UV absorption which they observed. Subsequently, in similar studies, Bevan and Johnson[77] observed the kinetics of ozone following pulse radiolysis of oxygen. They observed two transient species in their measurements of spectral band shape; these were attributed to two species labelled as O_3^{α} and O_3^{β} which are

probably vibrationally excited ozone molecules. Recently, Swanson and Celotta[129] have detected triplet ozone using electron energy loss spectra. This stable state might represent an important channel for recombination since both the triplet and singlet states of ozone correlate with the ground state of the reactants.

$$O(^3P) + O_2\ (^3\Sigma_g^-) + M \longrightarrow O_3 \text{ (triplet or singlet)} + M$$

The present results with He as the third body also imply that some transient species might reach a steady state in the system. Probable channels for the recombination might occur by either or both of the following mechanisms:

Mechanism 1, via singlet state ozone:

$$O + O_2 + M = X\ O_3^1 + M \qquad 1.1a$$

$$O + O_3^1 = 2O_2 \qquad 1.3b$$

where X = fraction of total ozone formed (both triplet and singlet)

Mechanism 2, via triplet state O_3:

$$O + O_2 + M = (1-X)\ O_3^3 + M \qquad 1.1b$$

$$O + O_3^3 = 2O_2 \qquad 1.3b$$

$$M + O_3^3 = O_3^1 + M \qquad 1.5$$

The treatment of ~~unimolecular~~ reactions based on the theory of Rice and Rampsperger[129] and Kassel[130] (RRK) relates the negative temperature coefficient to the average energy of the collisional complex formed by the two reactive species. The temperature dependence of the rate of reaction in the present work is in accord with this theory and Stater's[138]

theories of unimolecular decomposition for the reverse reaction. According to the RRK theory, a molecule is regarded as a collection of oscillators which are essentially harmonic but sufficiently coupled to allow flow of energy among them. Dissociation occurs when a critical energy accumulates in a particular oscillator. The Slater theory consideres the contributions of uncoupled normal vibrational modes of the molecule to the extension of a specified distance e.g. the distance between two bonded atoms. Dissociation occurs when the extension reaches a critical value.

The surface rate constants and surface recombination efficiency determined in this investigation are listed in Tables 2, 3, and 4. Two different systems were used in these laboratories for determining the surface rate constant. Ball[85] used system A which is essentially an apparatus in which O atom decay can be followed by sliding the detector (photomultiplier) to different positions along the reaction tube. System B, which has a fixed detector, was used in this work. Measurements of surface rate constant by system A is possible only at room temperature since the reaction system should be immersed in a thermostat to achieve different temperatures. However the value of k_w^* obtained from the direct measurements (i.e. system A) is the true value whereas values obtained from system B are apparent. The room temperature correspondence between k_w^* determined by Ball in system A and that determined in this work in system B provided a check on the latter method. k_w^* was calculated from the intercept of equation 20 and a typical plot is shown in Fig. 10. It is interesting to note that although the points lie on a reasonable straight line, the apparent values of k_w^* obtained at different temperatures show a negative temperature coefficient which

is contrary to the literature value[72]. At lower temperatures the surface recombination efficiency of the phosphoric acid coated pyrex approaches a value similar to that for clean pyrex ($\gamma \approx 8 \times 10^{-5}$). This indicates that the poisoned surface is acting like a clean pyrex surface. The increased recombination efficiency might be due to adsorption of some oxygen on the surface; this probably escapes from the surface at higher temperatures. This could account for the discrepancy between the results of temperature dependence observed here and those of other workers. The measured surface recombination coefficient at 298K, however, is in agreement (within the limits of experimental error) with that of Mulcahy and Williams[72] for a Teflon-coated pyrex surface ($\gamma \approx 0.7$ to 3×10^{-5}).

These workers also observed that the measurement of k_w becomes increasingly inaccurate at lower temperatures. The value of γ for phosphoric acid coated surface ($0.71 \pm 0.59 \times 10^{-5}$) can be compared with the corresponding value quoted by Kretschmer[135] ($\gamma \approx 0.3 \times 10^{-5}$ for O_2 - Ar increasing to 5×10^{-5} in pure oxygen).

Furthermore, the surface recombination efficiency appeared to decrease with the nature of the ambient gas in the order Ar, He > CO_2 (Tables 2, 3, and 4). This suggests that strong physical adsorption may reduce the catalytic efficiency and could explain the large range of values for γ^* reported in the literature, similar to the range observed in this work.

Although surface recombination efficiency varied by an order of magnitude at different temperatures and with different ambient gases, wall recombination caused no significant errors in $k_{1.1}$ because relative third body efficiencies and temperature coefficients of argon are in

close agreement with those obtained by static method where wall effects are absent.

The mechanism of wall recombination has been discussed by Linnett et al.[114-117] Oxygen atoms from the gas phase combine with loosely bound oxygen atoms on the surface, the active site thus produced is replaced at once by other oxygen atoms. It is supposed that the reactivity resides in a few oxygen atoms which are loosely bound or under some state of strain. Some or all of these loosely bound 0 atoms may be atoms that have adsorbed from the gas phase. The catalytic activity of the surface may be described by:

$$\text{Surface} - 0 + 0 \longrightarrow \text{Surface} - + O_2$$

$$\text{Surface} - + 0 \xrightarrow{\text{fast}} \text{Surface} - 0$$

where surface - 0 represents loosely bound 0 atoms. Such sequence will explain why the recombination is first order on a pyrex surface.

The data on the mole-fraction of NO, calculated from equation 20 for system B, needs some comment. One typical plot of the data according to this equation (Fig. 10) shows a linear relationships. The slope of the line provides the value of 2 F (NO) k_{12}^{Ar}. The recent value of k_{12}^{Ar} of Michael, Payne and Whytock[126] was used as a basis for the calculation of the mole-fraction of NO. The constancy of the mole-fraction in Tables 2 and 3 at different temperatures supports the temperature coefficient (n = 1.86) of Whytock et al.[126] for reaction 12.

The results of this work provided information on the homogeneous and wall reactions. It also gives indirectly some insight into reaction 12, but direct information is possible if [NO] can be determined. Wall effects do not constitute a serious drawback to the flow technique. Agreement

with the best static method can be expected over a wide temperature range and under very different conditions of pressure and time. This is significant for atomic reactions of higher kinetic order which are mainly studied by flow methods.

The experimental results of the kinetics study of the reaction:

$$O + SO_2 + M \longrightarrow SO_3 + M \qquad 2.1$$

emphasize the importance of the complete exclusion of water from the system. This is in agreement with the observation and conclusions of previous workers[98]. Unless all the glassware and reagents are dry, an oily layer, presumed to be H_2SO_4, is formed on walls of the reactor vessel, this has a pronounced catalytic effect on the reaction. This and the unsteady decay signal observed at high concentrations of O atoms might be partially responsible for the wide discrepancies and the large range of values of the rate constants reported in the literature. These difficulties were fully considered in the present investigation and it was found that reliable measurements of the decay signal could only be obtained at low concentration oxygen atoms. The rate constant of reaction 2.1 for M = SO_2 was measured under pseudo-first order conditions. The value of the rate constant at 298K is not in agreement with values reported previously with the exception of values reported by Westenberg and deHaas[98].

Mulcahy et al.[92] recognized that SO_3 produced by the reaction 2.1 eventually reached stationary concentration which is in equilibrium with a surface concentration $[SO_3]_w$. They also noted the possible complication

of an $O + SO_3$ step if it were fast enough. Since it has been reported[89] recently that the reaction of O with SO_3 is actually a termolecular process with a very high rate constant, SO_3 produced in reaction 2.1 might reach a steady state concentration. Westenberg and deHaas have recently demonstrated that SO_3 reached a steady state concentration in their experiments and also in some earlier investigations. They took account of the consecutive fast reaction.

$$O + SO_3 + M \longrightarrow SO_2 + O_2 + M \qquad 2.2$$

and divided their measured rate constant by 2 to get the true value. The situation is a slightly different, however, in the present investigation. An attempt was made to obtain the rate constant $k_{2.1}$ uncomplicated by a secondary step. Two sets of measurement at 298K were made for M = He, N_2 and Ar, one at a high $[O]/[SO_2]$ and the other one at a low $[O]/[SO_2]$ ratio. Although the first set of measurements gave a value, identical to the value measured originally by Westenberg and deHaas, the second set of measurements are in good agreement with their reported value. It is reasonable to suppose that at low concentrations of O atoms and high concentration of SO_2, the secondary reaction is unimportant; the rate constants (Table 12) were measured under these conditions. The experimental conditions used by earlier investigators[90, 92, 95] suggest that the secondary step should be effective in their investigation and their results have been divided by two to make them comparable with the present results. The results obtained by Davis[96] using a flash photolysis resonance fluorescence technique and by Atkinson and Pitts[97] using a modulated Hg- photosensitize technique are given without correction in Table 12 since in their techniques,

with short reaction times (10^{-3} ms), and large $[SO_2]/[O]$ ratios secondary reactions should be negligible.

The results are compared with those of other workers in Table 12. The rate constant $k_{2.1}^{SO_2}$ is in good agreement with the results of both Mulcahy et al.[92] and Westenberg and deHaas[98]. Both Timmons et al.[95] and Davis[96] report very high values for $k_{2.1}^{SO_2}$ which in view of our present experience are quite unreasonable. The flash photolysis results of Davis for $k_{2.1}^{M}$ when M = He, N_2 and Ar are lower than the present value by a factor of about 2.5. The possible reasons for such discrepancies are not immediately apparent since no details of these experiments are given[96]. However, the third body efficiencies relative to M = He for $He/Ar/N_2$ (1:2.02:2.25) are closely comparable with the work of Davis (1:1.92:2.23). The values of $k_{2.1}^{M}$ obtained for He, N_2 and SO_2 are in good agreement with those of Westenberg and deHaas. The values of the rate constants reported by Mulcahy et al, using a very different technique, for M = Ar and SO_2 are in reasonable agreement with the values obtained in the present work and both agree that the efficiency of SO_2 as a third body relative to that of an inert gas is not extraordinarily large. The rate constant for M = He and Ar reported by Timmons et al. using the discharge flow E.S.R. technique is good agreement with the present value. Atkinson and Pitts did not use any inert gas as a predominant third body and it is therefore difficult to compare these results with the present results or with the results of other workers.

The recombination of O atoms on a pyrex glass surface is measured as the fraction of the collisions of oxygen atoms with the surface

TABLE 12

Tabulated Values of $k^{M}_{2.1}$ for the Reaction: $O + SO_2 + M \longrightarrow SO_3 + M$

Reference	Method	Third Body M	$10^{-14} \times k^{M}_{2.1}$ at 298 ± 2 K/cm^6 mol^{-2} s^{-1}
This work	Discharge Flow chemi-luminescence technique	He	3.9 ± .335
		Ar	8.12 ± 0.475
		SO_2	30.5 ± 1.86
		N_2	8.7 ± 0.65
Halstead & Thrush[90]	"	Ar	24 ± 4
Timmons et al.[95]	Linear discharge flow, ESR	He	4
		Ar	5
		SO_2	205
Mulcahy et al.[92]	Homogeneous discharge flow ESR-NO glow	Ar	5.5 ± 1.5
		SO_2	33
Westenberg & deHaas[98]	Linear discharge flow ESR	He	3.0 ± 0.2
		N_2	7.2 ± 0.3
		SO_2	29 ± 8
Davis[96]	Flash photo-lysis resonance Fluorescence	He	1.3
		Ar	2.5
		N_2	2.9
		SO_2	174
Atkinsons & Pitts[97]	Modulated Hg-photosensitized N_2O-NO glow	N_2O	11.5 ± 1.5
		SO_2	<60

which are effective in leading to recombination. $(\gamma-\overset{*}{\gamma})$ values measured for this reaction are greater by an order of magnitude than the values reported for reaction 1.1. This is not surprising since pyrex in the reaction system was not poisoned by phosphoric acid, it is possible that the SO_3 - contaminated surface might increase recombination efficiency. This is supported by the fact that at higher temperatures there appeared to be formation of SO_3 on the walls. The view of Mulcahy et al. regarding surface reactions is that the wall reaction is strongly influenced by the rate of reaction 2.1 in the gaseous phase. Such a possibility can not be ruled out in the light of the present results. The values of $(\gamma-\overset{*}{\gamma})$ at 298K (Tables 6, 7, and 8) are comparable with the value of $\gamma \approx 1.2 \times 10^{-4}$ for clean pyrex[109]. As the temperature is increased from 240K (Table 6), the value of $(\gamma-\overset{*}{\gamma})$ decreased initially and then increased at higher temperatures. It is not immediately apparent whether it has positive or negative activation energy. The value of γ^* (Table 6) was measured in presence of argon and in absence of SO_2, its value is considerably less than that of $(\gamma-\gamma^*)$ which again suggest that a SO_3 - contaminated surface might increase surface recombination efficiency. The value obtained for γ^* at 298K is comparable, within the limits of experimental error, with that for reaction 1.1. In the temperature range 298-500K, there is a slight increase in the value of γ^*, this is in contrast to that observed for phosphoric acid-coated surfaces for reaction 1.1.

The rate constant data at different temperatures are plotted in the Arrhenius form (Fig. 24), from this plot the rate constant was found to satisfy the equation

$$k_{2.1}^{SO_2} = (5.31 \pm 0.357) \times 10^{16} \exp \frac{-(839.456 \pm 0.206)}{T}$$

The error limits represent the probable errors from a least square analysis. The temperature dependence of reaction 2.1 has also been investigated by other workers and it is generally agreed that the reaction has a positive activation energy. A comparison of the Arrhenius activation energy obtained in this work with value of other workers is given in Table 13. The activation energy for M = SO_2 measured here for the first time is comparable with value given by Atkinson and Pitts for M = N_2O.

TABLE 13. Activation Energies for Reaction

$$O + SO_2 + M \longrightarrow SO_3 + M \qquad 2.1$$

Reference	Temperature range/K	M	E/kJ mol^{-1}
This work	240-500	SO_2	6.98 ± 1.72
Atkinson & Pitts[97]	299-392	N_2O	8.37 ± 1.67
Davis[96]	220-353	N_2	9.21
Timmons et al.[95]	205-298	He	14.235
Westenberg & deHaas[98]	248-415	He	11.72 ± 0.42

The explanation for the observed positive temperature dependence is that third order reactions proceed via a two step mechanism. The first step involves the formation of the spin-allowed triplet SO_3 molecule. The second step, the intersystem crossing of SO_3 triplet, then gives rise to the observed positive temperature dependence. Webster and Walsh[137] and Mulcahy et al.[91] first discussed the lack of spin

conservation and the possible formation of triplet SO_3 in the reaction 2.1.

The mechanism of the reaction was discussed in some detail by Westenberg and deHaas[98] and a similar unsophisticated collision theory argument is given here to discuss reaction 2.1 in contrast to reaction 1.1. The mechanism of the reaction may be written in the form

$$O(^3P) + SO_2(^1A) \underset{k_b}{\overset{k_a}{\rightleftharpoons}} SO_3^*(^3A)$$

$$SO_3^*(^3A) + M \underset{k_d}{\overset{k_c}{\rightleftharpoons}} SO_3(^1A) + M$$

The overall third order reaction may be written in the form

$$k_{2.1} = (k_a/k_b)\, k_c = K_a\, k_c \qquad 22$$

Where K_a is the equibrium constant for the formation of the excited state from the initial reactants. The equilibrium constant for the overall reaction may be written in a manner similar to that outlined by Porter[23].

$$K = [SO_3]/[O]\,[SO_2] = K_a K_c = K_a k_c/k_d \qquad 23$$

$$\text{or } K\, k_d = K_a k_c \qquad 24$$

Comparing 22 and 24, the rate constant may be written as

$$k_{2.1} = k_d\, K \qquad 25$$

From statistical thermodynamics, the temperature dependent part of the overall K is given (neglecting vibrational contributions) by:

$$K \propto T^{-3/2} \exp(-\Delta E/RT) \qquad 26$$

where $\Delta E = -82$ k cal/mol is the exothermicity of the overall ground state reaction 2.1. The collision theory form[139] k_d is:

$$k_d \alpha T^{\frac{1}{2}} (E^*/RT)^m (1/m!) \exp(-E^*/RT) \qquad 27$$

Where E^* is the minimum energy (positive) for the excitation process $SO_3(^1A) \longrightarrow SO_3^* (^3A)$, and m is an empirical parameter related (vaguely) to the number of classical vibrations active in SO_3^*. Substituting K and k_d from equations 26 and 27 respectively in 25 gives

$$k_{2.1} \alpha T^{-1}(E^*/RT)^m (1/m!) \exp[-(E^* + \Delta E)/RT] \qquad 28$$

In the normal third-order reaction not requiring electronic excitation in the collision complex, one would have the situation that $E^* \sim \Delta E$, so that exponential factor in equation 28 drops out (ΔE being negative) and then $k \alpha T^{-(1 + m)}$ which is the type of inverse temperature dependence normally observed. In the present case, however, it is not unreasonable to suppose that the excitation to the triplet SO_3^* would require sufficient energy that $E^* > \Delta E$, i.e. enough so that the normal inverse T dependence would be overcome and a net effective positive temperature-dependence would exist.

The reaction between SO_2 and oxygen atoms has received considerable attention on account of its possible importance in the conversion of SO_2 to sulphuric acid aerosol in the well-known junge aerosol belt (16-22 km). In the light of the present results, the importance of this reaction to the aerosol conversion mechanism is negligible, since at typical atmospheric temperature where the ratio of $k_{2.2}/k_{2.1} > 10^3$, the main

effect of the presence of SO_2 on O in the atmosphere would be to catalyze its recombination with little or no net SO_3 formation.

Bibliography

1. R. J. Strutt, Proc. Phys. Soc., 23, 66, 147, (1910).

2. R. W. Wood, Proc. Roy. Soc., A 97, 455, (1920).

3. R. W. Wood, Proc. Roy. Soc., A 102, I, (1922).

   R. W. Wood, Phil. Mag., 42, 729, (1921).

   R. W. Wood, Phil., Mag., 44, 538, (1922).

4. E.W.R. Steacie, Atomic and Free Radical Reactions, Reinhold, New York, (1954).

5. F. Kaufman, Prog. Reaction Kinetics, I, I, (1961).

6. B. A. Thrush, Prog. Reaction Kinetics, 3, 63, (1965).

7. R. J. Cvetanovic, Advances in Photochemistry, I, 115, (1963).

8. G. Dixon-Lewis, M. M. Sutton and A. Williams, Disc. Faraday Soc. 33, 205 (1962).

9. K. Hilferding and W. Steiner, Z. Phys. Chem. B, 30, 399, (1935).

10. K. E. Russell and J. Simons, Proc. Roy. Soc., A 217, 271, (1953).

11. M. I. Christie, R. G. W. Norrish and G. Porter, Proc. Roy. Soc., A 216, 152, (1952).

12. M. I. Christie, A. J. Harrison, R. G. W. Norrish and G. Porter, Proc. Roy. Soc. A 231, 446, (1955).

13. R. L. Strong, J. C. W. Chien, P. E. Graf and J. E. Willard, J. Chem. Physics, 26, 1287, (1957).

14. D. L. Bunker and N. Davidson, J. Am. Chem. Soc., 80, 5085, 5090, (1958).

15. G. Porter, and J. A. Smith, Proc. Roy. Soc., A 261, 28, (1961).

16. R. Engleman and N. R. Davidson, J. Am. Chem. Soc., 82, 4770, (1960).

17. R. E. Dodd and E. W. R. Steacie, Proc. Roy. Soc., A 223, 283, (1954).

18. A. Shepp, J. Chem. Phys., 24, 939, (1956).

19. E. Rabinowitch, Trans. Faraday Soc. 33, 283, (1937).

20. D. L. Bunker, J. Chem. Phys., 32, I00I, (1960).

21. S. K. Kim, J. Chem. Phys., 46, 123, (1967).

22. M. Eusuf and K. J. Laidler, Trans. Faraday Soc., 59, 2750, (1963).

23. G. Porter, Disc. Faraday Society, 33, 198, (1962).

24. K. J. Laidler, Disc. Faraday Soc., 33, 294, (1962).

25. G. Porter and J. A. Smith, Nature, 184, 446, (1959).

26. S. J. Rand and R. L. Strong, J. Am. Chem. Soc., 82, 5, (1960).

27. T. A. Gover and G. Porter, Proc. Roy. Soc., A 262, 476, (1961).

28. B. A. Thrush, Chem. Britain, 287, (1966).

29. J. Berkowitz, W. A. Chupke and G. B. Kistiakowsky, J. Chem. Phys., 25, 457, (1956).

30. I. M. Cambell and B. A. Thrush, Proc. Roy. Soc., A 296, 201, (1967).

31. M. L. Spealman and W. H. Rodebush, J. Am. Chem. Soc., 57, 1474, (1935).

32. F. Kaufman, Proc. Roy. Soc. A 247, 123, (1958).

33. C. W. von Rosenberg, Jr. and D. W. Trainor, J. Chem. Phys., 59, 2142, (1973).

34. C. W. von Rosenberg, Jr. and D. W. Trainor, J. Chem. Phys., 61, 2442, 197, (1974).

35. C. W. von Rosenberg, Jr. and D. W. Trainor, J. Chem. Phys., 63, 5348, (1975).

36. R. G. O. Thomas and B. A. Thrush, J. Chem. Soc. Faraday (II) 71, 664, (1975).

37. P. N. Clough and B. A. Thrush, Trans. Faraday Soc., 63, 915, (1967).

38. C. J. Halstead and B. A. Thrush, Proc. Roy. Soc., A 295, 380, (1965).

39. B. A. Thrush, Ann. Rev. Phys. Chem., 19, 371, (1968).

40. M. J. Nicolet, Geophy. Res., 70, 679, (1965).

41. P. A. Leighton, Photochemistry of Air Pollution (Academic Press, New York, New York, (1961).

42. B. Bretta and H. J. Schumacher, Z. Phys. Chem. B, 17, 417, (1932).

43. H. J. Schumacher, Z. Phys. Chem. B17, 405, (1932).

44. D. H. Volman, J. Am. Chem. Soc., 73, 1018, (1951).

45. S. W. Benson and A. E. Axworthy, J. Chem. Phys., 26, 1718, (1957).

46. A. Glissman and H. J. Schumacher, Z. Phys. Chem., 21B, 323, (1933).

47. W. T. Sutphen "Kinetic Decomposition of Ozone", Doctoral thesis, Stanford University, Stanford, California (1955).

48. A. Eucken, Z. Phys. Chem., I07, 436, (1923).

49. J. T. Herron and F. S. Klein, J. Chem. Phys., 40, 2731, (1964).

50. W. Brennen and H. Niki, J. Chem. Phys. 42, 3725, (1965).

51. M. Ritchie, Proc. Roy. Soc., A146, 848, (1939).

52. H. J. Schumacher, J. Chem. Phys., 33, 938, (1960).

53. S. W. Benson and A. E. Axworthy, J. Chem. Phys., 33, 939, (1960).

54. D. J. Mckenney and K. J. Laidler, Can. J. Chem., 40, 539, (1962).

55. J. L. McCrumb and F. Kaufman, J. Chem. Phys., 57, 1270, (1972).

56. W. D. McGrath and R. G. W. Norrish, Proc. Roy. Soc. A254, 317, (1960)

57. F. Kaufman, Proc. Roy. Soc. A247, 123, (1958).

58. L. Elias, E. A. Ogryzlo and H. I. Schiff, Can. J. Chem., 37, 1680, (1959).

59. S. L. Foner and R. L. Hudson, J. Chem. Phys., 25, 601, (1956).

60. F. Kaufman and J. Kelso, Disc. Faraday Soc., 37, 26, (1964).

61. M. A. A. Clyne, B. A. Thrush and R. P. Wayne, Nature, (Physical Science), 199, 1057, (1963).

62. J. T. Herron and H. I. Schiff, Can. J. Chem., 36, 1159, (1958).

63. I. D. Clark, I. T. N. Jones and R. P. Wayne, Proc. Roy. Soc. 317, 407, (1970).

64. R. J. McNeal, and G. R. Cook, J. Chem. Phys., 46, 4541, (1967).

65. R. P. Wayne and J. N. Pitts, J. Chem. Phys., 50, 3644, (1969).

66. F. S. Larkin and B. A. Thrush, Disc. Faraday Soc., 37, 112, (1964).

67. A. Mathias and H. I. Schiff, Disc. Faraday Soc. 37, 38, (1964).

68. M. A. A. Clyne, D. J. McKenney and B. A. Thrush, Trans. Faraday Soc., 61, 2701, (1965).

69. S. W. Benson and A. E. Axworthy, J. Chem. Phys., 42, 2614, (1965).

70. E. Castellano and H. J. Schumacher, Z. Phys. Chem., 34, 198, (1962).

71. F. Kaufman and J. R. Kelso, J. Chem. Phys. 46, 4541, (1967).

72. M. F. R. Mulcahy and D. J. Williams, Trans. Faraday Soc., 64, 59, (1968).

73. M. C. Sauer, Jr., and Leon M. Dorfman, J. Am. Chem. Soc., 87, 3801, (1965).

74. M. C. Sauer, Jr., J. Phys. Chem., 71, 3311, (1967).

75. G. M. Meaburn, D. Perner, J. Leclavé, and M. Bourène, J. Phys. Chem. 72, 3920, (1968).

76. C. J. Hochanadel, J. A. Ghormley, and J. W. Boyle, J. Chem. Phys., 48, 2416, (1968).

77. P. L. T. Bevan and G. R. A. Johnson, J. Chem. Soc. (Faraday I), 69, 216, (1973).

78. T. G. Slanger and G. Black, J. Chem. Phys. 53, 3717, (1970).

79. F. Stuhl and H. Niki, J. Chem. Phys., 55, 3943, (1971).

80. R. E. Huie, J. T. Herron, D. D. Davis, J. Phys. Chem., 76, 2653, (1972).

81. J. A. Zaslowsky, H. B. Urbach, F. Leighton, R. J. Wnuk and J. A. Wojtowicz, J. Am. Chem. Soc., 82, 2682, (1960).

82. W. M. Jones and N. Davidson, J. Am. Chem. Soc. 84, 2868, (1962).

83. H. S. Johnston, National Stand. Ref. Ser., National Bureau of Standard (U.S.), 20, (1968).

84. K. H. Geib and P. Harteck, Trans. Faraday Soc., 30, 131, (1934).

85. M. J. Ball, Private Communication.

86. Walter G. Rothschild, J. Am. Chem. Soc., 86, 1307, (1964).

87. Adir Jacob and C. A. Winkler, J. Chem. Soc. (Faraday Transaction I) 68, 2077, (1972).

88. C. P. Fenimore and G. W. Jones, J. Phys. Chem., 69, 3593, (1965).

89. A. A. Westenberg and N. deHaas, J. Chem. Phys. 62, 725, (1975).

90. C. J. Halstead and B. A. Thrush, Proc. Roy. Soc., A295, 363, (1966).

91. M. F. R. Mulcahy, J. R. Steven, and J. C. Ward, J. Phys. Chem. 71, 2124, (1967).

92. M. F. R. ~~Mulcay,~~ Mulcahy, J. R. Steven, J. C. Ward and D. J. Williams 12th Symposium (International) on Combustion, (Combustion Institute, Pittsburgh, 1969), P. 323.

93. M. J. Ball and F. S. Larkin, Nature (Physical Science), 245, 63, (1973).

94. Sigmund Jaffe and F. S. Klein, Trans. Faraday Soc., 62, 2150, (1966).

95. R. B. Timmons, H. F. LeFevere and G. A. Hollinden, Chemical Reactions in Urban Atmospheres (Elsevier, Amsterdam, 1971), P. 159.

96. D. D. Davis, Can. J. Chem., 52, 1405, (1974).

97. R. Atkinson and J. N. Pitts, Jr., Chem. Phys. Lett, 29, 28, (1974).

98. A. A. Westenberg and N. deHaas, J. Chem. Phys., 63, 5411, (1975).

99. A. Farkas and H. W. Melville, "Experimental Methods in Gas Reactions" (MacMillan and Co., Lond., 1939), P. 42 & 145.

100. J. Strong, "Modern Physical Laboratory Practice" (Blackie and Son Ltd., Lond., 1951) P. 93.

101. J. Reilly and W. N. Rae, "Physico-Chemical Methods" (D. van Nostrand Company Inc., 1939), P. 237.

102. Z. Bay and W. Steiner, Z. Phys. Chem., Abt. B., 2, 146, (1929).

103. Z. Bay and W. Steiner, Z. Phys. Chem., B3, 149, (1929).

104. F. R. Bichowsky and L. C. Copeland, Nature, 120, 729, (1927).

105. K. R. Jennings and J. W. Linnett, Nature, 182, 597, (1958).

106. R. C. McCarthy, J. Chem. Phys., 22, 1360, (1954).

107. K. R. Jennings, Quart. Rev., 15, 237, (1961).

108. T. M. Shaw in "Formation and Trapping of free radicals", Ed. A. M. Bass and H. P. Broida (Academic Press, 1960), Ch. 3, P. 47.

109. J. W. Linnett and D. G. H. Marsden, Proc. Roy. Soc. A234, 489, (1956).

110. A. Fontijn, C. B. Meyer, and H. I. Schiff, J. Chem. Phys. 40, 64, (1964).

111. M. F. Golde and B. A. Thrush, Rep. Prog. Phys., 36, 1285, (1973).

112. H. M. Smallwood, J. Am. Chem. Soc., 51, 1958, (1929).

113. W. Steiner, Trans. Faraday Soc., 31, 623, (1935).

114. J. C. Greaves and J. W. Linnett, Trans. Faraday Soc. 54, 1323, (1958).

115. J. C. Greaves and J. W. Linnett, Trans. Faraday Soc., 55, 1338, (1959).

116. J. C. Greaves and J. W. Linnett, Trans. Faraday Soc., 55, 1346 (1959).

117. J. C. Greaves and J. W. Linnett, Trans. Faraday Soc., 55, 1355, (1959).

118. M. C. Johnson, Trans. Faraday Soc., 28, 162, (1932).

119. I. Langmuir, J. Chem. Soc., 511, (1940).

120. F. Kaufman, J. Chem. Phys., 28, 352, (1958).

121. J. T. Herron and H. I. Schiff, Can. J. Chem., 36, 1159, (1958).

122. P. Harteck, R. R. Reeves, Jr. and G. Mannella, J. Chem. Phys., 29, 1333, (1958).

123. S. Krongelb and M. W. F. Strandberg, J. Chem. Phys., 31, 1196, (1959).

124. H. Wise and C. M. Ablow, J. Chem. Phys., 35, 10, (1961).

125. S. W. Benson, "The Foundations of Chemical Kinetics" (McGraw-Hill Book Co. Inc., New York, 1960) P. 87.

126. J. V. Michael, W. A. Payne and D. A. Whytock, J. Chem. Phys., 65, 4830, (1976).

127. N. Swanson and R. J. Celotta, Phys. Rev. Lett., 35, 783, (1975).

128. JANAF Interim Thermochemical Tables (The Dow Chemical Co., Midland, MI, 1963).

129. O. K. Rice and H. C. Ramsperger, J. Amer. Chem. Soc., 50, 617, (1928).

130. L. S. Kassel, J. Phys. Chem., 32, 225, (1928).

131. R. J. Cvetanovic, J. Chem. Phys., 43, 1850, (1965).

132. M. Anbar and P. Perlstein, Trans. Faraday Soc., 62, 1803, (1966).

133. T. G. Slanger, J. Chem. Phys., 45, 4127, (1966).

134. R. J. Donovan, D. Husain and L. J. Kirsch, Trans. Faraday Soc., 66, 2551, (1970).

135. C. B. Kretschmer, AFOSR-TR-59-62, ASTIA No. 217-008, Aerojet Report No. 1611.

136. J. F. Riley and R. W. Cahil, J. Chem. Phys., 52, 3297, (1970).

137. P. Webster and A. D. Walsh, Tenth Symposium (International) on Combustion, Pittsburgh, (1965), P. 463.

138. N. B. Slater, Theory of Unimolecular Reactions (Mathuen, London, 1959).

139. R. Fowler and E. A. Guggenheim, Statistical Thermodynamics, Third Edition (Cambridge Univ., 1952, P. 497).